Volume 71A
Number 3
May–June 1967

Physics and Chemistry

U.S. DEPARTMENT OF COMMERCE

SECTION A

JOURNAL OF RESEARCH

NATIONAL BUREAU OF STANDARDS

Journal of Research

of the

National Bureau of Standards

A. Physics and Chemistry

May–June • 1967

VOLUME • 71A

NUMBER • 3

Editor: C. W. Beckett

Associate Editors: D. D. Wagman
J. M. Richardson

Publication dates:
Feb. 1, Apr. 1, June 1, Aug. 1, Oct. 1, Dec. 1, 1967

JOURNAL OF RESEARCH

The National Bureau of Standards Journal of Research reports research and development in the fields of activity shown at right. Also included from time to time are survey articles on topics closely related to the Bureau's scientific and technical program.

The Journal is published in three separate sections as follows:

A. Physics and Chemistry

Contains papers of interest primarily to scientists working in these fields. Issued six times a year. Annual subscription: domestic, $5.00; foreign, $6.00. Single copy, $1.00.

B. Mathematics and Mathematical Physics

Presents studies and compilations designed mainly for the mathematician and the theoretical physicist. Issued quarterly. Annual subscription: domestic, $2.25; foreign, $2.75. Single copy, 75c.

C. Engineering and Instrumentation

Reports research and development results of interest chiefly to the engineer and the applied scientist. Issued quarterly. Annual subscription: domestic, $2.75; foreign, $3.50. Single copy, 75c.

The National Bureau of Standards is a principal focal point in the Federal Government for assuring maximum application of the physical and engineering sciences to the advancement of technology in industry and commerce. Its responsibilities include development and maintenance of the national standards of measurement, and the provision of means for making measurements consistent with those standards; determination of physical constants and properties of materials; development of methods for testing materials, mechanisms, and structures, and making such tests as may be necessary, particularly for government agencies; cooperation in the establishment of standard practices for incorporation in codes and specifications; advisory service to government agencies on scientific and technical problems; invention and development of devices to serve special needs of the Government; assistance to industry, business and consumers in the development and acceptance of commercial standards and simplified trade practice recommendations; administration of programs in cooperation with United States business groups and standards organizations for the development of international standards of practice; and maintenance of a clearinghouse for the collection and dissemination of scientific, technical and engineering information. The scope of the Bureau's activities is suggested in the following listing of its three Institutes and their organizational units.

Institute for Basic Standards. Applied Mathematics. Electricity. Metrology. Mechanics. Heat. Atomic Physics. Physical Chemistry. Laboratory Astrophysics.* Radiation Physics. Radio Standards Laboratory.* Radio Standards Physics & Radio Standards Engineering. Office of Standard Reference Data.

Institute for Materials Research. Analytical Chemistry. Polymers. Metallurgy. Inorganic Materials. Reactor Radiations. Cryogenics.* Materials Evaluation Laboratory. Office of Standard Reference Materials.

Institute for Applied Technology. Building Research. Information Technology. Performance Test Development. Electronic Instrumentation. Textile and Apparel Technology Center. Technical Analysis. Office of Weights and Measures. Office of Engineering Standards. Office of Invention and Innovation. Office of Technical Resources. Clearinghouse for Federal Scientific and Technical Information.**

*Located at Boulder, Colo. 80302.
**Located at 5285 Port Royal Road, Springfield, Va. 22151.

U.S. DEPARTMENT OF COMMERCE
Alexander B. Trowbridge, Acting Secretary
NATIONAL BUREAU OF STANDARDS
A. V. Astin, Director

Order all publications from the Superintendent of Documents
U.S. Government Printing Office, Washington, D.C. 20402

Use of funds for printing this publication approved by the Director of the Bureau of the Budget (June 22, 1966).

JOURNAL OF RESEARCH of the National Bureau of Standards—A. Physics and Chemistry
Vol. 71A, No. 3, May–June 1967

Measured Relative Enthalpy of Anhydrous Crystalline Aluminum Trifluoride, AlF_3, from 273 to 1173 °K and Derived Thermodynamic Properties from 273 to 1600 °K[1]

Thomas B. Douglas and David A. Ditmars

Institute for Basic Standards, National Bureau of Standards, Washington, D.C. 20234

(January 27, 1967)

The enthalpy of a high-purity sample of anhydrous crystalline aluminum trifluoride, AlF_3, relative to that at 0 °C (273.15 °K), was precisely measured with an ice calorimeter and a "drop" method at 18 temperatures starting at 50 °C and proceeding in 50-deg steps to 900 °C (1173.15 °K). Thirty additional enthalpy measurements between 450 and 453 °C revealed a gradual transition. A simple general relation for the progress of transition when impurity is in solid solution is derived. The relation fits the observed transition data and indicates a first-order transition temperature of 455 °C (728 °K). X-ray powder patterns on the sample, measured in the Crystallography Section of the NBS, established the existence of a phase transition by showing not only the known hexagonal structure at room temperature (even after violent quenching from above the transition temperature region) but a new, simple-cubic structure at 570 °C (843 °K). The smooth heat-capacity curve formulated from the data merges very smoothly with that representing published precise low-temperature data. The common thermodynamic properties were derived, and are tabulated at and above 273.15 °K, with extrapolation up to 1600 °K.

Key Words: Aluminum trifluoride, drop calorimetry, enthalpy measurements, high-temperature calorimetry, phase transition, pretransition phenomena, specific heat, thermodynamic properties.

1. Introduction

During the past several years the National Bureau of Standards has conducted a comprehensive program of research to determine accurately the thermodynamic properties of substances that are important in high-temperature applications, such as chemical propulsion, yet for which accurate data have been lacking. Aluminum trifluoride, AlF_3, is a key example of prime importance in this area. In this research program the heat of formation at room temperature [1][2] and the vapor pressures at elevated temperatures [2] of AlF_3 have been accurately measured, and a current thermodynamic study of the AlF_3–$AlCl_3$ system involving vaporization equilibrium is in progress. Reliable thermodynamic properties of the solid up to high temperatures are needed, not only to obtain heats of formation and reaction at such temperatures but also to interpret accurately such vaporization data as those just referred to.

Low-temperature heat-capacity measurements (from 54 to 298 °K) on AlF_3, believed to be accurate, have been reported by King [3]. Lyashenko [4] measured the high-temperature enthalpy from 290 to 1305 °K. O'Brien and Kelley [5] repeated these measurements and extended them to 1401 °K. Though the results of these investigations did not differ seriously, those of O'Brien and Kelley have been regarded as somewhat more reliable. (For one thing, Lyashenko failed to detect the transition found by O'Brien and Kelley.) However, Frank [6] noted systematic differences between the results of O'Brien and Kelley and those of others for two other substances measured at the same time as the aluminum fluoride, and, concluding that O'Brien and Kelley's recorded temperatures were too high by amounts up to 20° at 1373 °K, made an adjustment of their smoothed data on AlF_3 which leads to corrected heat capacities in poor agreement with King's.

Because of the need for accurate high-temperature enthalpies of AlF_3 and the uncertainties in the existing data, the measurements reported in the present paper were undertaken.

2. Sample

The sample of aluminum fluoride was supplied by the Alcoa Research Laboratories of the Aluminum

[1] This work was sponsored by the U.S. Air Force, Office of Scientific Research, under Order No. OAR ISSA 65–8.

[2] Figures in brackets indicate the literature references at the end of this paper.

Company of America, New Kensington, Pa., who had purified it by sublimation at 1050 °C in a nickel retort. It was in the form of a fine white crystalline powder.

Specimens were analyzed chemically for aluminum and fluorine in the Applied Analytical Research Section of the NBS, and spectrochemically for a number of heavier chemical elements by a general qualitative method in the Spectrochemistry Section of the NBS. The results of these analyses are given in table 1. The supplier had indicated that the sample would contain "a small amount of aluminum oxide and a spectroscopic amount of nickel," and it will be noted that no analysis for oxygen was made. However, the percentages of aluminum and fluorine in table 1 agree with the theoretical composition within the precision of analysis, and hence no corrections for impurity were made other than adjustment of the enthalpy near the transition temperature as described in section 4.

TABLE 1. *Chemical composition of the sample of aluminum trifluoride as determined by chemical and qualitative spectrochemical analysis*

Element	Percentage by weight		
	Found		Theoretical
	Individual analysis	Mean	
Al	32.13 32.15 32.17	32.15	32.13
F	68.00 67.66 67.61	67.76	67.87
Mg	0.01–0.1		0
Ca, Cu, Fe, Mn, Ni, Si	[a] 0.001–0.01		0
Cr, V	[a] 0.0001–0.001		0
Ag, As, Au, B, Ba, Be, Bi, Cd, Ce, Co, Ga, Ge, Hf, Hg, In, Ir, La, Mo, Nb, Os, P, Pb, Pd, Pt, Rh, Ru, Sb, Sc, Sn, Sr, Ta, Te, Th, Ti, Tl, U, W, Y, Zn, Zr	Undetected		0

[a] For each of the elements listed.

3. Calorimetric Procedure and Thermal Data

The enthalpy measurements were made by a "drop" method employing a silver-core furnace and a precision ice calorimeter. The temperature of the furnace core, held constant to ±0.01 deg during a measurement, was measured up to 500 °C by a platinum resistance thermometer (ice-point resistance, about 25 Ω) that had been calibrated at the NBS and whose ice-point resistance was frequently rechecked. Above 500 °C the furnace temperatures were measured by two Pt – Pt-10 percent Rh thermocouples whose independent NBS calibrations were slightly adjusted to make them exactly concordant with the resistance thermometer below 500 °C when compared with it in the furnace of the calorimetric apparatus. The mass of the sample-plus-container was periodically checked for constancy during the series of measurements. Other details of the method and apparatus are discussed extensively in an earlier publication [7].

All the enthalpy measurements were made on a single specimen ("sample") of aluminum fluoride weighing about 5 g. The cylindrical sample container (wall thickness, about 0.015 in) was fabricated from annealed 99.9 percent-pure silver. One end was drawn down to a narrow neck, and, after introduction of the sample in the air atmosphere of a dry box at room temperature, the container was evacuated and filled with helium to a few torr pressure before pinching the neck and sealing if off with a torch.

The individual enthalpy measurements on the sample-plus-container, the corresponding mean net relative enthalpy of the sample at each temperature, and the deviations of these means from the empirical equations derived to represent them (sec. 5), are given in table 2 for the various furnace temperatures arranged in increasing order. Although the enthalpy measurements at a given furnace temperature are listed in chronological order, the temperatures themselves (particularly from 720 to 726 °K) are not. (The details of the empty-container measurements that were used to complete these calculations are given in another paper [8].) The tabulated values are those after correction for small differences between parts of the sample container and the empty container. The vapor pressure of aluminum fluoride at the highest furnace temperature involved, 900 °C, is only about 1 torr, and it can be shown that at this temperature the heat of evaporation to saturate the 3 cm^3 of gas space in the sample container was negligible (about 0.003 cal).

The enthalpy values of table 2 are further treated in sections 4 and 5.

4. Phase Transition

It is known that AlF_3 undergoes a solid-state transition, though the authors are unaware that anyone has previously investigated the nature of the structural change. O'Brien and Kelley's [5] enthalpy measurements showed a small but definite enthalpy increment (150 cal/mol), and over so small a temperature interval that it was attributed to a first-order transition reported to occur at 727 °K.

The present investigation likewise shows a transition with a heat and temperature approximately in agreement with the above values; so, in addition to a series of enthalpy measurements at furnace temperatures every 50 deg from 273 to 1173 °K, a special series of enthalpy values was determined at closely spaced temperatures between 722 and 727 °K, in an effort to distinguish between a first- and a second-order transition and also to define as closely as possible the true (equilibrium) transition temperature (or temperature range).

The individual unsmoothed enthalpy values obtained in this small range are shown in figure 1. The frame of reference which gives these points significance with regard to the transition is afforded by the two solid curves, calculated from the empirical equations derived later (sec. 5). The lower curve is part of that fitting closely all the values at and below 723 °K (except three values approached from higher temperatures, presently to be discussed), and the upper curve similarly fits closely the values from 773 to 1173 °K. Asso-

TABLE 2. *High-temperature enthalpy measurements on aluminum trifluoride, AlF_3*

Furnace temperature T [a]	Measured heat (sample plus container) [b,c]	$H_T - H_{273.15}$ of AlF_3 [c,d]		
		Individual measurement [e]	Mean observed	Mean observed–smoothed [f]
°K	*cal*	*cal mol*$^{-1}$	*cal mol*$^{-1}$	*cal mol*$^{-1}$
323.15	90.52	898.6	899.6	+3.1
	90.66	901.0		
	90.56	899.3		
373.15	186.12	1873.5	1871.8	+2.2
	186.05	1872.3		
	185.89	1869.6		
423.15	285.05	2896.9	2894.4	−4.1
	284.79	2892.6		
	284.86	2893.8		
473.15	386.95	3963.5	3965.0	−3.2
	387.08	3965.7		
	387.09	3965.9		
523.15	491.35	5066.0	5069.5	−0.2
	491.70	5071.9		
	491.63	5070.7		
573.15	598.42	6207.0	6206.8	+6.8
	598.39	6206.5		
623.15	706.54	7359.4	7363.1	+1.2
	706.85	7364.5		
	706.91	7365.6		
673.15	817.61	8554.4	8556.7	−7.3
	817.73	8556.4		
	817.90	8559.3		
719.78	[g] 934.92	[g] 9892.1		See figure 1. [f]
721.89	930.44	9788.8		
722.13	931.33	9800.7		
722.16	[g] 940.87	[g] 9959.6		
723.06	[g] 943.25	[g] 9987.2		
723.59	934.56	9834.9		
723.76	[g] 943.79	[g] 9986.9		
723.77	935.01	9840.1		
723.84	936.30	9860.7		
723.90	936.22	9858.5		
723.91	[g] 943.27	[g] 9976.2		
724.04	936.82	9866.7		
724.30	937.62	9876.6		
724.33	938.69	9894.1		
724.40	[g] 944.03	[g] 9982.4		
724.52	938.33	9885.4		
724.80	939.72	9905.0		
724.98	941.15	9926.4		
725.18	943.44	9962.1		
725.20	942.77	9950.4		
725.24	943.62	9964.1		
725.27	943.37	9959.6		
725.31	[g] 947.21	[g] 10023.3		
725.31	944.01	9969.8		
725.36	943.97	9968.1		

TABLE 2—*Continued*

Furnace temperature T [a]	Measured heat (sample plus container) [b,c]	$H_T - H_{273.15}$ of AlF_3 [c,d]		
		Individual measurement [e]	Mean observed	Mean observed–smoothed [f]
725.44	945.04	9985.2		See figure 1. [f]
725.54	945.57	9992.7		
725.60	946.56	10008.4		
725.70	947.01	10014.8		
725.89	947.71	10024.0		
726.08	948.73	10038.3		
726.64	949.96	10051.4		
733.00	963.89	10198.6	10198.6	−0.1
742.00	983.87	10411.2	10411.2	+2.3
763.06	1030.64	10908.2	10908.2	+6.5
773.15	1052.60	11138.2	11140.5	+2.2
	1052.92	11143.5		
	1052.69	11139.7		
783.22	1074.69	11370.5	11370.5	−4.2
793.31	1097.28	11610.5	11610.5	−1.9
803.20	1118.71	11833.6	11833.6	−11.2
812.99	1141.13	12074.2	12074.2	−1.3
818.07	1152.66	12197.2	12197.2	+1.8
820.84	1157.74	12244.0	12260.8	−16.8
823.15	1164.08	12318.2	12315.0	−0.3
	1163.69	12311.7		
	1163.89	12315.1		
873.15	1275.81	13494.3	13494.0	−5.7
	1275.77	13493.6		
923.15	1389.25	14690.2	14691.8	+0.8
	1389.31	14691.2		
	1389.48	14694.1		
973.15	1503.59	15892.2	15891.1	+1.9
	1503.41	15889.2		
	1503.57	15891.9		
1023.15	1619.16	17105.0	17100.0	+6.1
	1618.78	17098.7		
	1618.63	17096.2		
1073.15	1734.09	18297.0	18300.6	−4.5
	1734.35	18301.3		
	1734.49	18303.6		
1123.15	1851.71	19523.3	19521.1	−1.4
	1851.41	19518.3		
	1851.61	19521.6		
1173.15	1969.75	20745.7	20747.1	+1.0
	1970.00	20749.8		
	1969.76	20745.8		

[a] International Temperature Scale of 1948, as modified in 1954. 0 °C = 273.15 °K.
[b] Sample mass = 5.0248 g.
[c] 1 cal (defined) = 4.1840 J.
[d] Molecular weight = 83.9767.
[e] In calculating the net heat due to the sample, the gross heat (column 2) was decreased by the smoothed empty-container heat calculated from the equation

$$H_T - H_{273.15} = 0.76152(T-273.15) + 2.3649(10^{-5})(T-273.15)^2 + 0.42246(10^{-7})(T-273.15)^3 - 8.9987[(T-273.15)/T] \text{ cal at } T\,°K.$$

The observed values which this equation represents are given in table 3 of reference [8].
[f] The smoothed values below 728 °K were calculated from eq (14) and those above 728 °K from eq (15).
[g] In determining the enthalpy values so indicated in columns 2 and 3, the final sample temperature (column 1) was approached by cooling after first heating above 726 °K. In determining all other enthalpy values in this table, the final sample temperature was approached by heating only.

ciating these two curves with, respectively, the low-temperature (α) and high-temperature (β) forms of AlF_3, it is natural to take the vertical position of any point between as a linear measure (within the experimental precision) of the fraction of the sample which has converted from α to β, provided the sample can be assumed to have always reverted to the same state when cooled in the calorimeter to 273.15 °K.

On this basis the intermediate points approached from lower temperatures ("by heating") indicate a gradual transition between 723 and 726 °K, and it is believed that these represent approximately true equilibrium because two pairs of points involved equilibration times within the furnace which differed by factors of 4 and 10, respectively, without appreciably changing the enthalpy found. On the other hand the points approached by cooling after first heating above 726 °K (i.e., "by cooling") lie along the upper curve. It is believed that in these latter cases the sample completely converted to the β form but failed to revert partially to α (until quenched in the calorimeter). These points would then not correspond to phase equilibrium, and will not be discussed further.

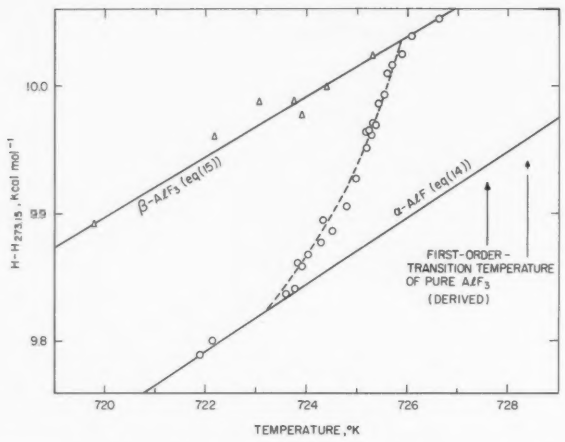

FIGURE 1. *Observed enthalpy of the sample of aluminum fluoride near the transition temperature.*

○ temperature approached by heating only; Δ, temperature approached by cooling after first heating above 726 °K. For the derivation of the dotted curve, see text.

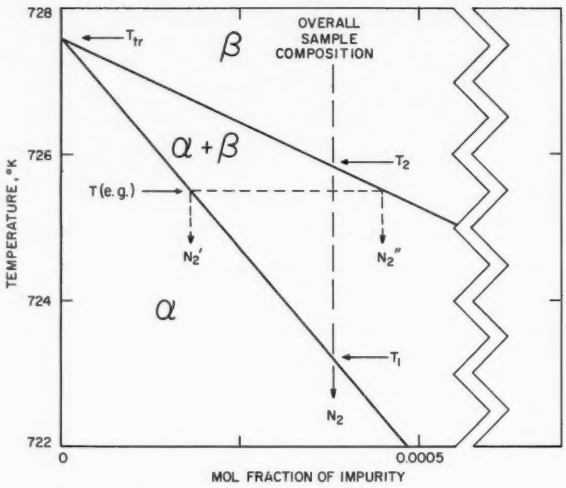

FIGURE 2. *Phase-diagram representation of the transition of the sample of aluminum fluoride as affected by impurity.*

(See text for definitions of symbols.)

It may be noted that the sharp upturn in the enthalpy between 723 and 726 °K, which would correspond to a hump in the heat-capacity curve, is in strong contrast to the gradual upward curvature of the heat-capacity curve over some 200 deg below 723 °K (fig. 3), so that the two phenomena appear to be of different origin. In order to throw light on the nature of the 3-deg upturn, x-ray powder patterns were taken in the Crystallography Section of the NBS on three specimens of the same aluminum-fluoride sample. These specimens were, respectively, one not used in the enthalpy measurements, one that had been heated well above 726 °K and then cooled slowly over two days to room temperature, and one that, after similar heating, had then been quenched in liquid nitrogen (i.e., much more drastically quenched than in the ice calorimeter). All three specimens gave at room temperature the same known pattern associated with the room-temperature hexagonal structure of AlF_3 [9]; it was therefore concluded that in all the enthalpy measurements the sample probably returned to this same form in the calorimeter, and consequently that the points in figure 1 are true measures of the relative enthalpy under the furnace conditions.

Additional x-ray patterns, however, were taken on one of the specimens while at approximately 840 °K, well above the transition region. In these cases the hexagonal pattern was missing, being replaced by a new pattern interpreted as due to a primitive (simple) cubic structure having a cell dimension of 3.580 Å (or possibly some multiple thereof). (TaF_3 is said to show a similar structure at certain temperatures.) From this result it is concluded that the transition in AlF_3 at about 726 °K involves a change in crystal structure. Since a true second-order transition is only compatible with a continuous change in structure not readily conceivable for most pairs of well-defined structures, the conclusion is that pure AlF_3 exhibits a true first-order transition. A quantitative explanation of the observed 3-deg transition is offered below after postulating the presence of impurity soluble in both forms of AlF_3 and then treating the sample as a two-component system.

Two-component systems which exhibit both appreciable solid solubility and a first-order transition of one component are very common, and enthalpy data on some such systems have been interpreted in accordance with these characteristics with as much care as the very common treatment of premelting. However, no one treatment is equally appropriate in every case, as in each one approximations must be made that are consistent with the amount and quality of the information available. With this fact in mind, the following very simple treatment was developed for application to the present case; obviously, it can be more generally applied.[3]

The situation tentatively assumed to exist is illustrated by the type of phase diagram shown in figure 2 (whose specific details are those subsequently derived for the present sample). For simplicity the principal component is assumed to be contaminated with a single component whose overall mole fraction, N_2, is so small that the temperature-composition phase boundaries may be taken as straight lines in this region. Also for simplicity, maintenance of complete phase equilibrium is assumed. In the example illustrated, the impurity depresses the transition temperature of the pure substance, T_{tr}, to a finite temperature interval T_1 to T_2, the sample at any intermediate temperature

[3] A similar treatment has been published by Mastrangelo and Dornte [12]. Their final equations, while derived for the fusion process only and expressed in terms of slightly less general parameters, can be shown to be equivalent to eqs (9) and (11) below.

T consisting of α and β phases of compositions N_2' and N_2'' respectively. Though in most known cases of this type the impurity does depress the transition temperature (as in fig. 2), some cases are known where this is elevated, but the following equations are equally applicable to both situations.

The two phase boundaries may be defined by

$$N_2' = A(T - T_{tr}); \tag{1}$$

$$N_2'' = B(T - T_{tr}), \tag{2}$$

where A and B are constants. The limits of the two-phase temperature region are then obviously given by

$$T_1 = T_{tr} + N_2/A; \tag{3}$$

$$T_2 = T_{tr} + N_2/B. \tag{4}$$

If at temperature T each mole of the principal component is distributed with n' moles in the α solid solution and n'' moles in the β solid solution, the overall mole balance of each component gives the well-known "lever" relations; on assuming that N_2, N_2', and N_2'' are negligible compared to unity, these relations are

$$n' = \frac{N_2 - N_2''}{N_2' - N_2''}; \tag{5}$$

$$n'' = \frac{N_2' - N_2}{N_2' - N_2''}. \tag{6}$$

It is convenient to define a constant parameter k by

$$B/A = k. \tag{7}$$

From these equations then follow the two relations

$$n'' = \left[\left(\frac{T_2 - T}{T - T_1}\right)k + 1\right]^{-1}; \tag{8}$$

$$T_{tr} = T_2 + \frac{T_2 - T_1}{k - 1}. \tag{9}$$

If ΔH_{tr} is the molal heat of transition, the molal enthalpy of the sample $n''\Delta H_{tr}$ at T in excess of that of the pure α phase may be calculated from eq (8); eq (9) gives the transition temperature corrected for the impurity. A well-known relation[4] applicable to dilute solutions exhibiting miscibility in both phases is, in the present notation (and with R as the gas constant),

$$\frac{N_2' - N_2''}{T - T_{tr}} = \frac{\Delta H_{tr}}{RT_{tr}^2}, \tag{10}$$

and this may be combined with previous equations to give the amount of impurity in the sample, N_2, causing the transition over the interval T_1 to T_2:

$$N_2 = \frac{k(T_2 - T_1)\Delta H_{tr}}{(1-k)^2 RT_{tr}^2}. \tag{11}$$

If T_1, T_2, k, and ΔH_{tr} can be evaluated from the thermal data such as that shown in figure 1, eq (9) and (11) may be readily solved.

Close examination of eq (8) shows, however, that some measure of the curvature of the "excess enthalpy" curve in the transition region ($n''\Delta H_{tr}$ versus T) is essential to assigning a value to k and hence using eq (9) and (11) significantly. If the impurity elevates the transition temperature ($T_{tr} < T_1$), then $k < 1$ and this curve is concave downward; but if the transition temperature is depressed ($T_{tr} > T_2$), then $k > 1$ and the curve is concave upward. In either event the curve begins (at T_1) and ends (at T_2) with finite positive slope.

The enthalpy values of figure 1 (excluding the points "by cooling"), though subject to apparently considerable scatter which is a result of the unusually small magnitude of the heat of transition and the correspondingly expanded scale of this plot,[5] were deemed sufficiently numerous and interconsistent to apply the above relations. An approximation to the best fit to the data gave

$$\left.\begin{aligned} T_1 &= 723.2\ ^\circ\text{K} \\ T_2 &= 725.85\ ^\circ\text{K} \\ k &= 2.5 \end{aligned}\right\}, \tag{12}$$

from which were calculated

$$\left.\begin{aligned} T_{tr} &= 727.6\ ^\circ\text{K} \\ N_2 &= 0.0004 \end{aligned}\right\} \tag{13}$$

and the dashed curve drawn through the transition region in figure 1. This curve fits the points within their precision, and it may be added that a value $N_2 = 0.0004$ is plausible (e.g., if due to MgF_2, this would correspond to 0.01 weight percent of Mg, which is consistent with table 1). This explanation of the observed transition data is thus regarded as acceptable, with the transition temperature of pure AlF_3 lying above 726 °K. Since the value derived above for the transition temperature must be considered uncertain by the order of 1 deg, it will be rounded to 728 °K for calculations on pure AlF_3.

[4] See, for example, reference [10].

[5] Note that in figure 1 the total ordinate distance between the two solid curves is equivalent to only about 1.5 percent of the measured relative enthalpy which determines any one point.

TABLE 3. *Thermodynamic functions for aluminum trifluoride, AlF_3, solid phases (in terms of defined calories per mole)*
(1 cal = 4.1840 J; T °K = t °C + 273.15; 1 mole = 83.9767 g.)

T	C_p°	$(H_T^\circ - H_0^\circ)$	$(H_T^\circ - H_0^\circ)/T$	S_T°	$-(G_T^\circ - H_0^\circ)$	$-(G_T^\circ - H_0^\circ)/T$
°K	cal deg^{-1} mol^{-1}	cal mol^{-1}	cal deg^{-1} mol^{-1}	cal deg^{-1} mol^{-1}	cal mol^{-1}	cal deg^{-1} mol^{-1}
			Alpha Phase			
273.15	17.045	2340.5	8.569	14.357	1581.2	5.789
298.15	17.957	2778.2	9.318	15.890	1959.4	6.572
300.00	18.021	2811.5	9.372	16.001	1988.9	6.630
325.00	18.828	3272.4	10.069	17.476	2407.5	7.408
350.00	19.526	3752.0	10.720	18.898	2862.3	8.178
375.00	20.119	4247.7	11.327	20.266	3352.0	8.938
400.00	20.623	4757.2	11.893	21.581	3875.2	9.688
425.00	21.053	5278.3	12.420	22.844	4430.6	10.425
450.00	21.426	5809.4	12.910	24.059	5017.0	11.149
475.00	21.754	6349.2	13.367	25.226	5633.1	11.859
500.00	22.054	6896.9	13.794	26.350	6277.9	12.556
550.00	22.625	8013.8	14.571	28.478	7649.2	13.908
600.00	23.258	9160.4	15.267	30.473	9123.5	15.206
650.00	24.071	10343.	15.912	32.365	10695.	16.454
700.00	25.181	11572.	16.532	34.188	12369.	17.656
728.00	25.978	12288.	16.880	35.190	13330.	18.311
			Beta Phase			
728.00	23.322	12423.	17.065	35.375	13330.	18.311
750.00	23.392	12937.	17.249	36.071	14116.	18.821
800.00	23.546	14110.	17.638	37.585	15958.	19.947
850.00	23.693	15291.	17.990	39.017	17873.	21.027
900.00	23.833	16480.	18.311	40.375	19858.	22.065
950.00	23.968	17675.	18.605	41.668	21910.	23.063
1000.00	24.099	18876.	18.876	42.900	24024.	24.024
1050.00	24.227	20084.	19.128	44.079	26199.	24.951
1100.00	24.353	21299.	19.363	45.209	28431.	25.847
1150.00	24.476	22520.	19.582	46.294	30719.	26.712
1200.00	24.598	23747.	19.789	47.339	33060.	27.550
1250.00	24.718	24979.	19.984	48.345	35452.	28.362
1300.00	24.837	26218.	20.168	49.317	37894.	29.149
1350.00	24.954	27463.	20.343	50.257	40383.	29.914
1400.00	25.071	28714.	20.510	51.166	42919.	30.656
1450.00	25.187	29970.	20.669	52.048	45500.	31.379
1500.00	25.302	31232.	20.822	52.904	48123.	32.082
1550.00	25.417	32500.	20.968	53.735	50790.	32.767
1600.00	25.531	33774.	21.109	54.544	53497.	33.435

H_0° is the enthalpy of the α form at 0 °K (and 1 atm pressure). Values for temperatures higher than 1150 °K are by extrapolation beyond the measuring range.

APPENDIX. *Thermodynamic functions for aluminum trifluoride, AlF_3, solid phases (in terms of joules per mole)*

(T °K = t °C + 273.15; 1 mole = 83.9767 g.)

T	C_p°	$(H_T^\circ - H_0^\circ)$	$(H_T^\circ - H_0^\circ)/T$	S_T°	$-(G_T^\circ - H_0^\circ)$	$-(G_T^\circ - H_0^\circ)/T$
°K	J deg^{-1} mol^{-1}	J mol^{-1}	J deg^{-1} mol^{-1}	J deg^{-1} mol^{-1}	J mol^{-1}	J deg^{-1} mol^{-1}
			Alpha Phase			
273.15	71.316	9792.6	35.853	60.070	6615.7	24.221
298.15	75.132	11624.	38.986	66.484	8198.1	27.497
300.00	75.400	11763.	39.212	66.948	8321.6	27.740
325.00	78.776	13692.	42.129	73.120	10073.	30.995
350.00	81.697	15698.	44.852	79.069	11976.	34.217
375.00	84.178	17772.	47.392	84.793	14025.	37.397
400.00	86.287	19904.	49.760	90.295	16214.	40.535
425.00	88.086	22084.	51.965	95.579	18538.	43.618
450.00	89.646	24306.	54.015	100.66	20991.	46.647
475.00	91.019	26565.	55.928	105.54	23569.	49.618
500.00	92.274	28857.	57.714	110.25	26267.	52.534
550.00	94.663	33530.	60.965	119.15	32004.	58.191
600.00	97.312	38327.	63.877	127.50	38173.	63.622
650.00	100.71	43275.	66.576	135.42	44748.	68.844
700.00	105.36	48417.	69.170	143.04	51752.	73.873
728.00	108.69	51413.	70.626	147.24	55773.	76.613
			Beta Phase			
728.00	97.579	51978.	71.400	148.01	55773.	76.613
750.00	97.872	54128.	72.170	150.92	59061.	78.747
800.00	98.516	59036.	73.797	157.26	66768.	83.458
850.00	99.132	63978.	75.270	163.25	74781.	87.977
900.00	99.717	68952.	76.613	168.93	83086.	92.320
950.00	100.28	73952.	77.843	174.34	91671.	96.496
1000.00	100.83	78977.	78.977	179.49	100520.	100.52
1050.00	101.36	84031.	80.032	184.43	109620.	104.40
1100.00	101.89	89115.	81.015	189.15	118960.	108.14
1150.00	102.41	94224.	81.931	193.69	128530.	111.76
1200.00	102.92	99357.	82.797	198.07	138320.	115.27
1250.00	103.42	104512.	83.613	202.28	148330.	118.67
1300.00	103.92	109696.	84.383	206.34	158550.	121.96
1350.00	104.41	114905.	85.115	210.28	168960.	125.16
1400.00	104.90	120139.	85.814	214.09	179570.	128.26
1450.00	105.38	125394.	86.479	217.77	190370.	131.29
1500.00	105.86	130675.	87.119	221.35	201350.	134.23
1550.00	106.34	135980.	87.730	224.83	212500.	137.10
1600.00	106.82	141310.	88.320	228.21	223830.	139.89

H_0° is the enthalpy of the α form at 0 °K (1 atm pressure). Values for temperatures higher than 1150 °K are by extrapolation beyond the measuring range.

5. Data-Smoothing; Derived Thermodynamic Functions

Pure aluminum fluoride was assumed to have a first-order transition at 728 °K, as derived in section 4, and two separate empirical equations were derived by the method of least squares to fit the observed enthalpy values as functions of temperature below and above this transition temperature. In this fitting, only the mean enthalpy values (given equal weight) at temperatures exactly 50 deg apart, from 323.15 to 1173.15 °K, were used.[6] After so trying several forms of equation to obtain acceptable smooth fits, the equations selected were as follows (with the enthalpy and standard deviation, σ, in cal mol^{-1} at T °K, relative to that of the α form at $T_0 = 273.15$ °K). Note that eq (15) is not intended to be applicable down to 273.15 °K.

α-AlF_3 (273 − 728 °K):

$$H_T - H_{T_0} = -6.27678(T - T_0) + 7.05597(10^{-2})(T^2 - T_0^2) - 8.25715(10^{-5})(T^3 - T_0^3) + 3.93984(10^{-8})(T^4 - T_0^4)$$

$$\sigma(\alpha) = 5.58 \qquad (14)$$

β-AlF_3 (728 − 1173.15 °K):

$$H_T(\beta) - H_{T_0}(\alpha) = 22.1387(T - T_0) + 1.08571(10^{-3})(T^2 - T_0^2) + 2.1078(10^5)\left(\frac{1}{T} - \frac{1}{T_0}\right)$$

$$\sigma(\beta) = 4.09 \qquad (15)$$

Smooth high-temperature thermodynamic functions of aluminum trifluoride that represent the present work and merge smoothly with those given by King's low-temperature heat capacities [3] are given in table 3 in terms of defined calories, and in the table in the appendix in joules. As a step in generating this table, a smooth heat capacity function was first evaluated from King's results alone, using a computer code which employs four-point Lagrangian interpolation and employing King's combination of Debye and Einstein functions[7] for temperatures below his range of measurement (below 51 °K). This procedure gave a Third-Law value for $S^\circ_{298.15}$ of 15.890 cal deg^{-1} mol^{-1} (King gave 15.89 ± 0.08). The value of $C_P^\circ(298.15)$ given by King (17.95 cal mol^{-1} deg^{-1}) is the same as that derived from eq (14) (which fits the high-temperature data of the present work alone). The smooth representation of King's heat capacity data was then joined to the high-temperature heat capacity derived from eq (14). In order to ensure a continuous temperature derivative of heat capacity in the region of joining, minor adjustments were made to the smoothed high-temperature heat capacity data below 360 °K. The net result of these adjustments was to increase the enthalpy increment ($H_{360} - H_{273.15\,°K}$) by less than 0.02 percent. The thermodynamic functions up to the transition point were generated using King's smoothed heat capacity data and heat capacity values determined from eq (14), adjusted below 360 °K.

Above the transition temperature eq (15) was used, the necessary integration constants being required to be consistent with the heat of transition, 134.6 cal mol^{-1}, given by the difference of eq (14) and (15) at the transition temperature, 728 °K.

6. Discussion

The heat capacities of α- and β-AlF_3 above 145 °K are shown as functions of temperature in figure 3. The high temperature experimental points were calculated in each case from the original enthalpy data employing a curvature correction according to a formula of Osborne et al. [13]. The smoothed results of O'Brien and Kelley were derived from their published enthalpy equation [5]. Lyashenko's smoothed values were derived from an enthalpy function which fit his observed data to 1.5 percent (several equations were tried, but none fit his data more closely). Over most of the temperature range, the solid curve, which represents the smoothed results of the present work (eq (14) or (15), or table 3), lies between that for O'Brien and Kelley's original work [5] and that for their results as adjusted by Frank [6]. King's values merge very smoothly with the authors' curve and nearly as well with O'Brien and Kelley's, but definitely not with Frank's. The authors' curve for the β form is closer to O'Brien and Kelley's than to Frank's. These considerations, taken together with the fact that Frank's adjustment of O'Brien and Kelley's data lowers the apparent α-β transition temperature by 9 °C (whereas the present work predicts a transition temperature essentially in agreement with that of O'Brien and Kelley), lead the authors to conclude that Frank's corrections to the AlF_3 data are completely invalid.

Just previous to the authors' measurements on AlF_3 they made checks on the calorimetric apparatus by repeating measurements of the enthalpy of Calorimetry-Conference standard-sample synthetic sapphire (Al_2O_3) at 373, 773, and 1173 °K relative to 273 °K. At all these temperatures the agreement with earlier work at the NBS using the same sample and the same apparatus was within 0.2 percent, which is within the present precision at 373 and 773 °K but slightly outside it at 1173 °K. Because the calorimetric apparatus used to measure AlF_3 was very recently used also to measure $BeO \cdot Al_2O_3$ and $BeO \cdot 3Al_2O_3$ over the same temperature range and with the same high precision, the authors feel that their general discussion of accuracy for the latter two substances [8, 11] is equally applicable to AlF_3. The actually observed enthalpy

[6] The measurements at 721.89 and 722.13 °K were used to compute the mean enthalpy at 723.15 °K.

[7] King states that this function fits his heat capacities to within 0.8 percent from 51 to 298 °K.

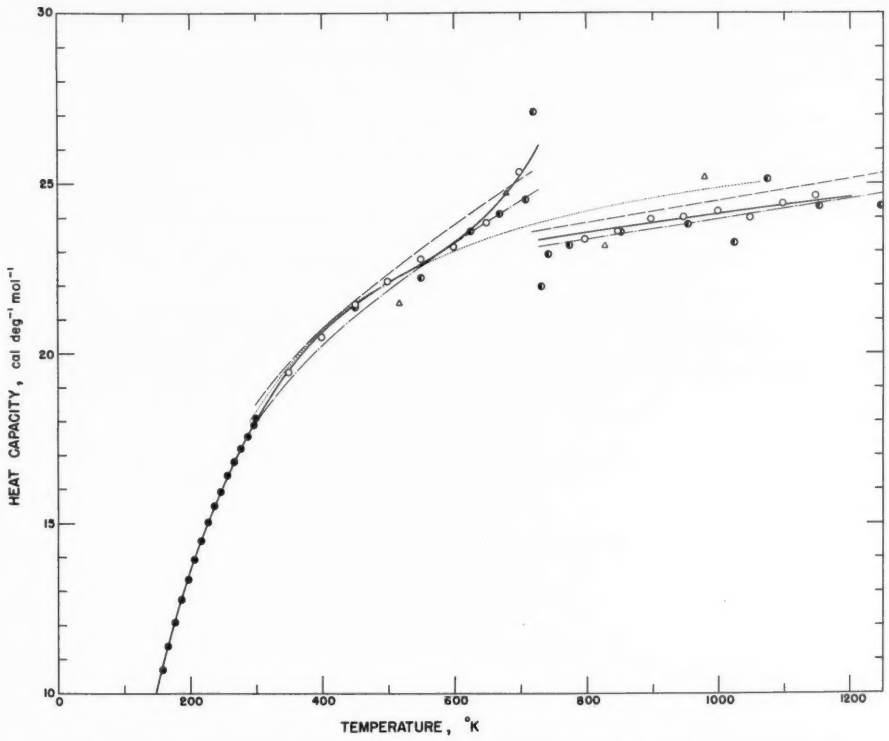

FIGURE 3. *Comparison of the heat capacity of α- and β-AlF_3 determined by independent investigations.*
For derivation of the curves (which represent smooth values), see text. ●, King, adiabatic method [3]; ○, NBS drop method (this work); ——, table 3 (this work); ◐ – – –, O'Brien and Kelley [5]; — —, O'Brien and Kelley as adjusted by Frank [6]; · · · · · ·, Δ, Lyashenko [4].

of the sample very near the transition temperature is, of course, subject to additional uncertainty owing to the possibility of incomplete phase equilibrium, but for other temperatures this introduces no uncertainty into the enthalpy and very little into the entropy.

The gradual upturn of the heat-capacity curve for about 200 deg below the transition temperature is interesting (fig. 3). Many solids show this behavior below their melting points or transition temperatures, and it is usually attributed to some type of disorder (of which lattice vacancies form a special case). Despite the x-ray diffraction results summarized in section 4, not enough structural data are presently available on β-AlF_3 to suggest how the lattice may tend to rearrange near the transition temperature.

The authors acknowledge the particularly helpful contributions of the following persons. George Long, of the Alcoa Research Laboratories, Aluminum Company of America, furnished the sample. It was analyzed by members of the National Bureau of Standards: for aluminum by E. June Maienthal, for fluorine by Rolf A. Paulson, and spectrochemically by Elizabeth K. Hubbard. Howard E. Swanson, also of the NBS, carried out the x-ray examinations and made the structural interpretations of them.

7. References

[1] E. S. Domalski and G. T. Armstrong, J. Research NBS **69A** (Phys. and Chem.), No. 2, 137 (1965).
[2] R. F. Krause, Jr., and T. B. Douglas, publication pending.
[3] E. G. King, J. Amer. Chem. Soc. **79,** 2056 (1957).
[4] V. S. Lyashenko, Metallurg. (USSR) **10,** No. 11, 85 (1935).
[5] C. J. O'Brien and K. K. Kelley, J. Amer. Chem. Soc. **79,** 5616 (1957).
[6] W. B. Frank, J. Phys. Chem. **65,** 2081 (1961).
[7] G. T. Furukawa, T. B. Douglas, R. E. McCoskey, and D. C. Ginnings, J. Res. NBS **57.** 67 (1956) RP 2694.
[8] D. A. Ditmars and T. B. Douglas, J. Res. NBS **71A** (Phys. and Chem.) No. 2, 89–96 (1967).
[9] F. Hanic, K. Matiasovsky, D. Stempelova, and M. Malinovsky, Acta Chim. Acad. Sci. Hung. **32,** (No. 3). 309 (1962).
[10] S. Glasstone, Textbook of Physical Chemistry, p. 650, eq (45), 2d ed. (D. Van Nostrand Co., Inc., New York, 1944).
[11] D. A. Ditmars and T. B. Douglas, J. Res. NBS **71A** (Phys. and Chem.) No. 2, 97–103 (1967).
[12] S. V. R. Mastrangelo and R. W. Dornte, J. Amer. Chem. Soc. **77,** 6200 (1955).
[13] N. S. Osborne, H. F. Stimson, T. S. Sligh, and C. S. Cragoe, BS Sci. Pap. **20,** 65 (1925) S501.

(Paper 71A3–450)

JOURNAL OF RESEARCH of the National Bureau of Standards—A. Physics and Chemistry
Vol. 71A, No. 3, May–June 1967

The Heat of Formation of Boron Trifluoride by Direct Combination of the Elements[1]

Eugene S. Domalski and George T. Armstrong

Institute for Basic Standards, National Bureau of Standards, Washington, D.C. 20234

(January 27, 1967)

The energy of combination of crystalline boron in gaseous fluorine was measured in a bomb calorimeter. The experimental data combined with reasonable estimates of all known errors may be expressed by the equation:

$$B(c) + 3/2F_2(g) = BF_3(g),\ \Delta H^\circ_{f298} = -271.03 \pm 0.51 \text{ kcal mol}^{-1}.$$

This result is compared with other recent work on and related to the heat of formation of boron trifluoride.

Key Words: Bomb calorimeter, boron, boron trifluoride, fluorine, heat of formation, Teflon.

1. Introduction

An accurate value for the heat of formation of boron trifluoride is of significant importance because this value is involved in the thermochemistry of many boron compounds. The study of the thermochemistry of boron compounds was for a long time hampered by difficulties in measuring a suitable reaction involving elemental boron. The heat of formation of boric oxide, for instance, was uncertain to several kilocalories per mole because of the difficulty of getting complete combustion of the element in oxygen, or of determining the amount of reaction, in the absence of complete combustion. The difficulty was apparently due to the glassy and nonvolatile character of the boric oxide formed, which tended to terminate the reaction before completion, and made the analysis of the product a complex problem.

The thermochemistry of boron was placed on a firm basis by the work of Prosen, Johnson, and Pergiel [1, 2][2] on the decomposition and hydrolysis of diborane, and of Johnson, Miller, and Prosen [3] on the heat of formation of boron trichloride from the elements. With the aid of the heats of these reactions and other data, they obtained reasonably consistent values for $B_2O_3(c)$, $H_3BO_3(c)$, $B_2H_6(g)$, and $BCl_3(g)$. While more recent work has suggested changes in some of the values, these changes have been small.

The heat associated with the direct combination of the elements in a bomb calorimeter was measured by Wise, Margrave, Feder, and Hubbard [41], who found the heat of formation of $BF_3(g)$ to be -269.88 ± 0.24 kcal mol^{-1}. Another study involving the direct combination of the elements by Gross, Hayman, Levi, and Stuart [5] gave -271.20 kcal mol^{-1} for the heat of formation of $BF_3(g)$.

More recent additional measurements by Johnson, Feder, and Hubbard [6] showed that the calorimetric work of Wise et al. [4], was correct, but reanalysis of the boron sample revealed impurities not previously taken into account. A recalculation of their earlier data gave for $\Delta H^\circ_{f298}[BF_3(g)]$, -271.6 ± 0.9 kcal mol^{-1}. The calorimetric measurements reported by Johnson et al. [6], were made using a boron sample of greater purity in both a conventional-type combustion bomb and a two-chambered combustion bomb and led to a value for $\Delta H^\circ_{f298}[BF_3(g)]$ of -271.65 ± 0.22 kcal mol^{-1}.

Research prior to the work of Wise et al. [4], is neither sufficiently detailed nor accurate enough to derive a value for the heat of formation of BF_3 having an uncertainty less than several kilocalories per mole, and hence, has not been considered. Gmelin [7] provides a review of the earlier work on this subject for the interested reader.

We felt that additional confirmatory work on the heat of formation of BF_3 was needed to establish more fully the recent work of Gross et al. [5], and Johnson et al. [6]. In addition, we have found that work in our laboratory on the measurement of the heats of combustion of several refractory boron compounds has produced values for their heats of formation very

[1] This research was sponsored by the Air Force Aero Propulsion Laboratory, Research and Development Division, Air Force Systems Command, Wright-Patterson Air Force Base, Ohio, under USAF Delivery Order No. 33(615)64-1003, and by the Air Force Office of Scientific Research under Order No. OAR ISSA 65-8.

[2] Figures in brackets indicate the literature references at the end of this paper.

sensitive to the auxiliary value used for the heat of formation of boron trifluoride. Some systematic errors in the calculated heats of formation may be avoided by measuring the heat of combustion of boron using a similar procedure in the same apparatus. The variations in the heat of formation of BF_3, as reported by other investigators, are large enough to make a significant difference in the heats of formation of metallic borides if calculated from their heats of combustion in fluorine.

2. Materials

2.1. Boron

The sample of β-rhombohedral boron was obtained from the Eagle-Picher Company and had been prepared by the hydrogen reduction of boron tribromide on a substrate of zone refined boron. The maximum particle size was 150 μ. The supplier reported traces of copper and silicon and a small amount of carbon in the sample. The sample was analyzed spectrographically for metallic impurities and quantitatively for individual metals to 0.001 percent. A nitrogen assay was made using the Kjeldahl method and the carbon content was determined by oxygen combustion of the sample and measurement of the CO_2 formed. This measurement gave a higher carbon content than was indicated by the supplier. We preferred our carbon analysis for the assay of our sample. The analysis for oxygen in our boron sample was performed by both neutron activation and inert-gas fusion methods. The oxygen analysis obtained by inert-gas fusion is preferred over the analysis by neutron activation because of suspected interference by isotopic species produced from irradiation of the boron itself [8]. Table 1 summarizes the analysis of the boron sample, showing the total boron content to be 99.68 percent by difference.

An x-ray diffraction pattern of the boron sample determined by the NBS Crystallography Section yielded lattice parameters in good agreement with data reported earlier. The lattice parameters were $a = 10.922$ Å and $c = 23.79$ Å (compared to $a = 10.944$ Å and $c = 23.811$ Å [10]) and the space group found was $R\bar{3}m$.

TABLE 1. *Analysis of the boron sample* [a]

Metal impurities								Total
Al	Fe	Mg	Mn	Sr	Ca	Si	Cu	
< 0.001	0.079	0.002	0.014	0.002	0.010	0.012 (0.0003)[b]	..... (0.0007)[b]	0.120

Nonmetallic impurities			
N	O	C	
< 0.005	0.088 [c] (0.161)[d]	0.11 (0.05)[e]	0.203

Assumed presence of nonmetallic impurities				
BN	B_2O_3	B_4C		
0.009	0.128	0.506		0.643
Total boron content.....			99.677	
Total boron as the element.....				99.237

[a] Analyses presented in table 1 were performed by the NBS Analysis and Purification Section, unless otherwise stated.

[b] Supplier's analysis (Eagle-Picher Co.).

[c] Inert-gas fusion (Ledoux and Co.).

[d] Neutron activation analysis (General Atomic).

[e] Supplier's analysis for carbon in boron by the method of Kuo, Bender, and Walker [9].

2.2. Teflon (Polytetrafluoroethylene)

The Teflon film and Teflon powder ("Teflon 7") used in preparing pelleted mixtures for combustion experiments were the same as we have described in an earlier publication [11]. Here again neither the Teflon powder nor the Teflon film were modified or treated in any special way prior to use. The energy of combustion, ΔE°_{303}, of the Teflon (film and powder) was $-10{,}372.8\ \mathrm{J\,g^{-1}}$ [11].

The fluorine used in the heat measurements assayed at 99.40 percent F_2. The fluorine was analyzed by absorbing the F_2 in mercury and observing the pressure and composition of the residual gases [12]. The composition of the residue was determined by examination in a mass spectrometer. Table 2 shows the results of typical analysis of a fluorine sample.

TABLE 2. *Composition of fluorine sample*

Constituent	Mole percent
F_2	[a] 99.40
O_2	0.0960
N_2	.2784
CO_2	.0175
CF_4	.1962
Ar	.0083
SO_2F_2	.0001
SiF_4	.0003
C_2F_6	.0023
SF_6	.0001
C_4F_8	.0002
C_3F_8	.0005
C_2F_4 or cyclic C_4F_8	.0001

[a] By difference.

3. Preparation of Sample Pellets

The first step of the procedure used to prepare the boron sample for combustion in fluorine was to mix the sample with Teflon powder in a bag made of Teflon film. The bagged mixture was then pelleted and provided with an additional coating of Teflon (method B of our earlier work [11]). Attempts to burn pelleted mixtures of boron and Teflon powder on which no outer Teflon coating was provided (method A, [11]) resulted in spontaneous combustion of the pellet during the fluorine-loading procedure. However, if method B was used, it was possible to carry out the calorimetric experiment, and the apparent heat transfer coefficients calculated for the calorimeter in these heat measurements were comparable to that of a normal combustion experiment in which no premature reaction was taking place.

Much care is needed in keeping track of the cumulative mass of the sample as the Teflon and boron are added because some losses are always observed and their distribution significantly affects the results of the experiment.

Table 3 gives average values for the amounts of Teflon and boron used in preparing a pellet and the losses detected in the process. The sample masses were adjusted for losses in the manner previously described [11].

The densities used for the Teflon film, Teflon powder, and boron in making buoyancy corrections were 2.15, 2.16, and 2.35 g $\mathrm{cm^{-3}}$ [13], respectively. Weighings of pelleted mixtures and intermediate stages were made to 0.01 mg.

TABLE 3. *Amounts of sample and losses incurred during pellet preparation (averages)*

1. Mass of Teflon bag.....g...	0.30
2. Mass of boron in mixture.....g...	.16
3. Mass of Teflon in mixture.....g...	1.88
4. Mass of Teflon coating.....g...	0.70
5. Loss of Teflon in sealing bag.....mg...	.32
6. Loss of mixture in pelleting.....mg...	.30
7. Total loss in preparation.....mg...	.62

4. Calorimetric System

No major changes had been made in the bomb calorimeter, thermometric system or combustion bomb since our earlier work [11] which was carried out with the same apparatus. The apparatus will be discussed here only briefly.

An isothermal-jacket, stirred-water calorimeter was used; the jacket was maintained at a constant temperature near 30 °C within 0.002 °C. Temperature changes in the calorimeter were measured to 0.0001 °C with a G–2 Mueller bridge in conjunction with a platinum resistance thermometer. Reactions were carried out in an "A" nickel combustion bomb, designed for service with fluorine, having a volume of approximately 360 ml. Two aluminum electrodes each suspended from the bomb head by a monel rod held a tungsten fuse (0.002 inch diam) which contributed about 20 J to the combustion energy, assuming complete combustion. The quantities of boron and Teflon in the pellets were adjusted to produce a temperature rise in the calorimeter of about 3 deg (27 to 30 °C). For procedures dealing with the loading and emptying of the combustion bomb, and for details of the design and construction of the fluorine manifold, our earlier work should be consulted [14].

5. Products of Combustion

Our previous work [11, 14] has established that Teflon burns in 15 to 21 atm of fluorine to carbon tetrafluoride as the only major product. Higher fluorocarbons were not detected in amounts greater than 0.02 mole percent. The product gases were analyzed in a mass spectrometer after absorption of the excess fluorine in mercury. It is interesting to note that the mass spectrometric examination of product gases from a boron-Teflon combustion experiment showed no sign of BF_3. We suspect that under the conditions of the reaction of fluorine with mercury, an interaction of some kind takes place between BF_3 and the mercury fluoride formed during the absorption of fluorine.

A typical analysis of the residual product gases from a combustion experiment is shown in table 4. The amounts of minor constituents found in the product

gases are greater than those expected on the basis of the amounts present as impurities in the original fluorine. The increments observed in the minor constituents were probably introduced during sampling and analysis procedures and were probably not involved in the actual bomb process.

Boron trifluoride was identified as a combustion product by infrared spectrometry. Examination in the region 650 to 400 cm^{-1} of a sample of the bomb product gases containing excess fluorine revealed the BF_3 band at 481 cm^{-1} and the CF_4 band at 630 cm^{-1}. Spectra of the evacuated cell and of BF_3 alone were taken over the region mentioned above to substantiate the identification. The cell used was 8 cm long and had polyethylene windows, 0.0625 in thick.

TABLE 4. *Composition of residual product gases from a combustion experiment (mass spectrometric examination)*

Component	Mole percent
N_2	0.74
O_2	.87
CO_2	.16
CF_4	98.4
BF_3	.....
SO_2F_2	0.008
SiF_4	.026
C_2F_6	.012
SF_6	.008

6. Calibration Experiments

Twenty calibration experiments were performed in which benzoic acid (Standard Sample 39i) was burned in 30 atm of oxygen and with 1 ml of distilled water in the nickel combustion bomb. Their consistency and reproducibility have been discussed in our earlier paper [11]. The average energy equivalent was calculated to be $14{,}803.27 \pm 0.99$ J deg^{-1}. The uncertainty cited is the standard deviation of the mean. The energy equivalent is that of the standard initial oxygen calorimeter which included the nickel combustion bomb with 30 atm of oxygen, a platinum crucible and fuse support wires, platinum fuse (2 cm long, 0.01 cm diam), a type 304 stainless-steel liner, monel pellet holder, and no sample. Fastened to the bomb was a heater and ignition leads. The mass of the calorimeter vessel and water was 3750.0 g.

Using the appropriate heat capacity data, the energy equivalent of the standard oxygen calorimeter was adjusted to the proper value for the fluorine experiments. This involved allowing for the heat capacities of 30 atm of oxygen, 1 ml of distilled water, the platinum ware, 21 atm of fluorine, and two aluminum electrodes. The application of these corrections gave 14,805.17 J deg^{-1} for the energy equivalent of the standard initial fluorine calorimeter over the temperature range used (27 to 30 °C).

7. Fluorine Combustion Experiments

The calorimetric measurements included seven experiments, which have been previously reported in detail [11], in which Teflon was burned in 21 atm of fluorine. The value listed in section 2.2 for the energy of combustion, ΔE°_{303}, was determined in these experiments. Ten heat measurements were performed in which boron-Teflon pellets were burned in 21 atm of fluorine. These measurements are summarized in table 5. In each experiment the sample pellet was placed in the recess of an "A" nickel plate on the bottom of the bomb. The bomb was attached to the fluorine manifold and filled to 21 atm with fluorine by the usual procedure. All bomb parts (bomb base, bomb-head assembly, electrodes, liner and nickel plate) were weighed before the first experiment and after each successive experiment. The bomb parts were washed with water and dried before the weighings were made.

The numbered entries in table 5 are as follows:

(1a) Mass of the boron mixed with Teflon in the pellet, corrected for weight loss in preparation, for recovery of unburned boron, and for a boron blank.

(1b) Mass of Teflon mixed with sample in the pellet, corrected for weight loss.

(2) Pressure of fluorine introduced into the bomb prior to combustion, corrected to 30 °C.

(3) Energy equivalent of the initial calorimeter for a given experiment.

(4) Temperature change of the calorimeter, corrected for heat of stirring and heat transfer.

(5) Total energy change in the bomb process.

(6) Energy liberated by the tungsten fuse assuming the fuse burns according to the reaction:

$$W(c) + 3F_2(g) = WF_6(g).$$

From the heat of formation of WF_6 [15], we calculate 9.44 J mg^{-1} for the energy of combustion of the fuse.

(7) Net energy correction for the hypothetical compression and decompression of bomb gases.

$$\Delta E \text{ gas} = \Delta E^{i}(\text{gas})]_{0}^{P_i^{(\text{gas})}} + \Delta E^{f}(\text{gas})]_{P_f(\text{gas})}^{0},$$

(8) Standard energy of combustion per gram of Teflon at 30 °C multiplied by the corrected mass of Teflon in the pellet, (1b).

(9) Standard energy of combustion per gram of the sample.

(10) Average standard energy of combustion per gram of the sample.

(11) Standard deviation of the mean of the average cited in (10).

(12) Energy contribution by impurities.

(13) Energy correction converting the reference temperature to 298 °K.

(14) Standard energy of combustion of the pure substance. Contributions from impurities have been accounted for both in mass and in energy.

(15) ΔnRT term.

(16) Standard heat of combustion at 298 °K.

The heat capacities at constant pressure, C_p, used in the calculation of entries (3) and (13) are as follows in cal deg^{-1} g^{-1} at 25 °C: boron, 0.245 [16]; and Teflon,

TABLE 5. *Boron-Teflon combustion experiments*

Experiment No.	1	2	3	4	5	6	7	8	9	10
(1a) m (sample)……g…	0.157378	0.153795	0.151406	0.153477	0.163715	0.149249	0.152208	0.153996	0.160486	0.167872
(1b) m (Teflon)……g…	2.767867	2.813748	2.675968	2.717357	2.880045	3.243633	3.168021	2.933396	3.053495	2.807121
(2) P (F_2)……atm…	21.2	21.6	21.4	21.6	21.4	21.8	21.6	21.9	22.0	21.9
(3) e)……J deg^{-1}…	14,798.95	14,796.70	14,805.56	14,803.17	14,804.61	14,803.77	14,804.26	14,799.88	14,805.01	14,803.61
(4) Δt_c……deg…	3.05494	3.06023	2.94249	2.98886	3.17645	3.33155	3.29647	3.14578	3.27706	3.15415
(5) e) $(-\Delta t_c)$……J…	−45,209.9	−45,281.3	−43,565.2	−44,244.6	−47,026.1	−49,319.5	−48,801.8	−46,557.1	−48,516.9	−46,692.8
(6) ΔE fuse……J…	20.2	20.5	20.3	20.4	20.4	20.4	20.4	16.9	17.4	18.5
(7) ΔE gas……J…	13.2	13.6	12.8	13.1	13.9	15.8	15.4	14.3	15.1	13.9
(8) ΔE° (Teflon)……J…	28,710.5	29,186.4	27,757.3	28,186.6	29,874.1	33,645.6	32,861.2	30,427.5	31,673.3	29,117.7
(9) ΔE°_{298} (sample)……Jg^{-1}…	−104,627	−104,430	−104,189	−104,410	−104,558	−104,776	−104,494	−104,538	−104,751	−104,500

(10) ΔE°_{298} (boron sample), $Jg^{-1} = -104{,}527$ Jg^{-1}
(11) Standard Deviation of the Mean = 54 $Jg^{-1} = 0.14$ kcal mol^{-1}
(12) Contribution from impurities = 545 Jg^{-1} for 0.763 percent impurities
(13) $\Delta E^\circ_{298} - \Delta E^\circ_{303} = 2$ Jg^{-1}
(14) ΔE°_{298} (boron) = −104,779 $Jg^{-1} = -270.74$ kcal mol^{-1}
(15) $\Delta nRT = -115$ Jg^{-1}
(16) ΔH°_{298} (boron) = −104,894 $Jg^{-1} = -271.03$ kcal mol^{-1}

0.28 [17]. The heat capacities at constant volume, C_v, used in the calculation of entries (3) and (13) were 5.52 [18], 12.62 [19], and 10.04 [16] cal deg^{-1} mol^{-1}, respectively for fluorine, carbon tetrafluoride, and boron trifluoride at 30 °C.

Washburn corrections, entry (7), were calculated following the procedure outlined by Hubbard [20] for experiments in which fluorine is used as an oxidant. The coefficients $[\partial E/\partial P]_T = -T[dB/dT]$ were found in tables compiled by Hirschfelder, Curtiss and Bird [21] using the appropriate force constants. The force constants used for fluorine, carbon tetrafluoride, and boron trifluoride were those determined by White, Hu, and Johnston [22], Douslin [23], and Brooks and Raw [24], respectively. Force constants appropriate to the mixtures F_2, CF_4, and BF_3 in the reaction products were calculated from those for the pure components.

We assumed that the metallic impurities in the boron sample were present as the elements and that the nonmetals, oxygen, nitrogen, and carbon were present as B_2O_3, BN, and B_4C, respectively.

In calculating the correction for the B_4C impurity in the boron sample, we have chosen $\Delta E^\circ_{298} = -97.84$ kJg^{-1} for the reaction: $B_4C(c) + 8F_2(g) = 4BF_3(g) + CF_4(g)$ based upon heat measurements performed in our laboratory. These latter data will be reported in more detail in a future publication.

Note that in adjusting the energy of combustion of the sample, entry (10), to the energy of combustion of pure boron, entry (14), the energy contributed by the impurities is subtracted from entry (10), and at the same time the mass of sample is reduced by the mass of the impurities. In calculating the corrections for the combustion of other impurities in the boron sample, the following heat of formation values were used and are given in kcal mol^{-1}: B_2O_3, −304.20 [25]; BN, −60.8 [25]; MgF_2, −268.7 [26]; CaF_2, −290.3 [27]; SiF_4, −385.98 [28]; FeF_3, −235 [29]; SrF_2, −290.3 [27]; MnF_3, −238 [29]; and AlF_3, −361.0 [11].

The raw data obtained in the benzoic acid calibration experiments were programmed for the IBM 7094 computer according to procedures outlined by Shomate [30] for the computer calculation of combustion bomb calorimetric data. The energy equivalent obtained was adjusted to that of the standard initial oxygen calorimeter as described in section 6. The combustion experiments were similarly programmed, however, the only valid data calculated by the computer were the corrected temperature rises, Δt_c, because the program used had not been modified to accommodate the use of fluorine as the oxidant.

Atomic weights were taken from the 1961 table of atomic weights based on $^{12}C = 12$ and adopted by the International Union of Pure and Applied Chemistry [31]. The unit of energy is the joule, and one calorie was defined as 4.1840 J.

About 500 mg of crystalline boron was transformed into boric acid solution by pyrohydrolysis [3] and the solution examined by surface emission mass spec-

[3] The authors are grateful to M. W. Lerner and L. J. Pinto, U.S.A.E.C. New Brunswick Laboratory, New Brunswick, New Jersey, for performing this task.

trometry [4] for the isotopic abundance of B^{10}/B^{11}. This study resulted in the atomic weight determination of our sample of 10.812 ± 0.005. As a result of the good agreement with the atomic weight of boron in the table based on $^{12}C = 12$ we have used the value 10.811 g mol^{-1} from this table in our calculations.

8. Discussion and Results

A residue amounting to less than 1 mg which was assumed to be unburned Teflon and/or carbon, was observed in heat measurements involving Teflon alone. No correction was applied to any experiment for this residue, and we assumed that the formation of the residue took place in all experiments approximately in proportion to the amount of Teflon initially present. The heat of combustion per gram of Teflon would be constant and the error due to residue formation would be eliminated when the energy due to the combustion of Teflon in the pelleted mixture was subtracted from the total energy released in the combustion.

After a boron-Teflon combustion experiment, a larger residue was found than when only Teflon was burned, which necessitated determining the amount of unburned boron and also finding a method for gathering the residue from the nickel support plate. The mass of the residue was obtained by weighing the plate before and after the experiment. The average mass found from these weighings was 3 mg.

The residue was taken up from the support plate by mixing and rubbing Na_2CO_3 into the residue with a spatula. To determine the amount of boron, the residue mixed with Na_2CO_3 was fused and put into solution with dilute acid. The *p*H of the solution was adjusted, mannitol added, and the liberated acid titrated with base. The mass of unburned boron found in the residues by this analysis ranged from 0.5 to 1.1 mg. To determine the reliability of the above procedure, control experiments were performed in which crystalline boron was mixed with Na_2CO_3 and the mixture was analyzed for boron using the same procedure. As a result of the control experiments a correction factor was applied to the boron recovered from the residues. Analysis of residues mixed with Na_2CO_3 was made by the NBS Analysis and Purification Section.

We attempted to assign a composition to the residue even though the mass was subject to effects difficult to estimate such as reaction of the support plate with fluorine, hygroscopicity of the residue, and spattering of molten tungsten onto the plate from the ignition process. Our estimate for the boron blank, boron recovery, unburned Teflon, and tungsten account for about two thirds of the mass of the combustion residue. The remainder could be attributed to one of the above effects, but in the absence of definite information no adjustment was made for it.

A test made to determine whether the presence of boron affected the residue of Teflon, indicated a negligible effect. A boron-Teflon combustion residue was analyzed for carbon, and the results showed an amount comparable to the carbon content of residues formed from burning Teflon alone. A test for weight changes of pellets on exposure to fluorine indicated a slow weight increase, which was not fully reversed on evacuation. A pellet which has been exposed to fluorine and later exposed to moist air showed additional small weight gains, indicating a hygroscopicity resulting from the exposure to fluorine. These effects were small and slow, and no corrections were applied for them. However, they have been taken into account in assessing possible errors.

9. Summary of Errors

We have tried to estimate the overall experimental uncertainty for the heat of formation of $BF_3(g)$ determined as a result of this investigation. Table 6 lists the errors considered in making the estimate. We have used the loss of sample found during the pelleting operation as a guide in estimating the error incurred in preparing a pellet (see table 3, line 6). From this source we estimate an error of 0.10 percent. The two oxygen analyses were 0.161 and 0.088 percent and the two carbon analyses were 0.05 and 0.11 percent. The effect that the differences of the analyses would have upon the heat data introduces an error of 0.06 percent.

TABLE 6. *Summary of errors*

Description of errors	Magnitude of error expressed in percent of ΔH°_{298} for boron
1. Weighing pellet	0.01
2. Loss during sample preparation	.10
3. Analysis of impurities	.06
4. Reaction prior to ignition	.03
5. Determining the amount of unburned boron	.06
6. Determining the composition of the combustion residue	.06
7. Fuse energy	.01
8. Bomb corrosion	.01
9. Calibration experiments	.01
10. Energy of combustion of Teflon [11]	.03
11. Boron combustion experiments	.12
12. Atomic weight of boron	.05
13. Total error (percent)	[a] .19

[a] (This is equivalent to 0.51 kcal mol^{-1}).

An error from the reaction of the sample in the bomb prior to ignition was estimated at 0.03 percent. This was based upon the assumption that prereaction occurring in the bomb prior to ignition was not more than 5 J hr^{-1} as suggested by mass increments of pelleted mixtures upon exposure to fluorine. We assumed that the determination of unburned boron was not in error by more than 0.1 mg (0.06 percent) and that the additional error in estimating the total composition of the combustion residue is similarly 0.06 percent. Since the carbon in the boron combustion residue was comparable to the carbon from the combustion of Teflon alone, no error has been attributed to the uncertainty in residue left by the combustion of Teflon.

[4] NBS Analysis and Purification Section.

Errors due to the weighing of the pellet, fuse energy, and bomb corrosion were estimated at 0.01 percent. Estimates of uncertainties arising from the benzoic acid calibration experiments, Teflon combustion experiments and combustions of boron-Teflon mixtures were made by multiplying the percent standard deviations of the means of the experiments by the appropriate factors for the Student t distribution at the 95 percent confidence level. Finally, we suggest that the error present in the determination of the atomic weight is 0.05 percent as a result of the experimental findings given in section 7.

The total percent error in this study was found by taking the square root of the sum of the squares of the individual errors cited.

10. Heat of Formation of Boron Trifluoride

On the basis of the calorimetric data given in table 5, we calculate for the standard heat of reaction (1),

$$\mathrm{B(c,\ \beta\text{-rhombohedral})} + 3/2\mathrm{F_2(g)} = \mathrm{BF_3(g)} \qquad (1)$$

and, hence, the standard enthalpy of formation of boron trifluoride at 298 °K, -271.03 ± 0.14 kcal mol^{-1}. The latter uncertainty is the standard deviation of the mean. We estimate our overall experimental uncertainty to be 0.51 kcal mol^{-1}.

Our value for the enthalpy of formation of $BF_3(g)$ is in good agreement with the result reported by Gross et al. [5], and differs from the result reported by Johnson et al. [6], by approximately our overall uncertainty.

Johnson et al. [6], have used some recent work by Gunn [32] on the solution of BF_3 in conc HF(aq), Good and Mansson [33] on the combustion of boron in oxygen in the presence of excess aqueous HF, their own data on $\Delta H^\circ_{f298}[BF_3(g)]$, and other appropriate auxiliary data to derive a value for $\Delta H^\circ_{f298}[HF \cdot 3H_2O(aq)] = -76.78$ kcal mol^{-1}. Insertion of our value for $\Delta H^\circ_{f298}[BF_3(g)]$ into this cycle, gives -76.58 kcal mol^{-1} for $\Delta H^\circ_{f298}[HF \cdot 3H_2O(aq)]$. Both our work and that of Johnson et al. [6], agree in showing that the heats of formation for aqueous solutions of HF should be more negative than those suggested by Wagman et al. [34], but less negative than those indicated by Cox and Harrop [35]. In this respect they substantiate our similar finding on the heat of formation of HF(aq) as derived from several other reactions in our study of the heat of formation of CF_4 [11]. Ludwig and Cooper [36] reported for the heat of reaction (2),

$$\mathrm{NF_3(g)} + \mathrm{B(c)} = \mathrm{BF_3(g)} + 1/2\mathrm{N_2(g)} \qquad (2)$$

$\Delta H^\circ_{298} = -239.7 \pm 1.2$ kcal mol^{-1}. Combining our data on $\Delta H^\circ_{f298}[BF_3(g)]$ with the heat of reaction (2), we calculate for $\Delta H^\circ_{f298}[NF_3(g)]$, -31.33 kcal mol^{-1}. Although this is in good agreement with the heat of formation of $NF_3(g)$, -31.44 kcal mol^{-1} reported by Sinke [37], the merits of the agreement are dubious because of the large uncertainty associated with the heat of reaction (2).

11. References

[1] E. J. Prosen, W. H. Johnson, and F. Y. Pergiel, J. Res. NBS **61,** 247–250 (1958), RP2901.

[2] E. J. Prosen, W. H. Johnson, and F. Y. Pergiel, J. Res. NBS **62,** 43–7 (1959), RP2927.

[3] W. H. Johnson, R. G. Miller, and E. J. Prosen, J. Res. NBS **62,** 213–217 (1959), RP2956.

[4] S. S. Wise, J. L. Margrave, H. M. Feder, and W. N. Hubbard, J. Phys. Chem. **65,** 2157–9 (1961).

[5] (a) P. Gross, C. Hayman, P. L. Levi, and M. C. Stuart, Fulmer Research Institute Report R. 146/4/23, Nov. 1960. (b) C. Hayman, private communication, April, 1966.

[6] G. K. Johnson, H. M. Feder, and W. N. Hubbard, J. Phys. Chem. **70,** 1–6 (1966).

[7] Gmelin's Handbuch der anorganische Chemie, System Nummer 13, Achte Auflage, Verlag Chemie G. M. B. H., (a) Hauptband, Leipzig-Berlin (1962), pp. 113–116; (b) Erganzungsband Weinheim/Bergstrasse (1954), p. 171.

[8] (a) G. H. Andersen, General Atomic, San Diego, California, private communication, March, 1966. (b) Kaman Nuclear, Technical Note (TN–105), 10 June 1965.

[9] C. Kuo, G. T. Bender, and J. M. Walker, Anal. Chem. **35,** 1505–9 (1963).

[10] J. L. Hoard and A. E. Newkirk, J. Am. Chem. Soc. **82,** 70–6 (1960).

[11] E. S. Domalski and G. T. Armstrong, J. Res. NBS **71A** (Phys. and Chem.), No. 2, 105–118 (1967).

[12] G. T. Armstrong and R. S. Jessup, J. Res. NBS **64A** (Phys. and Chem.), No. 1, 49–59 (1960).

[13] A. E. Newkirk, Preparation and Chemistry of Elementary Boron, in Borax to Boranes, Advances in Chemistry Series, No. 32, American Chemical Society, Washington, D.C., 1961.

[14] E. S. Domalski and G. T. Armstrong, J. Res. NBS **69A** (Phys. and Chem.), No. 2, 137–147 (1965).

[15] O. E. Myers and A. P. Brady, J. Phys. Chem. **64,** 591–4 (1960).

[16] W. H. Evans, NBS, private communication, January 1, 1961.

[17] W. D. Good, D. W. Scott, and G. Waddington, J. Phys. Chem. **60,** 1080–9 (1956).

[18] W. H. Evans, J. Hilsenrath, and H. W. Woolley, NBS, private communication, July 1, 1960.

[19] Dow Chemical Company, JANAF Thermochemical Tables, PB 168 370 (Clearinghouse for Federal Scientific and Technical Information, Springfield, Virginia, 1965).

[20] W. N. Hubbard, Fluorine Bomb Calorimetry, ch. 6, Experimental Thermochemistry, Vol. II, H. A. Skinner, editor (Interscience Publishers, Inc., New York, 1962).

[21] J. O. Hirschfelder, C. F. Curtiss, and R. B. Bird, Molecular Theory of Gases and Liquids (John Wiley & Sons, Inc., New York, N.Y., Copyright 1954, Second Printing 1964).

[22] D. White, H. Hu, and H. L. Johnston, J. Chem. Phys. **24,** 1149–52 (1953).

[23] D. R. Douslin, paper No. 11, pp. 135–46, PVT Relations and Intermolecular Potentials for Methane and Carbon Tetrafluoride in Progress in International Research on Thermodynamics and Transport Properties, J. F. Masi and D. H. Tsai, editors (Academic Press, New York, 1962).

[24] G. L. Brooks and C. J. G. Raw, Trans. Faraday Soc. **54,** 972–4 (1958).

[25] D. D. Wagman, W. H. Evans, I. Halow, V. B. Parker, S. M. Bailey, and R. H. Schumm, NBS Technical Note 270–2, May 6, 1966.

[26] E. Rudzitis, H. M. Feder, and W. N. Hubbard, J. Phys. Chem. **68,** 2978–81 (1964).

[27] F. D Rossini, D. D. Wagman, W. H. Evans, S. Levine, and I. Jaffe, Selected Values of Chemical Thermodynamic Properties, NBS Circular 500 (U.S. Government Printing Office, Washington, D.C., 1952).

[28] S. S. Wise, J. L. Margrave, H. M. Feder, and W. N. Hubbard, J. Phys. Chem. **67,** 815–21 (1963).

[29] L. Brewer, L. A. Bromley, P. W. Gilles, and N. Lofgren, The Thermodynamic Properties of the Halides, paper 6, Chemistry and Metallurgy of Miscellaneous Materials: Thermodynamics, L. L. Quill, editor (McGraw-Hill Book Company, Inc., New York, 1950).

248-733 O–67—2

[30] C. H. Shomate, Computer Calculations of Combustion Bomb Calorimetric Data, Technical Progress Report 327, NOTS TP 3288, U.S. Naval Ordnance Test Station, China Lake, California, August 1963.
[31] A. E. Cameron and E. Wichers, J. Am. Chem. Soc. **84,** 4175–97 (1962).
[32] S. R. Gunn, J. Phys. Chem. **69,** 1010–5 (1965).
[33] W. D. Good and M. Månsson, J. Phys. Chem. **70,** 97–104 (1966).
[34] D. D. Wagman, W. H. Evans, I. Halow, V. B. Parker, S. M. Bailey and R. H. Schumm, NBS Technical Note 270–1, October 1, 1965.
[35] J. D. Cox and D. Harrop, Trans. Faraday Soc. **61,** 1328–37 (1965).
[36] J. R. Ludwig and W. J. Cooper, J. Chem. Eng. Data **8,** 76–7 (1963).
[37] G. C. Sinke, J. Phys. Chem. **71,** 359–360 (1967).

(Paper 71A3–451)

JOURNAL OF RESEARCH of the National Bureau of Standards—A. Physics and Chemistry
Vol. 71A, No. 3, May–June 1967

An Equation of State for Fluid Parahydrogen from the Triple-Point to 100 °K at Pressures to 350 Atmospheres

Robert D. Goodwin*

Institute for Materials Research, National Bureau of Standards, Boulder, Colo. 80302

(December 19, 1966)

This equation of state may be useful for interpolation and for computations which include thermodynamic properties of parahydrogen. A principal advantage is that it employs only one set of 24 coefficients for all fluid states. The basic form is relatively simple. An adjustment term for the critical region leads to good agreement with published PVT data and specific heats in this especially difficult area. The forms of fitting functions were developed by systematic trial methods using least squares to find the coefficients.

Key Words: Equation of state, hydrogen, parahydrogen, *PVT*-relations, thermodynamic properties.

List of Symbols and Units

$A(\rho)$, $B(\rho)$, $C(\rho)$ density-dependent parameters.
C_v, specific heat at constant volume; C_v° for ideal gas states.
d, density.
d_c, d_t, critical-point, and triple-point densities.
$\Delta_p \equiv (100/n) \cdot \sum_1^n |P/P_{\text{calc}} - 1|$ for n data.
J, the joule.
l, the liter, defined as 1000 cm³ (12th Gen. Conf. Wts. Measures, Paris, October 1964).**
P, pressure.
P_c, P_t, critical-point, and triple-point pressures.
$P_t = 0.0695$ atm [6].
$\Pi(\rho)$, a density-dependent, parametric pressure.
R, the gas constant, 82.0597 cm³ atm/g mol deg [3].
$\rho \equiv d/d_t$, density reduced at the triple point.
$\sigma \equiv d/d_c$, density reduced at the critical point.
T, temperature, deg Kelvin (NBS 1955 low-temp. scale).
T_c, T_t critical-point, and triple-point temperatures.
$\tau \equiv T/T_c$, temperature reduced at the critical point.
$v \equiv 1/d$, molal volume.
$x \equiv T/T_t$, temperature reduced at the triple point.
Y, a defined function of P, Π, T, d.
$Z(\sigma, \tau)$, a defined function.
$\varphi(\sigma, \tau)$, a defined function.

1. Introduction

Our initial computations of thermodynamic properties of parahydrogen [1][1] were accomplished by use of the Benedict-Webb-Rubin equation of state as modified by Strobridge [2]. To obtain the required accuracy, however, it was necessary to evaluate two sets of constants for two regions of the P–V–T surface. Serious computational complications then arose from the need to establish a practical continuity of thermodynamic properties over the boundaries of these regions. Partly for this reason, we used polynomial methods in our formal publication on the thermodynamic properties [3]. Despite these tabulations, there remains a need for an equation of state which can be used for interpolation, and for a multitude of computational investigations. A prerequisite of the following work has been that the equation of state shall require but a single set of constants for all fluid states of the substance (to avoid the above-mentioned problem of continuities).

Well-behaved descriptions of P–ρ–T behavior are obtained with the form $P(\rho, T)$, that is, with density and temperature as arguments or parameters. Density-dependence of specific heats then is obtained from P–ρ–T data via the thermodynamic relation,

$$(\partial C_v/\partial \rho)_T = (-T/\rho^2)(\partial^2 P/\partial T^2)_\rho.$$

Thus an exacting requirement upon any equation of state is to give the curvature of isochores, $(\partial^2 P/\partial T^2)_\rho$, accurately as a function of density and temperature.

We have elected to develop an isochoric form of equation, i.e., an expression for pressure in terms of

*Cryogenics Division, NBS Laboratories, National Bureau of Standards, Boulder, Colo. 80302.
**NBS Misc. Publ. 279, p. 203 (1965).
[1] Figures in brackets indicate the literature references at the end of this paper.

temperature. As any accurate equation for high densities must be empirical, we considered that temperature dependence along isochores (fixed mean intermolecular distance) probably would be less complicated than density-dependence along isotherms [4]. We have allowed the density-dependence of parameters in the equation to be given by P–ρ–T data on isochores. These data are interpolated from experimental isotherms [5].

2. The Behavior of $P-\rho-T$ Data on Isochores

In this section we survey the set of interpolated data on isochores with a view to discovering any useful generalities. This survey is possible because the experimental data on isotherms are dense, covering a wide range of conditions, and because they have been interpolated quite accurately on isochores [5]. For convenience in obtaining derivatives for this survey, we take values computed from polynomial representations of the isochores with coefficients given by [3]. The derivatives therefore may be of low accuracy in some regions.

Plots of P versus T at constant density (isochores) appear to be a family of straight lines. (This emphasizes the need for extreme accuracy in $P-\rho-T$ data used to obtain derivatives.) First derivatives $(\partial P/\partial T)_\rho$, however, reveal useful characteristics. Figure 1 gives dimensionless slopes, $v\cdot(\partial P/\partial T)/R$, versus T on isochores. For $d > 0.013$ g mol/cm^3 each plot has a maximum, corresponding to an inflection in the $P(T)$ relation. Curvatures, $(\partial^2 P/\partial T^2)_\rho$, are positive at low temperatures and negative at high temperatures. The locus of these inflections is important for the computation of specific heats on isotherms, due to the inversion of sign of the integrand. Figures 2 and 3 give the approximate $P-T$ and $T-\rho$ coordinates of the locus. On isotherms from 33 to about 52 °K we

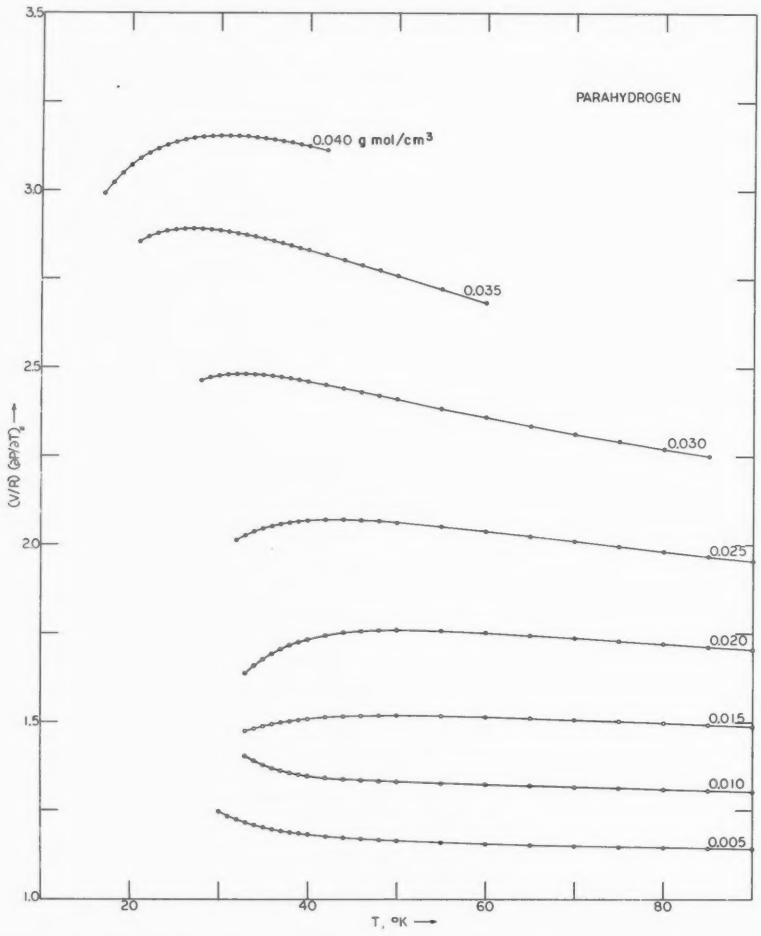

FIGURE 1. *Slopes of selected isochores versus* T.

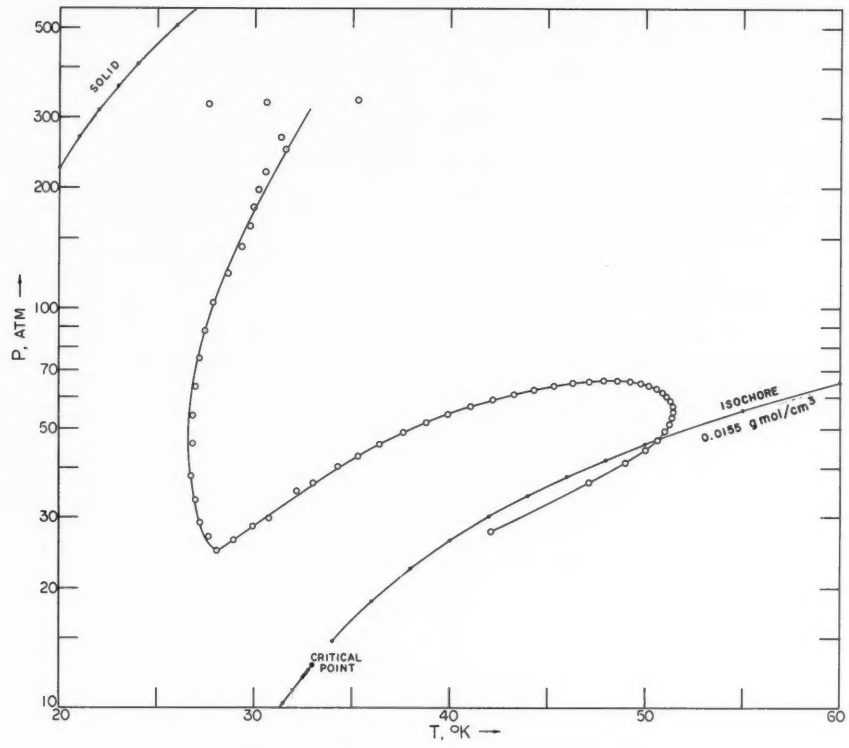

FIGURE 2. *Locus of isochore inflection points in* P−T *coordinates.*

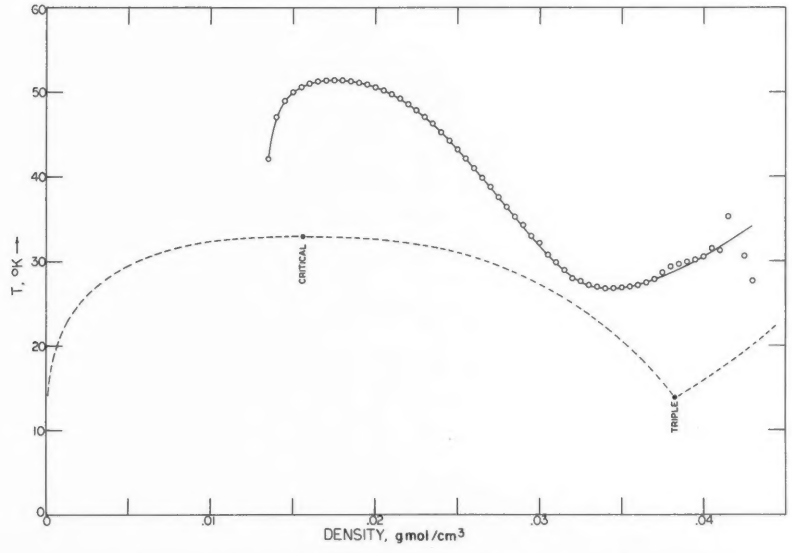

FIGURE 3. *Locus of isochore inflection points in* T−ρ *coordinates.*
The dashed line from left to right represents saturated vapor, saturated liquid, and freezing liquid, respectively.

see that $(\partial^2 P/\partial T^2)_\rho$ might have three inversions of sign as the density increases from zero to very high values. Part of this behavior already is known [16].

A further important characteristic of isochores is seen only by careful examination of differences in the data. The terminating ranges near saturation (low temperatures) exhibit sharp curvatures $(\partial^2 P/\partial T^2)_\rho$ as $T \rightarrow T_{sat}$, appropriately named "hooks." In the critical region these curvatures are negative for $\rho < \rho_c$ and positive for $\rho > \rho_c$.

3. A Preliminary Equation

We at first sought an elementary form for the sigmoid behavior of isochores. It should reduce to perfect gas behavior at low densities and also at high temperatures. We may include the purely density-dependent, parametric pressure found in the van der Waals and Beattie-Bridgeman equations, using the symbol $\Pi(\rho)$ [4].

Assume that the inflection-point temperature, $\theta(\rho)$, is known for each isochore. For each, define a new temperature scale, $t(\rho,T) \equiv T/\theta$, and assume that $\theta(0) = 0$, (fig. 3). The simple form,

$$[P + \Pi(\rho)]/(R \cdot \theta \cdot d) = t \cdot \exp\,[(1-m)/(m \cdot t^m)],$$

with $0 < m \neq 1$, then yields a derivative, $(\partial^2 P/\partial T^2)_\rho$, which is positive for $T < \theta$ and is negative for $T > \theta$.

Woolley et al., used an exponential form for hydrogen at high temperatures, omitting the term $\Pi(\rho)$ [6]. We have, therefore, investigated the general form

$$\log_e Y = \sum_{i=1}^{N} A_i \cdot T^{-n_i}, \qquad (1)$$

using the definition,

$$Y \equiv (P + \Pi)/(R \cdot T \cdot d).$$

One must discover necessary values for exponents, n_i, and the corresponding number of terms, N. Density-dependence of the A_i then is obtained from $P(T)$ data by least squares under an iterative search for $\Pi(\rho)$ on each isochore.

Lengthy investigations failed to yield a behavior for $\Pi(\rho)$ which was sufficiently regular to permit analytical representation. With more than three terms (of the numerous powers in T investigated), the behavior of $\Pi(\rho)$ and all $A_i(\rho)$ was exceedingly irregular. With three terms, the behavior of $\Pi(\rho)$ above 0.01 g mol/cm^3 was in rough accord with the Beattie-Bridgeman description, which we adopted for the constrained form of Π,

$$\Pi(\rho) \equiv P_1 \cdot \rho^2 - P_2 \cdot \rho^3. \qquad (2)$$

When P_1 and P_2 have been found (by iterative methods), the A_i have a regular dependence on ρ. The lowest deviation, Δ_p (see list of symbols), was obtained with the equation

$$\log_e Y = A \cdot \rho \cdot x^{-1/4} + B \cdot \rho \cdot x^{-1} + C \cdot x^{-3}. \qquad (3)$$

where $x \equiv T/T_t$, and symbols A, B, C, replace the A_i of eq (1).

In each of the first two terms on the right one power of ρ has been introduced explicitly to diminish density-dependence of A and B. We note that exponent $n_1 = 1/4$ is required for description of virial coefficients at low densities [7], and exponent $n_3 = 3$ is found in the Beattie-Bridgeman equation. At sufficiently low densities, the term with $n_2 = 1$ combines with $\Pi(\rho)$, independent of temperature. With $P_1 = 703.2813$ atm and $P_2 = 88.3125$ atm, one obtains the behavior for $A(\rho)$, $B(\rho)$, $C(\rho)$ shown by figure 4.

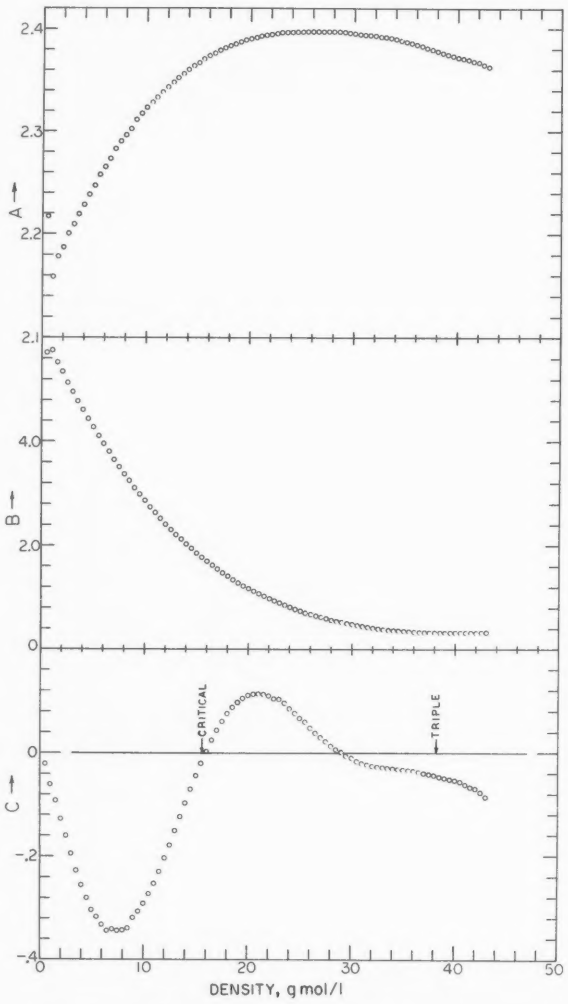

FIGURE 4. *Parameters of eq (3), Π constrained.*

Data needed for developing analytical descriptions of the parameters $A(\rho)$, $B(\rho)$, $C(\rho)$ were obtained as described in appendix 6.1. The form of each description, given below, is the result of a considerable investigation, imposed by the need for high percision (appendix 6.2). In each, the number of terms and the values of exponents were explored systematically. In brief, the behaviors of figure 4 have been described as follows:

$$A(\rho) = A_1 + A_2 \cdot \rho \cdot \exp(-A_3 \cdot \rho), \tag{3-a}$$

$$B(\rho) = B_1 + \exp(B_2 + B_3 \cdot \rho + B_4 \cdot \rho^2 + B_5 \cdot \rho^4 + B_6 \cdot \rho^5), \tag{3-b}$$

$$C(\rho) = C_1 \cdot \rho + C_2 \cdot \rho^2 + C_3 \cdot \rho^3 + C_4 \cdot \rho^4 + C_5 \cdot \rho^5 + C_6 \cdot \rho^7 + C_7 \cdot \rho^{10} + C_8 \cdot \rho^{14}. \tag{3-c}$$

We found constants for eqs (3-a) to (3-c), omitting one datum at the lowest temperature (near saturation) from each of 85 isochores of interpolated data, $1.0 \leq d \leq 43.0$ g mol/liter [5]. Mean deviation for the remaining 2002 points was $\Delta_p = 0.026$ percent. Excessive deviations near the critical point, however, precluded calculation of specific heats in this region.

Anticipating an adjustment function for the critical region, we redetermined a set of 19 constants for eq (3), excluding an additional 59 data in the domain, $32 \leq T \leq 35$ °K, $8.5 \leq d \leq 22.5$ g mol/liter. The pressure was constrained at the liquid triple-point by means of a relatively small adjustment to the value of constant C_8.

These 19 constants, P_1, . . ., C_8, are given in table 1. Mean deviations for eq (3) appear in table 2, and individual deviations $(P - P_{calc})/P_{calc}$ appear in table 3, given in parts per ten-thousand at temperatures through 42 °K. For higher temperatures they do not exceed a few parts in ten-thousand. (Where data do not exist, as in two-phase regions, or at $P > 350$ atm, tables 3 and 5 contain zero entries.) Figure 5 gives the difference between left and right sides of eq (3), multiplied by 10^4, on the 33-deg isotherm.

TABLE 1. *Constants for eqs (3) and (4)*

Equation (3)						Equation (4)		
Constant	Value		Constant	Value		Constant	Value	
T_t.....°K.....	13.803	[6]	B_4	−0.2410	0077	n	8	
T_c.....°K.....	32.976	[12]	B_5	1.8319	9451			
d_t.....g mol/cm³.....	(1/26.176)	[6]	B_6	−0.9445	7676	d_c, g mol/cm³	0.0154	40
						C_8	−.7702	5578
P_1.....atm.....	697.0		C_1	−2.0176	0851	D_1	.0004	5110
P_2.....atm.....	81.0		C_2	−13.9844	7635	D_2	.0166	2606
A_1.....	2.1350	2896	C_3	128.3251	2808	D_3	−.0105	4950
A_2.....	1.0170	4119	C_4	−294.2851	8710	D_4	7.28	
A_3.....	1.4268	4000	C_5	239.1130	5168	E_1	3.32	
B_1.....	−1.1427	1000	C_6	−67.1458	8122			
B_2.....	1.9682	3016	C_7	10.7210	8689			
B_3.....	−2.2337	9180	C_8	−0.7702	5591			

TABLE 2. *Mean deviations for eqs (3) and (4)*

Equation number.....	(3)	(4)
Number of constants.....	19	19 + 6
No. of points used.....	[a] 1943	[b] 781
Value of exponent n.....	.....	8
No. of points for deviation	Mean deviation, Δ_p, %	
[c] 88	0.3576	0.0252
781	.....	.0456
1943	.0223	.....
2087	.0497	.0305

[a] One point omitted at lowest temperature of each of 85 isochores, and all points in domain, $32 \leq T \leq 35$ °K, $8.5 \leq d \leq 22.5$ g mol/liter.

[b] For the six constants in $Z(\sigma, \tau)$, data used in the domain, $17 \leq T \leq 40$ °K, $1.0 \leq d \leq 36.0$ g mol/liter.

[c] Points in the arbitrary critical domain, $32 \leq T \leq 35$ °K, $8.5 \leq d \leq 22.5$ g mol/liter.

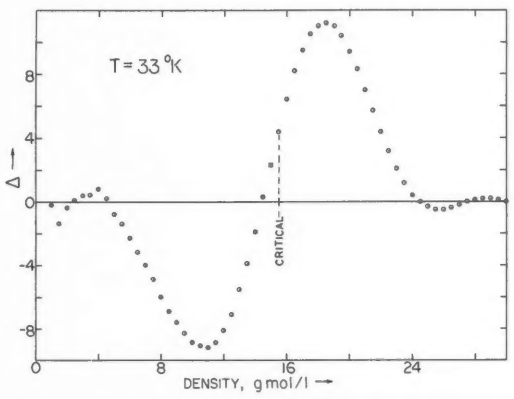

FIGURE 5. *Difference between left and right sides of eq (3), multiplied by 10^4, on 33-deg isotherm.*

4. The Adjusted Equation

The deviation plot (fig. 5) shows behavior of an adjustment on isotherms which must be made to the preliminary equation in the critical region. We see that it may correspond at least to an incipient level spot or shelf in the $P(\rho, T)$ surface in three-dimensions, and we should not expect the preliminary equation to describe this sharp irregularity. We have, therefore, added an adjustment term, $Z(\sigma, \tau)$, a function of reduced variables $\sigma \equiv d/d_c$, $\tau \equiv T/T_c$, as follows,

$$\log_e Y = A \cdot \rho \cdot x^{-1/4} + B \cdot \rho \cdot x^{-1} + C \cdot x^{-3} + Z(\sigma, \tau). \tag{4}$$

The adjustment diminishes rapidly at densities away from the critical point, and at temperatures above the critical point.

Recent work suggests nonanalytic *PVT* behavior at the critical point, corresponding to a logarithmic infinity in C_v [8, 9, 10, 11]. The form of adjustment needed here, however, already is restricted by the preliminary equation of state. We have chosen an analytic form, with the justification that it describes the experimental facts quite well in the range investigated.

The form of Z, below, permits representation of the deviations in table 3 and also yields an acceptable set of specific heats in the critical region. With five coefficients $D_1, \ldots, E_1$ the function is

$$Z(\sigma, \tau) \equiv D(\sigma) \cdot \exp\,[-\phi(\sigma, \tau)], \tag{4-a}$$

$$D(\sigma) \equiv D_1 \cdot \sigma + (D_2 \cdot \sigma + D_3 \cdot \sigma^2) \cdot (\sigma - 1), \tag{4-b}$$

$$\phi(\sigma, \tau) \equiv D_4 \cdot (\sigma - 1)^2 + E_1 \cdot (\tau^n - 1). \tag{4-c}$$

We discuss briefly the basis for eq (4-a). Deviations at 33 deg (very near the critical isotherm at 32.976 deg) require at least a cubic polynomial in density, with roots at $\sigma = 0$, $\sigma \approx 1$, $\sigma > 1$; yet these deviations diminish rapidly at the highest densities. Equation (4-a) describes this behavior on isotherms. Temperature-dependence of these deviations is strong: when $\tau = 1.1$ the deviations have about vanished. For this reason we introduced the factor $\exp(-E_1 \cdot \tau^n)$. It gives the sharp isochore curvatures or "hooks" which contribute to calculated specific heats in the critical region. It also allows the calculated deviations to persist at temperatures below critical at densities near the saturation envelope.

On the right of eq (4-c) we selected the form of the first term, $D_4 \cdot (\sigma - 1)^2$, following some tedious work with the form $D_4 \cdot (\sigma^m - 1)$. Using the latter at $m \approx 4$, it was necessary to increase the powers of σ in eq (4-b) by two or more, e.g.,

$$D(\sigma) \approx D_1 \cdot \sigma^3 + (D_2 \cdot \sigma^4 + D_3 \cdot \sigma^5) \cdot (\sigma - 1),$$

to obtain a deviation, Δ_p, comparable with that found via eq (4-b) above. Even so the magnitudes and the signs of coefficients D_1, D_2, D_3 exhibited radical behaviors, and we abandoned this search.

The constants of eq (4-a) have been determined for 781 data in the domain $17 \leq T \leq 40$ °K; $1.0 \leq d \leq 36.0$ g mol/liter, as described in section 5, below. Our general method was the following: We assumed values for exponent n, and then found D_4, E_1 by iterative procedures which minimize Δ_p. In every step we used D_1 for constraint to the assigned critical-point pressure, and D_2, D_3 to ensure that $\partial P/\partial\sigma = \partial^2 P/\partial\sigma^2 = 0$ at the assigned critical point. (An estimate of $n \approx 10$ at first was obtained by assuming that $\exp[-E_1 \cdot (\tau^n - 1)] \approx 0.02$ at $\tau = 1.1$, and that its maximum positive curvature shall occur near $\tau = 1$.)

We have used the critical temperature established by Roder et al., $T_c = 32.976$ °K [12]. The critical pressure is computed at this temperature by means of the vapor-pressure equation of Weber et al., for accurate consistency, $P_c = 12.759\,263$ atm [13]. The critical density has been varied within limits of uncertainty [14] to obtain consistency between specific heats from eq (4) and those tabulated in [3], as described below.

5. Examination of the Equation

An exacting test of the equation is behavior of calculated specific heats, $C_v = C_v^\circ + C_v^*$, where the "residual specific heat" is

$$C_v^* \equiv \text{const.} \cdot (-T) \cdot \int_0^\rho (\partial^2 P/\partial T^2)_\rho d\rho/\rho^2, \tag{5}$$

with const. $= (0.101325$ J/cm^3 atm$)/(d_l)$ when d_l is in g mol/cm^3. As a rough guide, deviations within 5 to 10 percent of C_v often are considered satisfactory. In this work we use the tabulations of [3] for comparison, as they are in good agreement with experimental data.

We have varied parameters n and d_c of eq (4), examining behavior of the mean deviation Δ_p and also of the mean deviation ΔC_v between 470 specific heats from eq (4) and from [3]. Table 4(A) presents these results. In general, a minimum in Δ_p does not coincide with the best minimum in ΔC_v. We have made an arbitrary selection of $n = 8$, $d_c = 15.44$ g mol/liter. Corresponding values for C_8, D_1, D_2, D_3, D_4, and E_1 are given in table 1.

Table 5 presents residual specific heats from eq (4) with above constants and compares them with values from [3]. The first row at $d = 0$ gives C_v° from [6]. At $T < T_c$ the reference states for liquid are saturated liquid (not ideal gas), with properties given by table 6. Mean deviation for the 470 points of table 5 is 0.077 J/g mol deg, or roughly half of 1 percent. The greatest deviations are about 3 percent in neighborhood of the critical point.

It is interesting to see that integration on the 33 °K isotherm (within 0.02 °C of the critical point) yields satisfactory specific heats at the higher densities. Nevertheless, the maximum in C_v on this isotherm

Table 3. Individual relative deviations from eq (3).

DEVIATIONS OF PRESSURES ON ISOCHORES, PARTS PER TEN THOUSAND

T,K=	17	18	19	20	21	22	23	24	25	26	27	28	29	30	31	32	33	34	35	36	37	38	39	40	42
DEN																									
1.0	0	0	0	0	0	0	0	4	-1	2	-0	-1	-1	-1	-4	-2	-0	-2	0	-1	2	1	1	0	0
1.5	0	0	0	0	0	0	0	-2	2	1	1	3	-1	-0	-1	-2	-2	-1	-0	-1	1	0	0	1	1
2.0	0	0	0	0	0	0	0	0	0	1	1	1	1	-1	-1	-0	1	0	-1	1	-0	1	1	0	1
2.5	0	0	0	0	0	0	0	0	0	0	1	2	1	2	0	1	0	-1	1	0	0	1	1	2	1
3.0	0	0	0	0	0	0	0	0	0	0	0	-1	-0	1	1	1	1	0	1	0	1	2	2	1	1
3.5	0	0	0	0	0	0	0	0	0	0	0	0	-4	-2	1	-0	0	1	0	1	1	2	2	1	1
4.0	0	0	0	0	0	0	0	0	0	0	0	0	0	-4	-2	-1	0	1	0	2	2	2	2	2	2
4.5	0	0	0	0	0	0	0	0	0	0	0	0	0	-4	-4	-1	0	1	2	2	2	2	2	2	2
5.0	0	0	0	0	0	0	0	0	0	0	0	0	0	0	-6	-3	-1	0	2	2	2	2	2	2	2
5.5	0	0	0	0	0	0	0	0	0	0	0	0	0	0	-8	-4	-2	0	2	2	2	2	2	2	2
6.0	0	0	0	0	0	0	0	0	0	0	0	0	0	0	-10	-5	-2	0	2	2	2	2	2	2	2
6.5	0	0	0	0	0	0	0	0	0	0	0	0	0	0	-12	-6	-3	0	2	2	2	2	2	2	2
7.0	0	0	0	0	0	0	0	0	0	0	0	0	0	0	-14	-7	-3	0	2	2	2	2	2	2	2
7.5	0	0	0	0	0	0	0	0	0	0	0	0	0	0	-16	-8	-4	0	2	2	2	2	2	2	2
8.0	0	0	0	0	0	0	0	0	0	0	0	0	0	0	-18	-9	-4	0	2	2	2	2	2	2	2
8.5	0	0	0	0	0	0	0	0	0	0	0	0	0	0	-20	-10	-5	0	2	2	2	2	2	2	2
9.0	0	0	0	0	0	0	0	0	0	0	0	0	0	0	-22	-11	-5	0	2	2	2	2	2	2	2
9.5	0	0	0	0	0	0	0	0	0	0	0	0	0	0	-24	-12	-6	0	2	2	2	2	2	2	2
10.0	0	0	0	0	0	0	0	0	0	0	0	0	0	0	-26	-13	-6	0	2	2	2	2	2	2	2
10.5	0	0	0	0	0	0	0	0	0	0	0	0	0	0	-28	-14	-7	0	2	2	2	2	2	2	2
11.0	0	0	0	0	0	0	0	0	0	0	0	0	0	0	-30	-15	-7	0	2	2	2	2	2	2	2
11.5	0	0	0	0	0	0	0	0	0	0	0	0	0	0	-32	-16	-8	0	2	2	2	2	2	2	2
12.0	0	0	0	0	0	0	0	0	0	0	0	0	0	0	-34	-17	-8	0	2	2	2	2	2	2	2
12.5	0	0	0	0	0	0	0	0	0	0	0	0	0	0	-36	-18	-9	0	2	2	2	2	2	2	2
13.0	0	0	0	0	0	0	0	0	0	0	0	0	0	0	-38	-19	-9	0	2	2	2	2	2	2	2
13.5	0	0	0	0	0	0	0	0	0	0	0	0	0	0	-40	-20	-10	0	2	2	2	2	2	2	2
14.0	0	0	0	0	0	0	0	0	0	0	0	0	0	0	-42	-21	-10	0	2	2	2	2	2	2	2
14.5	0	0	0	0	0	0	0	0	0	0	0	0	0	0	-44	-22	-11	0	2	2	2	2	2	2	2
15.0	0	0	0	0	0	0	0	0	0	0	0	0	0	0	-46	-23	-11	0	2	2	2	2	2	2	2
15.5	0	0	0	0	0	0	0	0	0	0	0	0	0	0	-48	-24	-12	0	2	2	2	2	2	2	2
16.0	0	0	0	0	0	0	0	0	0	0	0	0	0	0	-50	-25	-12	0	2	2	2	2	2	2	2
16.5	0	0	0	0	0	0	0	0	0	0	0	0	0	0	-52	-26	-13	0	2	2	2	2	2	2	2
17.0	0	0	0	0	0	0	0	0	0	0	0	0	0	0	-54	-27	-13	0	2	2	2	2	2	2	2
17.5	0	0	0	0	0	0	0	0	0	0	0	0	0	0	-56	-28	-14	0	2	2	2	2	2	2	2
18.0	0	0	0	0	0	0	0	0	0	0	0	0	0	0	-58	-29	-14	0	2	2	2	2	2	2	2
18.5	0	0	0	0	0	0	0	0	0	0	0	0	0	0	-60	-30	-15	0	2	2	2	2	2	2	2
19.0	0	0	0	0	0	0	0	0	0	0	0	0	0	0	-62	-31	-15	0	2	2	2	2	2	2	2
19.5	0	0	0	0	0	0	0	0	0	0	0	0	0	0	-64	-32	-16	0	2	2	2	2	2	2	2
20.0	0	0	0	0	0	0	0	0	0	0	0	0	0	0	-66	-33	-16	0	2	2	2	2	2	2	2
20.5	0	0	0	0	0	0	0	0	0	0	0	0	0	0	-68	-34	-17	0	2	2	2	2	2	2	2
21.0	0	0	0	0	0	0	0	0	0	0	0	0	0	0	-70	-35	-17	0	2	2	2	2	2	2	2
21.5	0	0	0	0	0	0	0	0	0	0	0	0	0	0	-72	-36	-18	0	2	2	2	2	2	2	2
22.0	0	0	0	0	0	0	0	0	0	0	0	0	0	0	-74	-37	-18	0	2	2	2	2	2	2	2
22.5	0	0	0	0	0	0	0	0	0	0	0	0	0	0	-76	-38	-19	0	2	2	2	2	2	2	2
23.0	0	0	0	0	0	0	0	0	0	0	0	0	0	0	-78	-39	-19	0	2	2	2	2	2	2	2
23.5	0	0	0	0	0	0	0	0	0	0	0	0	0	0	-80	-40	-20	0	2	2	2	2	2	2	2
24.0	0	0	0	0	0	0	0	0	0	0	0	0	0	0	-82	-41	-20	0	2	2	2	2	2	2	2
24.5	0	0	0	0	0	0	0	0	0	0	0	0	0	0	-84	-42	-21	0	2	2	2	2	2	2	2
25.0	0	0	0	0	0	0	0	0	0	0	0	0	0	0	-86	-43	-21	0	2	2	2	2	2	2	2
25.5	0	0	0	0	0	0	0	0	0	0	0	0	0	0	-88	-44	-22	0	2	2	2	2	2	2	2
26.0	0	0	0	0	0	0	0	0	0	0	0	0	0	0	-90	-45	-22	0	2	2	2	2	2	2	2
26.5	0	0	0	0	0	0	0	0	0	0	0	0	0	0	-92	-46	-23	0	2	2	2	2	2	2	2
27.0	0	0	0	0	0	0	0	0	0	0	0	0	0	0	-94	-47	-23	0	2	2	2	2	2	2	2
27.5	0	0	0	0	0	0	0	0	0	0	0	0	0	0	-96	-48	-24	0	2	2	2	2	2	2	2
28.0	0	0	0	0	0	0	0	0	0	0	0	0	0	0	-98	-49	-24	0	2	2	2	2	2	2	2
28.5	0	0	0	0	0	0	0	0	0	0	0	0	0	0	-100	-50	-25	0	2	2	2	2	2	2	2
29.0	0	0	0	0	0	0	0	0	0	0	0	0	0	0	-102	-51	-25	0	2	2	2	2	2	2	2
29.5	0	0	0	0	0	0	0	0	0	0	0	0	0	0	-104	-52	-26	0	2	2	2	2	2	2	2
30.0	0	0	0	0	0	0	0	0	0	0	0	0	0	0	-106	-53	-26	0	2	2	2	2	2	2	2
30.5	0	0	0	0	0	0	0	0	0	0	0	0	0	0	-108	-54	-27	0	2	2	2	2	2	2	2
31.0	0	0	0	0	0	0	0	0	0	0	0	0	0	0	-110	-55	-27	0	2	2	2	2	2	2	2
31.5	0	0	0	0	0	0	0	0	0	0	0	0	0	0	-112	-56	-28	0	2	2	2	2	2	2	2
32.0	0	0	0	0	0	0	0	0	0	0	0	0	0	0	-114	-57	-28	0	2	2	2	2	2	2	2
32.5	0	0	0	0	0	0	0	0	0	0	0	0	0	0	-116	-58	-29	0	2	2	2	2	2	2	2
33.0	0	0	0	0	0	0	0	0	0	0	0	0	0	0	-118	-59	-29	0	2	2	2	2	2	2	2
33.5	0	0	0	0	0	0	0	0	0	0	0	0	0	0	-120	-60	-30	0	2	2	2	2	2	2	2
34.0	0	0	0	0	0	0	0	0	0	0	0	0	0	0	-122	-61	-30	0	2	2	2	2	2	2	2
34.5	0	0	0	0	0	0	0	0	0	0	0	0	0	0	-124	-62	-31	0	2	2	2	2	2	2	2
35.0	0	0	0	0	0	0	0	0	0	0	0	0	0	0	-126	-63	-31	0	2	2	2	2	2	2	2
35.5	0	0	0	0	0	0	0	0	0	0	0	0	0	0	-128	-64	-32	0	2	2	2	2	2	2	2
36.0	0	0	0	0	0	0	0	0	0	0	0	0	0	0	-130	-65	-32	0	2	2	2	2	2	2	2
36.5	0	0	0	0	0	0	0	0	0	0	0	0	0	0	-132	-66	-33	0	2	2	2	2	2	2	2
37.0	0	0	0	0	0	0	0	0	0	0	0	0	0	0	-134	-67	-33	0	2	2	2	2	2	2	2
37.5	0	0	0	0	0	0	0	0	0	0	0	0	0	0	-136	-68	-34	0	2	2	2	2	2	2	2
38.0	0	0	0	0	0	0	0	0	0	0	0	0	0	0	-138	-69	-34	0	2	2	2	2	2	2	2
38.5	0	0	0	0	0	0	0	0	0	0	0	0	0	0	-140	-70	-35	0	2	2	2	2	2	2	2
39.0	0	0	0	0	0	0	0	0	0	0	0	0	0	0	-142	-71	-35	0	2	2	2	2	2	2	2
39.5	0	0	0	0	0	0	0	0	0	0	0	0	0	0	-144	-72	-36	0	2	2	2	2	2	2	2
40.0	0	0	0	0	0	0	0	0	0	0	0	0	0	0	-146	-73	-36	0	2	2	2	2	2	2	2
40.5	0	0	0	0	0	0	0	0	0	0	0	0	0	0	-148	-74	-37	0	2	2	2	2	2	2	2
41.0	0	0	0	0	0	0	0	0	0	0	0	0	0	0	-150	-75	-37	0	2	2	2	2	2	2	2
41.5	0	0	0	0	0	0	0	0	0	0	0	0	0	0	-152	-76	-38	0	2	2	2	2	2	2	2
42.0	0	0	0	0	0	0	0	0	0	0	0	0	0	0	-154	-77	-38	0	2	2	2	2	2	2	2
42.5	0	0	0	0	0	0	0	0	0	0	0	0	0	0	-156	-78	-39	0	2	2	2	2	2	2	2
43.0	0	0	0	0	0	0	0	0	0	0	0	0	0	0	-158	-79	-39	0	2	2	2	2	2	2	2

TABLE 4. *Effects of parameters in eq (4)*
Part A. $T_c = 32.976$ °K

n	d_c, g mol/l	$(\Delta_p, \%) \cdot 100$			ΔC_v, J/mol deg
		88[a]	781[b]	2087[c]	470[d]
6	15.40	3.05	4.37	2.97	0.106
6	15.42	2.51	4.45	3.00	.092
6	15.44	2.99	4.54	3.04	.089
8	15.36	2.68	4.47	3.01	.104
8	15.38	2.38	4.40	2.99	.092
8	15.40	2.32	4.40	2.99	.086
8	15.42	2.36	4.47	3.01	.079
8	15.44	2.52	4.56	3.05	.077
8	15.46	2.70	4.67	3.09	.078
10	15.36	2.90	4.54	3.04	.094
10	15.38	2.52	4.46	3.01	.089
10	15.40	2.41	4.46	3.01	.092
10	15.42	2.32	4.54	3.04	.095
10	15.44	2.41	4.62	3.07	.098
10	15.46	2.43	4.72	3.11	.106

TABLE 4. *Effects of parameters in eq (4) (continued)*
Part B. $n = 8$

T_c deg K	d_c, g mol/l	$(\Delta_p, \%) \cdot 100$			ΔC_v, J/mol deg
		88[a]	781[b]	2087[c]	470[d]
32.982	15.40	2.51	4.41	2.99	0.086
32.982	15.44	2.60	4.57	3.05	.076
32.982	15.48	3.11	4.78	3.13	.083
32.984	15.43	2.59	4.51	3.03	.077
32.984	15.44	2.67	4.56	3.05	.075
32.984	15.45	2.74	4.61	3.07	.076
32.984	15.46	2.88	4.67	3.09	.077
32.986	15.40	2.55	4.42	2.99	.086
32.986	15.44	2.69	4.56	3.05	.076
32.986	15.48	3.24	4.78	3.13	.082
32.990	15.40	2.74	4.43	3.00	.088
32.990	15.44	2.88	4.56	3.05	.079
32.990	15.48	3.50	4.78	3.13	.079

[a] 88 Points, $32 \leq T \leq 35$ °K, $8.5 \leq d \leq 22.5$ g mol/liter.
[b] 781 Points, $17 \leq T \leq 40$, $1.0 \leq d \leq 36.0$.
[c] 2087 Points, $17 \leq T \leq 100$, $1.0 \leq d \leq 43.0$.
[d] 470 Values of C_v, [3] and table 5.

Table 5. Calculated specific heats from eq (4) with n = 8, d_c = 15.44 g mol/l‡

SPECIFIC HEAT AT CONSTANT VOLUME, JOULE/GMOL DEG.
TEMPERATURE, DEG.K

DENSTY	30.00		31.00		32.00		33.00		34.00		35.00		36.00	
GMOL/L	CALCD	REFER	CALCD	REFER	CALCD	REFER	CALCD	REFER	CALCD	REFER	CALCD	REFER	CALCD	REFER
0.000	12.47	12.47	12.47	12.47	12.47	12.47	12.47	12.47	12.47	12.47	12.47	12.47	12.48	12.48
1.000	0.35	0.31	0.33	0.29	0.30	0.28	0.28	0.27	0.26	0.25	0.24	0.24	0.23	0.22
2.000	0.75	0.70	0.69	0.66	0.64	0.62	0.59	0.58	0.55	0.53	0.50	0.49	0.47	0.45
3.000	1.18	1.17	1.10	1.09	1.02	1.01	0.93	0.95	0.86	0.85	0.78	0.76	0.72	0.68
4.000	1.65	1.73	1.54	1.59	1.43	1.47	1.31	1.37	1.19	1.20	1.08	1.06	0.98	0.93
5.000	2.15	2.37	2.02	2.16	1.89	1.98	1.72	1.85	1.55	1.58	1.38	1.37	1.24	1.19
6.000	0.00	0.00	2.56	2.80	2.41	2.55	2.19	2.37	1.94	2.00	1.70	1.70	1.50	1.46
7.000	0.00	0.00	0.00	0.00	3.01	3.19	2.74	2.95	2.39	2.45	2.04	2.06	1.76	1.74
8.000	0.00	0.00	0.00	0.00	3.72	3.70	3.38	3.66	2.89	2.96	2.40	2.35	2.01	2.02
9.000	0.00	0.00	0.00	0.00	0.00	0.00	4.11	4.33	3.45	3.44	2.78	2.66	2.26	2.30
10.000	0.00	0.00	0.00	0.00	0.00	0.00	4.91	4.89	4.05	3.80	3.16	2.99	2.48	2.55
11.000	0.00	0.00	0.00	0.00	0.00	0.00	5.74	5.50	4.65	4.37	3.59	3.33	2.68	2.76
12.000	0.00	0.00	0.00	0.00	0.00	0.00	6.48	6.16	5.19	4.85	3.96	3.63	2.84	2.92
13.000	0.00	0.00	0.00	0.00	0.00	0.00	7.03	6.81	5.58	5.28	4.06	3.82	2.93	3.01
14.000	0.00	0.00	0.00	0.00	0.00	0.00	7.27	7.26	5.74	5.54	4.14	3.88	2.95	3.02
15.000	0.00	0.00	0.00	0.00	0.00	0.00	7.15	7.36	5.64	5.55	4.09	3.80	2.87	2.95
16.000	0.00	0.00	0.00	0.00	0.00	0.00	6.66	7.16	5.27	5.28	3.81	3.32	2.72	2.62
17.000	0.00	0.00	0.00	0.00	0.00	0.00	5.86	6.36	4.68	4.71	3.43	2.99	2.50	2.41
18.000	0.00	0.00	0.00	0.00	0.00	0.00	4.88	5.23	3.95	3.94	2.98	2.59	2.24	2.17
19.000	0.00	0.00	0.00	0.00	0.00	0.00	3.86	3.98	3.20	3.09	2.50	2.18	1.97	1.89
20.000	0.00	0.00	0.00	0.00	0.00	0.00	2.91	2.79	2.50	2.29	2.05	1.79	1.71	1.61
21.000	0.00	0.00	0.00	0.00	0.00	0.00	2.13	1.83	1.91	1.63	1.67	1.46	1.47	1.35
22.000	0.00	0.00	0.00	0.00	0.00	0.00	1.54	1.42	1.46	1.31	1.37	1.23	1.28	1.15
23.000	0.00	0.00	0.00	0.00	-0.07	-0.05	1.12	1.17	1.14	1.10	1.14	1.05	1.12	1.00
24.000	0.00	0.00	0.00	0.00	-0.38	-0.29	0.85	0.97	0.93	0.93	0.98	0.90	1.00	0.87
25.000	0.00	0.00	0.00	0.00	-0.58	-0.48	0.68	0.81	0.79	0.79	0.87	0.79	0.92	0.78
26.000	0.00	0.00	-0.13	-0.16	-0.70	-0.63	0.58	0.69	0.70	0.69	0.80	0.70	0.86	0.71
27.000	-0.03	-0.04	-0.22	-0.29	-0.77	-0.74	0.52	0.60	0.65	0.62	0.75	0.65	0.82	0.67
28.000	-0.11	-0.15	-0.28	-0.39	-0.82	-0.81	0.49	0.54	0.62	0.58	0.73	0.62	0.81	0.66
29.000	-0.17	-0.23	-0.32	-0.44	-0.84	-0.85	0.47	0.52	0.62	0.57	0.73	0.62	0.81	0.66
30.000	-0.20	-0.27	-0.34	-0.47	-0.84	-0.86	0.48	0.52	0.63	0.58	0.75	0.64	0.83	0.69
31.000	-0.21	-0.28	-0.33	-0.47	-0.83	-0.85	0.49	0.53	0.65	0.60	0.77	0.67	0.86	0.72
32.000	-0.20	-0.27	-0.32	-0.45	-0.81	-0.83	0.52	0.57	0.68	0.64	0.81	0.71	0.90	0.77
33.000	-0.19	-0.25	-0.30	-0.42	-0.78	-0.80	0.56	0.60	0.72	0.68	0.86	0.76	0.95	0.82
34.000	-0.16	-0.23	-0.27	-0.39	-0.75	-0.76	0.60	0.65	0.77	0.73	0.91	0.81	1.00	0.87
35.000	-0.14	-0.20	-0.24	-0.36	-0.71	-0.72	0.64	0.69	0.81	0.77	0.95	0.85	1.06	0.92
36.000	-0.12	-0.18	-0.21	-0.33	-0.68	-0.69	0.68	0.72	0.86	0.81	1.00	0.90	1.11	0.97
37.000	-0.10	-0.17	-0.19	-0.31	-0.65	-0.67	0.71	0.75	0.90	0.85	1.05	0.94	1.16	1.02
38.000	-0.09	-0.16	-0.17	-0.30	-0.63	-0.64	0.74	0.78	0.93	0.88	1.09	0.98	1.20	1.06
39.000	-0.09	-0.16	-0.16	-0.29	-0.61	-0.63	0.76	0.80	0.96	0.91	1.12	1.01	1.24	1.10
40.000	-0.09	-0.16	-0.16	-0.29	-0.60	-0.62	0.78	0.82	0.98	0.93	1.15	1.04	1.27	1.14
41.000	-0.11	-0.16	-0.16	-0.29	-0.60	-0.62	0.79	0.83	0.99	0.94	1.17	1.06	1.30	1.15
42.000	-0.12	-0.18	-0.18	-0.30	-0.61	-0.62	0.78	0.82	1.00	0.94	1.18	0.00	1.31	0.00

Table 5. (continued)

SPECIFIC HEAT AT CONSTANT VOLUME, JOULE/GMOL DEG.

DENSTY	TEMPERATURE, DEG.K 40.00		50.00		60.00		70.00		80.00		90.00		100.00	
GMOL/L	CALCD	REFER	CALCD	REFER	CALCD	REFER	CALCD	REFER	CALCD	REFER	CALCD	REFER	CALCD	REFER
0.000	12.49	12.49	12.64	12.64	13.09	13.09	13.99	13.99	15.31	15.31	16.94	16.94	18.69	18.69
1.000	0.18	0.18	0.12	0.12	0.09	0.09	0.08	0.06	0.07	0.06	0.06	0.05	0.06	0.04
2.000	0.36	0.35	0.24	0.24	0.18	0.18	0.15	0.13	0.13	0.11	0.12	0.10	0.12	0.08
3.000	0.55	0.51	0.35	0.35	0.26	0.27	0.22	0.20	0.20	0.17	0.18	0.14	0.17	0.12
4.000	0.74	0.66	0.46	0.44	0.34	0.35	0.29	0.27	0.26	0.22	0.24	0.18	0.23	0.15
5.000	0.92	0.80	0.56	0.53	0.42	0.43	0.35	0.33	0.32	0.27	0.29	0.23	0.28	0.19
6.000	1.09	0.93	0.66	0.61	0.49	0.51	0.41	0.39	0.37	0.32	0.35	0.27	0.33	0.22
7.000	1.24	1.05	0.75	0.68	0.56	0.58	0.47	0.45	0.42	0.37	0.40	0.31	0.38	0.25
8.000	1.38	1.21	0.83	0.75	0.62	0.63	0.52	0.50	0.47	0.42	0.45	0.37	0.43	0.32
9.000	1.49	1.38	0.89	0.81	0.67	0.67	0.57	0.54	0.52	0.47	0.50	0.43	0.48	0.40
10.000	1.58	1.51	0.95	0.86	0.72	0.70	0.62	0.57	0.57	0.52	0.54	0.49	0.53	0.48
11.000	1.63	1.62	0.99	0.90	0.76	0.73	0.66	0.61	0.62	0.57	0.58	0.56	0.58	0.56
12.000	1.67	1.69	1.02	0.92	0.79	0.75	0.70	0.64	0.66	0.61	0.64	0.61	0.63	0.63
13.000	1.67	1.73	1.04	0.94	0.82	0.78	0.74	0.67	0.71	0.66	0.69	0.67	0.68	0.69
14.000	1.66	1.72	1.05	0.95	0.85	0.80	0.78	0.71	0.75	0.70	0.74	0.72	0.73	0.76
15.000	1.62	1.68	1.05	0.96	0.87	0.82	0.81	0.74	0.79	0.74	0.78	0.77	0.78	0.81
16.000	1.56	1.62	1.04	0.95	0.90	0.84	0.85	0.78	0.84	0.79	0.84	0.82	0.83	0.86
17.000	1.49	1.52	1.03	0.95	0.92	0.87	0.89	0.82	0.88	0.83	0.89	0.86	0.89	0.91
18.000	1.41	1.40	1.02	0.94	0.94	0.90	0.93	0.86	0.93	0.87	0.94	0.91	0.95	0.95
19.000	1.32	1.28	1.01	0.93	0.96	0.93	0.97	0.90	0.98	0.92	1.00	0.96	1.01	1.00
20.000	1.24	1.16	1.01	0.93	0.99	0.96	1.01	0.94	1.04	0.97	1.06	1.01	1.07	1.05
21.000	1.16	1.05	1.00	0.93	1.02	1.00	1.06	0.99	1.09	1.02	1.12	1.06	1.13	1.11
22.000	1.08	0.96	1.00	0.93	1.05	1.04	1.11	1.05	1.15	1.08	1.18	1.13	1.20	1.17
23.000	1.02	0.88	1.01	0.94	1.09	1.08	1.16	1.10	1.22	1.15	1.25	1.19	1.27	1.24
24.000	0.97	0.82	1.03	0.96	1.14	1.13	1.22	1.16	1.28	1.21	1.32	1.26	1.35	1.32
25.000	0.94	0.79	1.05	0.99	1.19	1.18	1.29	1.23	1.35	1.28	1.40	1.34	1.42	1.40
26.000	0.92	0.77	1.09	1.03	1.25	1.24	1.36	1.30	1.43	1.36	1.47	1.42	1.50	1.49
27.000	0.91	0.77	1.13	1.07	1.31	1.30	1.43	1.37	1.51	1.44	1.56	1.51	1.58	1.58
28.000	0.93	0.78	1.19	1.13	1.38	1.37	1.51	1.45	1.59	1.52	1.64	1.60	1.67	0.00
29.000	0.95	0.82	1.25	1.19	1.46	1.45	1.60	1.53	1.68	1.61	1.73	1.69	1.76	0.00
30.000	0.99	0.86	1.32	1.26	1.54	1.53	1.68	1.62	1.77	1.70	1.82	0.00	1.85	0.00
31.000	1.04	0.91	1.39	1.33	1.63	1.61	1.78	1.71	1.86	1.81	1.92	0.00	1.94	0.00
32.000	1.10	0.97	1.47	1.41	1.72	1.70	1.87	1.81	1.96	0.00	2.01	0.00	2.04	0.00
33.000	1.16	1.04	1.56	1.49	1.81	1.79	1.97	1.92	2.06	0.00	2.11	0.00	2.14	0.00
34.000	1.23	1.10	1.64	1.58	1.91	1.89	2.07	0.00	2.16	0.00	2.21	0.00	2.24	0.00
35.000	1.30	1.16	1.73	1.66	2.00	2.00	2.17	0.00	2.26	0.00	2.31	0.00	2.34	0.00
36.000	1.36	1.23	1.82	1.75	2.10	0.00	2.27	0.00	2.36	0.00	2.42	0.00	2.44	0.00
37.000	1.43	1.29	1.90	1.85	2.20	0.00	2.37	0.00	2.47	0.00	2.52	0.00	2.55	0.00
38.000	1.49	1.35	1.99	1.96	2.29	0.00	2.47	0.00	2.57	0.00	2.62	0.00	2.65	0.00
39.000	1.54	1.42	2.07	0.00	2.39	0.00	2.57	0.00	2.67	0.00	2.73	0.00	2.75	0.00
40.000	1.59	0.00	2.15	0.00	2.48	0.00	2.67	0.00	2.78	0.00	2.83	0.00	2.86	0.00
41.000	1.64	0.00	2.22	0.00	2.57	0.00	2.77	0.00	2.88	0.00	2.94	0.00	2.96	0.00
42.000	1.67	0.00	2.29	0.00	2.65	0.00	2.86	0.00	2.98	0.00	3.04	0.00	3.06	0.00

FOR 470 POINTS, MEAN = 0.077 J/GMOL DEG.

†At $T<T_c$ the reference states for liquid are the saturated liquid (not ideal gas) with properties given by table 6.

TABLE 6. *Properties of saturated liquid used in the specific heat calculations*

T, °K	d, g mol/liter [15]	C_v, J/g mol deg [3]
30.0	26.753	13.07
31.0	25.103	13.33
32.0	22.825	13.79

near $d=14.0$ g mol/liter may be an imperfection, even though it is consistent with the estimated sign inversion of $(\partial^2 P/\partial T^2)$ near 13.0 g mol/liter at 33 °K (fig. 3). This could be the subject of another, lengthy investigation, which might include adjustment of data for gravitational effects, nonanalytic functions, etc. [8].

Further to validate the behavior of eq (4), we have made the following examinations. (1) A table of relative deviations, similar to table 3 in this report, shows that they are comparable in the critical region with those elsewhere, and that many near the saturation envelope at $T<T_c$ have been appreciably diminished relative to table 3. (2) A table of pressures and derivatives $\partial P/\partial\rho$, $\partial^2 P/\partial\rho^2$ on the critical isotherm shows that $\partial P/\partial\rho \geq 0$, and that $\partial^2 P/\partial\rho^2 \lessgtr 0$ as $\rho \lessgtr \rho_c$. Differences in $\partial^2 P/\partial\rho^2$ give the estimate $\partial^3 P/\partial\rho^3 = 9.0$ atm at ρ_c (where $\rho \equiv d/d_l$). (3) A table of calculated pressures at all ρ, T arguments of the interpolated data [5] shows monotonic increase of P with either ρ or T in single-phase regions. (4) A table of calculated densities of the saturated vapor and liquid phases, and of the freezing liquid phase, shows acceptable agreement with previously derived results [15].

In conclusion, we mention a further examination of eq (4-a). Effects of varying T_c (P_c obtained from [13]) are in table 4(B). We do not feel that these results justify a change of T_c from [12]. Constants corresponding to the minimum deviation, $\Delta C_v = 0.075$ J/g mol deg, nevertheless are given in table 7 because the critical point constants are close to those determined initially by Hoge and Lassiter, namely $T_c = 32.984 \pm 0.02$ °K, $d_c = 15.27 \pm 0.30$ g mol/liter, $P_c = 12.77 \pm 0.04$ atm [14].

The National Aeronautics and Space Administration has supported this work from the beginning. Mr. William J. Hall generously helped the author with initial computer programs, and contributed the essential iteration routine and the high-speed, least-squares

TABLE 7. *Constants for alternate* T_c
Equation (4–a)

Constant	Value
n	8
T_c, °K	32.984
d_c, g mol/liter	15.44
P_c, [13], atm	12.774 257
C_R	−0.7702 5576
D_1	.0004 4993
D_2	.0161 4536
D_3	−.0102 2498
D_4	7.22
E_1	3.32

routine in machine language. Mrs. Levelt Sengers kindly suggested improvements in the manuscript and encouraged us to seek a form which would be non-analytic at the critical point.

6. Appendixes

6.1. Method Used To Find Data for $A(\rho)$, $B(\rho)$, $C(\rho)$

With reference to eq (3) and determination of coefficients on the right side by least squares on isochores, we used a method whereby deviations introduced by the arbitrary form of the first coefficient, $A(\rho)$, will appear in data for the second coefficient, $B(\rho)$, and so forth. After adjusting the constants in $A(\rho)$ we used its representation on the left side, and redetermined data for B and for C by least squares on isochores in the transposed form,

$$\{\log Y - A_{\text{calc}} \cdot \rho \cdot x^{-1/4}\} = B \cdot \rho \cdot x^{-1} + C \cdot x^{-3},$$

and so forth.

6.2. The Requirement for High Precision in $A(\rho)$, Etc.

The explicit form of eq (3) for pressure,

$$P = -\Pi(\rho) + F(\rho, T)$$

shows that P is obtained as a difference of two principal terms. At high densities the value of Π may exceed 700 atm. At high densities and low temperatures the value of P may be as low as 0.0695 atm (triple point). Values for the parameters $A(\rho)$, $B(\rho)$, etc., therefore may be required with a precision ten thousand-fold greater than desired in the calculated pressure.

7. References

[1] H. M. Roder and R. D. Goodwin, Provisional thermodynamic functions for para-hydrogen, NBS Tech. Note 130, 1961.

[2] T. R. Strobridge, The thermodynamic properties of nitrogen from 64 to 300 °K between 0.1 and 200 atmospheres, NBS Tech. Note 129, 1962.

[3] H. M. Roder, L. A. Weber, and R. D. Goodwin, Thermodynamic and related properties of para-hydrogen from the triple-point to 100 °K at pressures to 340 atmospheres, NBS Mono. 94, 1965.

[4] J. O. Hirshfelder, C. F. Curtiss, and R. B. Bird, Molecular Theory of Gases and Liquids (John Wiley & Sons, Inc., New York, N.Y., 1954).

[5] R. D. Goodwin, D. E. Diller, H. M. Roder, and L. A. Weber, Pressure-density-temperature relations of fluid parahydrogen from 15 to 100 °K at pressures to 350 atmos., J. Res. NBS **67A** (Phys. and Chem.), No. 2, 173–192 (1962).

[6] H. W. Woolley, R. B. Scott, and F. G. Brickwedde, Compilation of thermal properties of hydrogen in its various isotopic and ortho-para modifications, J. Res. NBS **41**, 379–475 (1948) RP1932.

[7] R. D. Goodwin, D. E. Diller, H. M. Roder, and L. A. Weber, Second and third virial coefficients for hydrogen, J. Res. NBS **68A** (Phys. and Chem.) No. 2, 121–126 (1964).

[8] M. S. Green, and J. V. Sengers, editors, Critical phenomena, NBS Miscellaneous Publication 273, December 1, 1966.

[9] S. Y. Larsen and J. M. H. Levelt Sengers, On the behavior of the compressibility along the critical isotherm, pp. 74–75, in Advances in Thermophysical Properties at Extreme Temperatures and Pressures, Serge Gratch, editor, Am. Soc. Mechanical Engineers, 345 E. 47th St., N.Y., N.Y. 10017 (1965).

[10] A. V. Voronel, and Yu. R. Chashkin, Specific heat C_v of argon as a function of density near the critical point, Zh. Eksperim. (i) Teor. Fiz. **51** (2), 394–400 (1966).

[11] B. Widom, Equation of state in neighborhood of the critical point, J. Chem. Phys. **43** (11), 3898–3905 (1965).

[12] H. M. Roder, D. E. Diller, L. A. Weber, and R. D. Goodwin, The orthobaric densities of parahydrogen, derived heats of vaporization, and critical constants, Cryogenics **3** (1), 16–22 (1963).

[13] L. A. Weber, D. E. Diller, H. M. Roder, and R. D. Goodwin, The vapor pressure of 20 °K equilibrium hydrogen, Cryogenics **2** (4), 236–238 (1962).

[14] H. J. Hoge, and J. W. Lassiter, Critical temperatures, pressures, and volumes of hydrogen, deuterium, and hydrogen deuteride, J. Res. NBS **47**, 75–79 (1951) RP2229.

[15] R. D. Goodwin, Density-temperature formulae for coexisting liquid and vapor and for freezing liquid parahydrogen, J. Res. NBS **70A** (Phys. and Chem.) No. 6, 541–544 (1966).

[16] V. A. Rabinovich, Analysis of experimental thermal values and equation of state for hydrogen, Inzhenerno–Fiz. Zhur. Akad. Nauk Belorus S.S.R. **5** (5), 30–37 (1962).

(Paper 71A3–452)

JOURNAL OF RESEARCH of the National Bureau of Standards—A. Physics and Chemistry
Vol. 71A, No. 3, May–June 1967

The Dissociation Constants of Some Disubstituted Anilines and Phenols in Aqueous Solution at 25 °C

R. A. Robinson

Institute for Materials Research, National Bureau of Standards, Washington, D.C. 20234

(February 21, 1967)

The dissociation constants of six disubstituted anilines and of five disubstituted phenols in aqueous solution at 25 °C have been measured using the spectrophotometric method. Consideration is given to the extent to which these dissociation constants can be predicted from corresponding values for monosubstituted anilines and phenols. In addition, the question as to whether the *pK* value of a substituted aniline can be predicted from the *pK* value of a phenol with substituents in the same positions is also investigated.

Key Words: Dissociation constant, substituted anilines, substituted phenols.

1. Introduction

In an earlier paper [1][1] the results of measurements of the *pK* values of the six dichloroanilines and the six dichlorophenols in aqueous solution at 25 °C have been reported. The conclusions drawn from this work can be summarized briefly in two statements. In the first place, the *pK* value of any one of ten dichlorosubstituted compounds (2,6-dichloroaniline and 2,6-dichlorophenol being exceptions) could be predicted knowing the *pK* values of the monosubstituted chlorocompounds. This utilizes an additivity rule which can be illustrated as follows; the *pK* value of phenol itself is 9.998, that of *m*-chlorophenol is 9.130 and that of *p*-chlorophenol is 9.418 [2]. Thus, *m*-Cl substitution lowers the *pK* value of phenol by 0.868 and *p*-Cl substitution by 0.580. If the substituent effects were strictly additive, 3,4-dichloro substitution should lower the value of *pK* by 1.448 and the *pK* value of 3,4-dichlorophenol should be 8.550. The observed value is 8.585, differing from the calculated by only 0.035. The additivity rule predicts *pK* values with an accuracy which varies from 2,4-dichloroaniline ($pK_{obs}=2.02$, $pK_{calc}=2.03$) to 2,3-dichloroaniline ($pK_{obs}=1.76$, $pK_{calc}=1.92$). Only in the case of 2,6-dichloroaniline and 2,6-dichlorophenol did the additivity rule fail to predict the observed value within these limits, the difference between observed and calculated *pK* values being 0.28 in the case of 2,6-dichloroaniline and 0.27 in the case of 2,6-dichlorophenol. In these two instances we have compounds with three substituent groups in adjacent positions, Cl, NH_2 (or OH), Cl, and it is not surprising that there should be steric effects which interfere with the additivity relation.

Secondly, it was found that a linear relationship existed between the *pK* value of a dichloroaniline, pK_A, and the *pK* value of the corresponding dichlorophenol, pK_P. This could be expressed by the equation

$$pK_A = -9.047 + 1.401\, pK_P.$$

For example, it was found that pK_P was 6.791 for 2,6-dichlorophenol, whence this equation gives $pK_A=0.467$. The experimental value is 0.422. It should be noted that this relationship holds for 2,6-disubstituted compounds, although the additivity rule, mentioned above, fails in this instance.

These conclusions are valid for a particular class of disubstituted anilines and phenols, the dichloro compounds. It is of interest, however, to inquire whether they have application to a wider group of disubstituted anilines and phenols. For this reason, measurements have now been made on a group of disubstituted compounds in which the substituent groups are $-Br$, $-Cl$, $-CH_3$, and $-NO_2$.

2. Experimental Procedure

2.1. Materials

4-Chloro-2-methylaniline hydrochloride was recrystallized twice from 80 percent ethanol, Cl found 19.92 percent, calc 19.91 percent, ϵ_2 2,510 at 291 mμ in alkaline solution. 2,4-Dibromoaniline was recrystallized first from heptane and then from a mixture of

[1] Figures in brackets indicate the literature references at the end of this paper.

heptane and petroleum ether, mp 80 °C, ϵ_2 2,160 at 300 mμ in alkaline solution, ϵ_1 280 at 273 mμ and 200 at 280 mμ in acid solution. 2,6-Dibromoaniline was recrystallized twice from heptane, mp 83.5 °C, ϵ_2 2,550 at 294 mμ, ϵ_1 350 at 272 mμ and 370 at 279 mμ. 2-Methyl-5-nitroaniline was recrystallized once from benzene, mp 108 °C, ϵ_2 2,060 at 355 mμ. 4-Methyl-2-nitroaniline was recrystallized once from benzene, mp 117.5 °C, ϵ_2 4,230 at 427 mμ. 4-Methyl-3-nitroaniline was recrystallized twice from benzene, mp 79.5 °C, ϵ_2 1,580 at 357 mμ. 4-Chloro-2-methylphenol was recrystallized three times from petroleum ether, mp 47.5–48 °C ϵ_2 3,030 at 300 mμ, ϵ_1 1,680 at 281 mμ, and isosbestic points ϵ 1,010 at 271 mμ and 1,600 at 284 mμ. 2,4-Dibromophenol was recrystallized three times from heptane, mp 36 °C, ϵ_2 3,700 at 309 mμ, ϵ_1 2,090 at 286 mμ, ϵ 1,280 at 274 mμ and 1,970 at 291 mμ. 2,6-Dibromophenol was recrystallized twice from petroleum ether, mp 56 °C, ϵ_2 5,250 at 304 mμ, ϵ_1 2,170 at 276 mμ and 2,170 at 284 mμ, ϵ 1,130 at 269 mμ and 2,160 at 284 mμ. 2-Methyl-4-nitrophenol was recrystallized twice from water, mp 96 °C, ϵ_2 13,310 at 414 mμ, ϵ_1 6,340 at 327 mμ, ϵ 3,510 at 358 mμ. 4-Methyl-3-nitrophenol was recrystallized from benzene and then from a mixture of heptane and petroleum ether, mp 77.5–78 °C, ϵ_2 1,410 at 390 mμ, ϵ_1 2,050 at 340 mμ, ϵ 1,340 at 369 mμ.

2.2. Outline of Method

The principle of the spectrophotometric determination of a pK value is as follows. Consider three solutions of a phenol, all at the same stoichiometric concentration. Let there be added to one enough acid to convert the phenol entirely into the molecular form, HN. To the second let there be added sufficient alkali to convert the phenol entirely into its ionized form, N^-. Let the third contain a buffer solution in which the phenol is present partly in its molecular form and partly in its ionized form. Let α be the degree of dissociation of the phenol. Then if D_1, D_2, and D, respectively, are the optical densities of these three solutions, measured at the same wavelength in cells of the same length, it follows that

$$\alpha = (D-D_1)/(D_2-D_1) \text{ and } \alpha/(1-\alpha) = (D-D_1)/(D_2-D). \quad (1)$$

This dissociation constant for the process

$$HN \rightleftharpoons H^+ + N^-$$

is

$$K = \frac{a_{H^+} \cdot m_{N^-}}{m_{HN}} \frac{\gamma_{N^-}}{\gamma_{HN}} = a_{H^+} \cdot \frac{\alpha}{1-\alpha} \frac{\gamma_{N^-}}{\gamma_{HN}} \quad (2)$$

which can be written as

$$pK = p(a_H\gamma_{Cl}) - \log \alpha/(1-\alpha) - \log \gamma_{N^-}/(\gamma_{HN}\gamma_{Cl^-}) \quad (3)$$

where $p(a_H\gamma_{Cl})$ is a characteristic of the buffer solution employed and γ designates an activity coefficient.

Accurate values of the pK are obtained if $\alpha \approx 0.5$, which means that pK should be approximately equal to $p(a_H\gamma_{Cl})$. Thus, the measurement of the pK value of a phenol is best performed with a buffer solution which satisfies this condition. The buffer solutions used in this work were (1) an equimolal mixture of potassium dihydrogen phosphate and disodium hydrogen phosphate, $p(a_H\gamma_{Cl}) \approx 7.0$; (2) a mixture of tris(hydroxymethyl)aminomethane (m) and its hydrochloride ($0.9845m$), $p(a_H\gamma_{Cl}) \approx 8.3$; (3) a mixture of borax (m) and sodium chloride ($1.855m$), $p(a_H\gamma_{Cl}) \approx 9.2$. The $p(a_H\gamma_{Cl})$ values of the buffer solutions depend on the concentrations of the buffer constituents; the requisite values have been tabulated by Bates and Gary [3]. These $p(a_H\gamma_{Cl})$ values are altered to a small extent by the phenol in the buffer solution whose dissociation into hydrogen ions increases the acidity of the buffer solution slightly. The correction to the $p(a_H\gamma_{Cl})$ values has already been considered [4].

It would be expected that the last term in eq (3) would be either small or negligible; in the former case an extrapolation can be made to give the true value of pK at infinite dilution. For the phenols studied in this work, the value of pK proved to be independent of the buffer concentration, indicating that the last term of eq (3) was negligible and, therefore, the best value of pK was assumed to be the average of those found at different concentrations of the buffer solution.

The dissociation of the anilinium ion or a substituted anilinium ion can be represented as

$$BH^+ \rightleftharpoons H^+ + B$$

with a dissociation constant

$$K = \frac{m_{H^+} \cdot \alpha}{1-\alpha} \frac{\gamma_{H^+} \cdot \gamma_B}{\gamma_{BH^+}} \quad (4)$$

or

$$pK = -\log m_{H^+} - \log \alpha/(1-\alpha) - \log (\gamma_{H^+} \cdot \gamma_B)/\gamma_{BH^+}. \quad (5)$$

The pK values of most substituted anilines are less than 3 and it is therefore preferable to make measurements in solutions of a strong acid of known concentration. In this work, hydrochloric acid was used. Then, if m_{HCl} is the stoichiometric concentration of hydrochloric acid added to the aniline solution and m is the stoichiometric concentration of aniline, m_{H^+} in eq (5) can be equated to $m_{HCl} - m(1-\alpha)$. Again it is desirable to use hydrochloric acid solutions of concentration such that $\alpha \approx 0.5$. If dilute solutions of hydrochloric acid are used, the last term of eq (5) should be negligible and this proved to be the case. But if pK was small, so that moderately concentrated solutions of hydrochloric acid had to be used, as in the case of 2,6-dibromoaniline and 4-methyl-2-nitro-

aniline, this term could no longer be neglected and the true value of pK had to be obtained by extrapolation of $[-\log m_{H^+} - \log \alpha/(1-\alpha)]$ to zero acid concentration; this procedure has already been used for 2,6-dichloroaniline [1] and for *o*-nitroaniline [2].

In one instance, 4-chloro-2-methylaniline, with a pK value ≈ 3.8, it was necessary to use a succinic acid-sodium hydrogen succinate buffer solution. The equation for the dissociation constant now becomes

$$pK = p(a_H\gamma_{Cl}) - \log \alpha/(1-\alpha) + \log (\gamma_{BH^+} \cdot \gamma_{Cl^-})/\gamma_B. \quad (6)$$

Values of $p(a_H\gamma_{Cl})$ for this buffer solution have been tabulated [3] and the activity coefficient term can be written

$$\log (\gamma_{BH^+} \cdot \gamma_{Cl^-})/\gamma_B = -2AI^{1/2}/(1+1.5I^{1/2}) \quad (7)$$

where A is the parameter of the Debye-Hückel equation (0.5108 $kg^{-1/2}$ $mole^{1/2}$ at 25 °C).

3. Results and Discussion

3.1. Additivity Effects

The detailed experimental results are given in tables 1–11 and summarized in table 12. The pK value for 4-methyl-2-nitrophenol is taken from a previous publication [5]. Table 12 also contains values of pK calculated on the assumption that the effect of double substitution in an aniline or phenol can be compounded as the sum of the separate monosubstitution effects. Thus the pK value of phenol itself, 9.99_8, [2] is raised to 10.28_7 in *o*-cresol, [6] the substitution effect of the *o*-methyl group being -0.28_9; the pK value of *p*-chlorophenol is 9.41_8 [2] so that the substitution effect of the *p*-chloro group is 0.58_0. If these effects are strictly additive, the combined effects of *o*-methyl and *p*-chloro substitution should be 0.29_1 giving $pK = 9.70_7$ for 4-chloro-2-methylphenol, which agrees very well with the observed value of 9.70_6. Substituent effects were calculated from the pK values of *o*-nitrophenol [7], *m*-nitrophenol [8], and *m*-nitroaniline [10]; for other groups the data of Biggs [6] or of Biggs and Robinson [2] were used.

Inspection of table 12 shows that the additivity rule holds with varying degrees of success. It is remarkably good with 4-chloro-2-methylphenol and 4-methyl-3-nitrophenol and not so good with 4-methyl-2-nitrophenol. It is possible that the additivity rule fails when bulky ortho substituted groups are present because these can produce steric inhibition of resonance. Thus the rule fails badly with 2,6-dibromoaniline and 2,6-dibromophenol as it does with the corresponding dichloro compounds [1] and with 2,6-dinitrophenol [10]. Perhaps the most remarkable failure of additivity is found with 4-methyl-2-nitroaniline; the additivity rule holds for the corresponding phenol with only moderate success.

TABLE 1. *Dissociation constant of 4-chloro-2-methylaniline*

Aniline concentration 2.27×10^{-4} M, cell length 1 cm, wavelength 291 mμ, D_1 0, D_2 0.569

I	m	$p(a_H\gamma_{Cl})$	D	$\log \frac{D-D_1}{D_2-D}$	2 log γ	pK	pK(corr)
0.02017	0.02	3.898	0.257	−0.084	−0.117	3.865	3.853
.03018	.03	3.892	.251	−.103	−.140	3.855	3.848
.04019	.04	3.887	.245	−.121	−.157	3.851	3.848
.05019	.05	3.884	.239	−.140	−.171	3.853	3.851
.06020	.06	3.882	.236	−.150	−.183	3.849	3.847
.08021	.08	3.878	.229	−.172	−.203	3.847	3.846
.10021	.10	3.875	.223	−.191	−.219	3.847	3.846

The buffer solution was a mixture of sodium hydrogen succinate (m) and hydrochloric acid (0.6667m) equivalent to a mixture of sodium hydrogen succinate (0.3333m), succinic acid (0.6667m), and sodium chloride (0.6667m).

TABLE 2. *Dissociation constant of 2,4-dibromoaniline*

Aniline concentration 9.31×10^{-5} M, cell length 4 cm, wavelength 300 mμ, D_1 0.009, D_2 0.804

$m_{HCl} \times 10^3$	D	$\log \frac{D-D_1}{D_2-D}$	$-\log m_{H^+}$	pK
5.846	0.568	0.375	2.235	1.860
6.852	.535	.291	2.166	1.875
9.591	.474	.149	2.020	1.871
13.80	.408	.003	1.862	1.859
16.28	.370	−.080	1.790	1.870
16.39	.375	−.069	1.787	1.856
21.02	.322	−.188	1.679	1.867
29.59	.257	−.344	1.530	1.874

TABLE 3. *Dissociation constant of 2,6-dibromoaniline*

Aniline concentration 4.92×10^{-5} M, cell length 4 cm, wavelength 294 mμ, D_1 0, D_2 0.502

m_{HCl}	D	$\log \frac{D-D_1}{D_2-D}$	$\log m_{H^+}$	pK'	pK'(calc)
0.1021	0.436	0.817	−0.991	0.174	0.182
.2042	.382	.499	−.690	.191	.195
.3063	.337	.306	−.514	.208	.209
.4084	.300	.167	−.389	.222	.222
.5105	.271	.065	−.292	.227	.236
.6126	.242	−.037	−.213	.250	.249
.7147	.218	−.121	−.146	.267	.263
.8168	.196	−.200	−.088	.288	.277
.9189	.183	−.248	−.037	.285	.290
1.021	.165	−.318	.009	.309	.304

$pK'(\text{calc}) = 0.168 + 0.133\ m_{HCl}$.

TABLE 4. *Dissociation constant of 2-methyl-5-nitroaniline*

Aniline concentration $5.05 \times 10^{-4} M$ cell length 1 cm, wavelength 355 mμ, D_1 0.105, D_2 1.042

$m_{HCl} \times 10^3$	D	$\log \frac{D-D_1}{D_2-D}$	$-\log m_{H^+}$	pK
2.004	0.772	0.393	2.731	2.338
4.007	.613	.074	2.424	2.350
6.011	.522	−.096	2.242	2.338
8.014	.451	−.232	2.114	2.346
10.02	.403	−.331	2.014	2.345
14.03	.336	−.485	1.865	2.350

TABLE 5. *Dissociation constant of 4-methyl-2-nitroaniline*

Aniline concentration 1.752×10^{-4} *M*, cell length 1 cm, wavelength 427 mμ, D_1 0, D_2 0.740

m_{HCl}	D	$\log \frac{D-D_1}{D_2-D}$	$-\log m_{H^+}$	pK'	pK'(calc)
0.1037	0.581	0.563	0.984	0.421	0.422
.2075	.471	.243	.683	.440	.442
.3112	.390	.047	.507	.460	.461
.4150	.326	−.104	.382	.486	.480
.5187	.280	−.216	.285	.501	.499
.6224	.243	−.311	.206	.517	.519
.7262	.210	−.402	.139	.541	.538
.8299	.185	−.477	.081	.558	.557
.9337	.163	−.549	.030	.579	.577
1.037	.146	−.609	−.016	.593	.596

$pK'(\text{calc}) = 0.403 + 0.186\ m_{HCl}$.

TABLE 6. *Dissociation constant of 4-methyl-3-nitroaniline*

Aniline concentration 3.49×10^{-4} *M*, cell length 1 cm, wavelength 357 mμ, D_1 0.088, D_2 0.551

$m_{HCl} \times 10^3$	D	$\log \frac{D-D_1}{D_2-D}$	$-\log m_{H^+}$	pK
1.002	0.336	+0.062	3.076	3.014
1.503	.284	−.134	2.885	3.019
2.004	.250	−.269	2.750	3.019
2.505	.225	−.377	2.646	3.023
3.006	.207	−.461	2.561	3.022
3.507	.193	−.533	2.490	3.027
4.008	.181	−.600	2.428	3.028
5.010	.165	−.700	2.326	3.026

TABLE 7. *Dissociation constant of 4-chloro-2-methylphenol*

Phenol concentration 3.25×10^{-4} *M*, cell length 1 cm, wavelength 300 mμ, D_1 0.012, D_2 0.984

I	$p(a_H\gamma_{Cl})$	D	$\log \frac{D-D_1}{D_2-D}$	pK	pK(corr)
0.010	9.234	0.254	−0.480	9.714	9.702
.015	9.237	.257	−.472	9.709	9.701
.020	9.237	.258	−.470	9.707	9.701
.025	9.238	.257	−.472	9.710	9.705
.030	9.239	.256	−.475	9.714	9.710
.035	9.239	.256	−.475	9.714	9.711
.040	9.239	.256	−.475	9.714	9.711

The buffer solution was a mixture of borax (*m*) and sodium chloride (1.855*m*), $I = 3.855m$.

TABLE 8. *Dissociation constant of 2,4-dibromophenol*

Phenol concentration 1.76×10^{-4} *M*, cell length 1 cm, wavelength 399 mμ, D_1 0.007, D_2 0.652

I	$p(a_H\gamma_{Cl})$	D	$\log \frac{D-D_1}{D_2-D}$	pK	pK(corr)
0.01	8.176	0.461	0.376	7.800	7.790
.02	8.207	.471	.409	7.798	7.793
.03	8.232	.480	.439	7.793	7.790
.04	8.251	.486	.460	7.791	7.789
.05	8.266	.491	.478	7.788	7.786
.06	8.280	.495	.492	7.788	7.786
.07	8.292	.499	.507	7.785	7.784
.08	8.302	.499	.507	7.795	7.794
.09	8.312	.502	.518	7.794	7.793
.10	8.321	.505	.530	7.791	7.790

The buffer solution was a mixture of tris(hydroxymethyl)amino methane (*m*) and its hydrochloride (0.9845*m*), $I = 0.9845m$.

TABLE 9. *Dissociation constant of 2,6-dibromophenol*

Phenol concentration 3.05×10^{-5} *M*, cell length 4 cm, wavelength 300 mμ, D_1 0.008, D_2 0.641

I	$p(a_H\gamma_{Cl})$	D	$\log \frac{D-D_1}{D_2-D}$	pK	pK(corr)
0.01	7.111	0.467	0.421	6.690	6.684
.02	7.080	.463	.408	6.672	6.669
.03	7.058	.456	.384	6.674	6.672
.04	7.040	.452	.371	6.669	6.667
.05	7.026	.443	.342	6.684	6.683
.06	7.013	.444	.345	6.668	6.667
.08	6.992	.433	.310	6.682	6.681
.10	6.974	.432	.307	6.667	6.666

The buffer solution was an equimolal mixture of potassium dihydrogen phosphate (*m*) and disodium hydrogen phosphate (*m*), $I = 4m$.

TABLE 10. *Dissociation constant of 2-methyl-5-nitrophenol*

Phenol concentration 4.04×10^{-4} *M*, cell length 1 cm, wavelength 430 mμ, D_1 0.005, D_2 0.685

I	$p(a_H\gamma_{Cl})$	D	$\log \frac{D-D_1}{D_2-D}$	pK	pK(corr)
0.01	8.176	0.190	0.427	8.603	8.593
.02	8.207	.202	.390	8.597	8.592
.03	8.232	.209	.368	8.600	8.597
.04	8.251	.217	.344	8.595	8.593
.05	8.266	.223	.326	8.592	8.590
.06	8.280	.226	.317	8.597	8.595
.07	8.292	.232	.300	8.592	8.591
.08	8.302	.237	.286	8.588	8.587
.09	8.312	.239	.280	8.592	8.591
.10	8.321	.244	.266	8.587	8.586

The buffer solutions were mixtures of tris(hydroxymethyl)amino methane (*m*) and its hydrochloride (0.9845*m*), $I = 0.9845m$.

TABLE 11. *Dissociation constant of 4-methyl-3-nitrophenol*

Phenol concentration 4.69×10^{-4} *M*, cell length 1 cm

I	$p(a_H\gamma_{Cl})$	D	$\log \frac{D-D_1}{D_2-D}$	pK	pK(corr)
Wavelength 390 mμ, D_1 0.232, D_2 0.660					
0.02	8.207	0.352	−0.409	8.616	8.611
.04	8.251	.360	−.370	8.621	8.619
.05	8.266	.362	−.360	8.626	8.624
.06	8.280	.362	−.360	8.640	8.638
.08	8.302	.371	−.318	8.620	8.619
.10	8.321	.377	−.290	8.611	8.610
Wavelength 430 mμ, D_1 0.010, D_2 0.493					
0.02	8.207	0.146	−0.407	8.614	8.609
.04	8.251	.152	−.381	8.632	8.630
.05	8.266	.157	−.359	8.625	8.623
.06	8.280	.157	−.359	8.639	8.637
.08	8.302	.165	−.326	8.628	8.627
.10	8.321	.172	−.297	8.618	8.617

The buffer solutions were mixtures of tris(hydroxymethyl)amino methane (m) and its hydrochloride (0.9845m), I=0.9845m.

TABLE 12. pK *values of substituted anilines and phenols in aqueous solution at 25 °C*

	pK(Aniline)			pK(Phenol)		
	Obsd.	Calcd.	Diff.	Obsd.	Calcd.	Diff.
4-Chloro-2-methyl	3.848	3.822	0.026	9.706	9.707	−0.001
2,4-Dibromo	1.867	1.794	.073	7.790	7.805	−.015
2,6-Dibromo	0.168	0.463	−.295	6.674	6.888	−.214
2-Methyl-5-nitro	2.345	2.306	.039	8.592	8.644	−.052
4-Methyl-2-nitro	0.403	0.210	.193	7.597	7.494	.103
4-Methyl-3-nitro	3.022	2.933	.089	8.622	8.619	.003

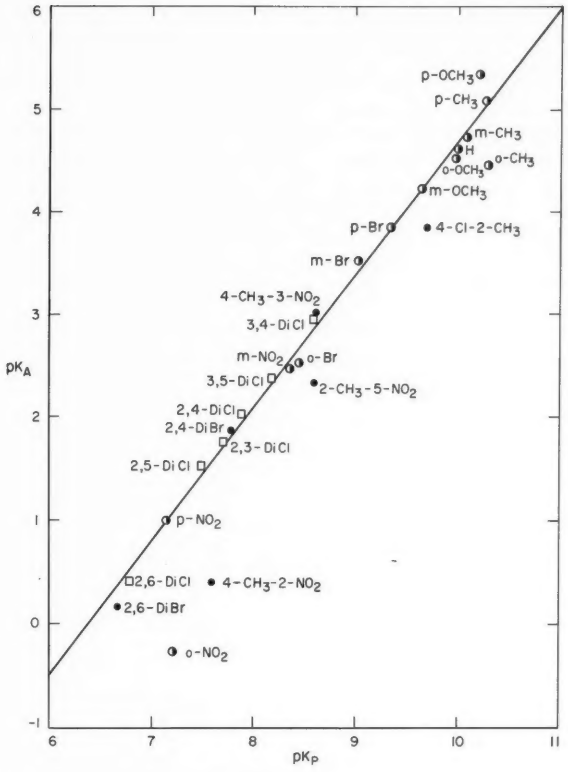

FIGURE 1. pK_A *values of substituted anilines versus* pK_P *values of substituted phenols.*

◑, Monosubstituted compounds
□, Dichloro compounds
●, Present work.

3.2. A Linear Relation Between the *pK* Values of Substituted Anilines and Those of Substituted Phenols

Figure 1 is a plot of the pK values of 25 substituted anilines (pK_A) against the pK value of the corresponding substituted phenol (pK_P). It is clear that, with six exceptions, the experimental values lie close to a straight line. The exceptions are *o*-methyl, *p*-methoxy, *o*-nitro, 4-chloro-2-methyl, 2-methyl-5-nitro, and 4-methyl-2-nitroaniline and phenol. The best straight line through the remaining 19 points in figure 1, determined by the method of least squares, is given by the equation:

$$pK_A = a\,pK_P - b, \tag{8}$$

with $a=1.293$ and $b=8.254$. This equation is essentially an expression of the Hammett Rule [11]. It enables the pK value of a substituted aniline to be predicted from the pK value of the corresponding phenol (or vice versa) with an average difference between observed and calculated values of 0.07_7, the smallest difference being found in the case of *p*-nitro substitution (0.00_1) and the greatest in the case of 2,6-dibromo substitution (0.20_6). In a previous publication [1], a similar linear relationship was discussed but two linear equations were proposed, one for the monosubstituted anilines and phenols and another for dichloroanilines and dichlorophenols. Naturally, the use of four parameters leads to better agreement with the experimental data; a two-parameter equation is used here because it is not so much agreement with the experimental data that is of interest but the exceptional cases which are widely divergent. The exceptions among the monosubstituted anilines and phenols are *o*-methyl, *p*-methoxy, and *o*-nitro compounds for which deviations from the straight line of figure 1 of 0.59_8, -0.39_8, and 1.35_9, respectively, are found, a positive sign being used if the observed pK_A value of a substituted aniline is greater than that calculated using eq (8). Three exceptions are found among the disubstituted anilines and phenols, the 4-chloro-2-methyl, 2-methyl-5-nitro, and 4-methyl-2-nitroanilines and phenols. The discrepancies amount to 0.44_8, 0.51_0, and 1.16_6, respectively. It will be noted that there is *o*-methyl substitution in two instances and *o*-nitro substitution in the third. Both substituents lead to anomalies in the monosubstituted

248-733 O-67—3

compounds. Moreover, the anomaly is about the same in both monosubstituted and disubstituted compounds. Thus it is 0.59_8 for *o*-methyl monosubstitution and 0.44_8 or 0.51_0 if there is an *o*-methyl radical in a disubstituted compound; it is 1.35_9 for *o*-nitro monosubstitution and 1.16_6 if there is an *o*-nitro group in a disubstituted compound. This suggests that anomalies in monosubstituted compounds carry over more or less unchanged on further substitution by a "well-behaved" radical. On the average, the anomaly is 0.51_9 for *o*-methyl substitution and 1.26_2 for *o*-nitrosubstitution; eq (8) can, therefore, be extended by retaining the value of $a=1.293$ but reducing b to -9.516 for *o*-nitro substitution and b to -8.773 for *o*-methyl substitution. The agreement between observed pK_A values and those calculated with the aid of these b values in eq (8) is now -0.09_5 for *o*-nitro monosubstitution and -0.07_9 for *o*-methyl monosubstitution; in the case of disubstituted compounds, the discrepancy is 0.09_6 for the 4-methyl-2-nitro compounds, 0.07_1 for the 4-chloro-2-methyl compounds, and 0.00_9 for the 2-methyl-5-nitro compounds.

4. References

[1] R. A. Robinson, J. Res. NBS **68A** (Phys. and Chem.) No. 2, 159 (1964).
[2] A. I. Biggs and R. A. Robinson, J. Chem. Soc. (London) 388 (1961).
[3] R. G. Bates and R. Gary, J. Res. NBS **65A** (Phys. and Chem.) No. 6, 495 (1961).
[4] R. A. Robinson and A. K. Kiang, Trans. Faraday Soc. **51,** 1398 (1955).
[5] R. A. Robinson and R. G. Bates, J. Res. NBS **70A** (Phys. and Chem.) No. 6, 553 (1966).
[6] A. I. Biggs, Trans. Faraday Soc. **52,** 35 (1956).
[7] R. A. Robinson and A. Peiperl, J. Phys. Chem. **67,** 1723 (1963).
[8] R. A. Robinson and A. Peiperl, J. Phys. Chem. **67,** 2860 (1963).
[9] E. E. Sager, R. A. Robinson, and R. G. Bates, J. Res. NBS **68A** (Phys. and Chem.) No. 3, 305 (1964).
[10] R. A. Robinson, M. M. Davis, M. Paabo, and V. E. Bower, J. Res. NBS **64A** (Phys. and Chem.) No. 4, 347 (1960).
[11] L. P. Hammett, Physical organic chemistry, ch. VII (McGraw-Hill Book Co., Inc., New York, N.Y., 1940).

(Paper 71A3–453)

JOURNAL OF RESEARCH of the National Bureau of Standards—A. Physics and Chemistry
Vol. 71A, No. 3, May–June 1967

Third Virial Coefficient for Air-Water Vapor Mixtures*

R. W. Hyland and E. A. Mason**

Institute for Basic Standards, National Bureau of Standards, Washington, D.C. 20234

(January 9, 1967)

The third interaction virial coefficient C_{aww} for air-water vapor mixtures is estimated in the temperature range 0 to 100 °C, by means of an approximate method based on molecular association. The results are believed accurate to within a factor of two. The value of C_{aww} can be combined with previous estimates of the other interaction coefficient C_{aaw} and the values of the third virial coefficients of pure air and pure water vapor, to give a quantitative description of the equation of state of air-water vapor mixtures through the complete third virial coefficient. It is shown that the maximum total contribution from both C_{aww} and C_{aaw} to the compressibility factor is only of the order of parts in 10^4 up to 100 °C and 100 atmospheres total pressure. At −50 °C, it can be shown by extrapolation of C_{aww} that the contribution of the C_{aww} term to the compressibility factor is only on the order of parts in 10^{11}.

Key Words: Chemical association, Lennard-Jones potential parameters, virial coefficients, water vapor-air mixtures.

1. Introduction

The thermodynamic properties of air-water vapor mixtures near atmospheric pressure have been determined and tabulated by Goff and his co-workers [1–4].[1] Close correlation was found between the equation of state in the virial form and experimental observations; since the virial form has a sound theoretical basis, Goff was able to make accurate interpolations and extrapolations. In this work, Goff neglected terms involving the third interaction virial coefficients C_{aaw} and C_{aww}, which account respectively for interactions among two air molecules and one water molecule, and one air molecule and two water molecules. This neglect was dictated at least in part by necessity, since no information on C_{aaw} and C_{aww} was available at that time, but the good agreement between theory and experiment indicated that the neglect was probably justified. However, the effects of C_{aaw} and C_{aww} increase with increasing pressure, and it cannot be taken for granted that they can be neglected at high pressures, where interactions among three molecules become important. The situation was improved somewhat in 1963, when Mason and Monchick [5] presented theoretical estimates of C_{aaw}, believed accurate within a factor of two. Only C_{aww} then remained unknown in the treatment of the equation of state of moist air through the third virial coefficient.

The purpose of this paper is to present theoretical estimates of C_{aww}. Internal evidence in the calculations indicates that the results are reliable within a factor of two from 0 to 100 °C; even order of magnitude reliability would be valuable, however, because no other information whatever is available on C_{aww}. The results can be extrapolated down to −50 °C with no loss in overall accuracy in the equation of state, since the maximum water content of moist air is so small at low temperatures. The results can also be extrapolated above 100 °C, but the upper limit of usefulness is uncertain. At 100 °C and pressures up to 100 atm, however, the total contribution from both C_{aaw} and C_{aww} to the compressibility factor is only of the order of parts in 10^4, so considerable extrapolation is possible if only moderately accurate equation of state information is needed.

The rigorous calculation of C_{aww} is difficult because one of the pair interactions, ww, is qualitatively different from the other two, aw, inasmuch as a long-range dipole-dipole force is involved. However, if the dipole-dipole interaction is strong enough, a good approximation can be obtained by assuming that the two water molecules form a quasi-stable dimer, w_2, whose interaction with a single air molecule is relatively easy to calculate. This is the physical basis for the present theoretical estimates.

2. The Virial Equation of State

The virial equation of state through the third virial coefficient for a mixture is

$$\frac{PV}{RT}=1+\frac{B_{\text{mix}}}{V}+\frac{C_{\text{mix}}}{V^2}+\ldots \qquad (1)$$

*This work was supported in part by the U.S. Army Research Office—Durham.
**Institute for Molecular Physics, University of Maryland, College Park, Md. 20740.
[1] Figures in brackets indicate the literature references at the end of this paper.

which can also be written as a series in the pressure,

$$\frac{PV}{RT}=1+B_{\text{mix}}\frac{P}{RT}+(C_{\text{mix}}-B_{\text{mix}}^2)\left(\frac{P}{RT}\right)^2+\ldots \quad (2)$$

where

P = absolute pressure, atm,
V = molar volume of mixture, cm³/mol,
T = absolute temperature, °K,
R = gas constant, cm³-atm/mol-°K,
B_{mix} = second virial coefficient of the mixture, cm³/mol, and
C_{mix} = third virial coefficient of the mixture, (cm³/mol)².

The virial coefficients of a mixture depend on both temperature and composition, but the composition dependence is simple. For a binary mixture of a and w, it is

$$B_{\text{mix}}=x_a^2B_{aa}+2x_ax_wB_{aw}+x_w^2B_{ww} \quad (3)$$

$$C_{\text{mix}}=x_a^3C_{aaa}+3x_a^2x_wC_{aaw}+3x_ax_w^2C_{aww}+x_w^3C_{www} \quad (4)$$

where

x_a, x_w = mole fractions of air and water vapor, respectively,

B_{aa}, B_{ww} = second virial coefficients of pure air and pure water vapor, respectively,

B_{aw} = second interaction virial coefficient for one air molecule and one water molecule,

C_{aaa}, C_{www} = Third virial coefficients of pure air and pure water vapor, respectively, and

C_{aaw}, C_{aww} = third interaction virial coefficients for two air molecules and one water molecule and for one air molecule and two water molecules, respectively.

All the B_{ij} and C_{ijk} are functions of temperature only, and are independent of composition.

3. Association Treatment of Virial Coefficients

Our approximation is based on the treatment of the equation of state in terms of chemical association, as has been discussed, for example, by Woolley [6]. In this treatment, a single-component gas is considered to be an ideal mixture of molecular clusters consisting of monomers, dimers, trimers, etc. The actual nonideal behavior of the gas is thus accounted for by the change in the total number of molecules due to the association—an ideal gas would consist only of monomers. This treatment leads to the following equation of state for one mole of a single-component gas:

$$\frac{PV}{RT}=1-K_2P+(3K_2^2-2K_3)P^2+\ldots \quad (5)$$

where K_2 is the equilibrium constant for dimer formation, K_3 that for trimer formation, and so on.

At this point the results are completely rigorous, and in fact there is a one-to-one correspondence between the equilibrium constants and the Mayer cluster integrals of statistical-mechanical theory. Approximations enter only in the evaluation of the equilibrium constants, and the chemical association method is most useful in those cases where the interactions are strong enough that K_2, for instance, can be obtained by considering only those pairs of molecules which are bound together in their lowest energy state. If all states of binding are considered, then the ordinary virial equation of state is recovered, but couched in somewhat different language than usual.

For example, for pure water vapor, treated as a mixture of monomers, dimers, etc., comparison of eq (5) and the virial equation of state for water monomer shows that

$$B_{ww}=-K_2RT,\ C_{www}=(4K_2^2-2K_3)(RT)^2, \text{ etc.} \quad (6)$$

According to the law of mass action,

$$K_2=\frac{x_{w_2}V}{x_w^2RT} \quad , \quad (7)$$

where x_{w_2} is the mole fraction of dimers and x_w the mole fraction of monomers. Combination of eqs (6) and (7) leads to

$$B_{ww}=-\frac{x_{w_2}V}{x_w^2} \text{ or } \frac{B_{ww}}{V}=-\frac{x_{w_2}}{x_w^2} \quad (8)$$

and

$$\frac{PV}{RT}=1-\frac{x_{w_2}}{x_w^2}+\ldots\approx 1-x_{w_2}+\ldots \quad (9)$$

for $x_{w_2}\ll x_w$.

The treatment is easily extended to gas mixtures, and a hybrid description is even possible, in which strongly interacting components of the mixture are handled by the chemical association method, and weakly interacting components by the ordinary virial coefficient method. Such a hybrid description is appropriate for mixtures of air and water vapor. We will not, however, calculate B_{ww} from eq (6), but will take B_{ww} as an experimental quantity and use eq (8) to calculate the mole fraction of dimers, which will be needed in the estimation of C_{aww}.

Barua, et al. [7] have shown that for polar molecules a fairly good approximation to B and K_2 can be obtained by considering only those pairs of molecules which interact strongly enough to be bound together

in the lowest energy state—that is, by considering only dimers whose component molecules have their dipoles alined head-to-tail. The contributions from other dimer configurations can be ignored if the temperature is not too high. This study thus gives quantitative evidence for the validity of the concept of dimers of water molecules.

For a description only through the third virial coefficient, we can consider the three-molecule interactions either as trimer formation, or else as the nonideal interaction between a dimer and a monomer. Our model of a mixture of air and water vapor through the third virial coefficient will be that of a mixture of three species—air monomers, water monomers, and water dimers. All of these species interact with one another except for two water monomers, whose interaction is already taken into account by the existence of the water dimers. The equation of state of this ternary mixture is

$$\frac{PV}{RT}=1+(x_a'^2B_{aa}+2x_a'x_w'B_{aw}+x_w'^2B_{ww})\frac{1}{V}+(2x_a'x_{w_2}B_{aw_2}+2x_w'x_{w_2}B_{ww_2})\frac{1}{V}+(x_a'^3C_{aaa}+3x_a'^2x_w'C_{aaw})\left(\frac{1}{V}\right)^2+\ldots \quad (10)$$

in which we have written B_{ww} explicitly rather than use eq (8), since we will take B_{ww} as an experimental quantity. Other interactions, such as those involving $B_{w_2w_2}$ or C_{aaw_2}, contribute to the fourth virial coefficient and are neglected. The mole fractions have been written with primes to indicate that they are not the same as those appearing in eqs (3) and (4).

The degree of dimerization is on the order of parts per thousand of the total number of water molecules. We therefore make the approximation that the x_a' and x_w' of eq (10) are equal to the x_a and x_w of eqs (3) and (4). By comparison of these equations, we see that

$$C_{\text{mix}}=(2x_ax_{w_2}B_{aw_2}+2x_wx_{w_2}B_{ww_2})V+(x_a^3C_{aaa}+3x_a^2x_wC_{aaw}). \quad (11)$$

Solving eq (8) for x_{w_2} and substituting into the first term on the right, we find

$$3x_ax_w^2C_{aww}+x_w^3C_{www}=-2x_ax_w^2B_{aw_2}B_{ww}-2x_w^3B_{ww_2}B_{ww} \quad (12)$$

and therefore

$$C_{aww}=-\frac{2}{3}B_{aw_2}B_{ww} \quad (13)$$

$$C_{www}=-2B_{ww_2}B_{ww}. \quad (14)$$

The quantity sought, C_{aww}, has therefore been related to a product of second virial coefficients, one of which (B_{ww}) is known experimentally, and the other of which (B_{aw_2}) remains to be calculated. In addition, if C_{www} is known experimentally, we can use eq (14) as a check on the internal consistency of our above calculations or as a source of information on the dimer properties (through B_{ww_2}).

4. Calculation of B_{ww_2}

We can now calculate values of B_{ww_2} from eq (14), and compare with values obtained by methods described in this section. This affords a check on our procedures to this point.

It must be emphasized that we are not trying to derive values for B_{ww_2} as an end in itself—rather, we wish to determine the ranges within which the molecular potential parameters for the dimer-monomer interaction lie. This is important, for these parameters will be used to obtain, in order, the molecular potential parameters associated with the air-dimer interaction, B_{aw_2} itself, and finally C_{aww} from eq (13).

The values of B_{ww} and C_{www} are listed in table 1, as taken from the correlations of Goff [4] and Keyes [8]. The respective values of B_{ww} warrant using the average value in all calculations. The respective C_{www} values, however, should be considered individually. Goff [4] assigns a tolerance of ±120 percent at 60 °C and of ±30 percent at 90 °C to his values of C_{www}, with the tolerances taken as twice the probable error. This points out the large uncertainty in this quantity, particularly when we have used Goff's relations to extrapolate his values below 60 °C.

TABLE 1. *Experimental values of the second and third virial coefficients of water vapor; extrapolated values in parentheses*

Temp.	$-B_{ww}$ cm³/mol			$-C_{www}$ liter²/mol²	
	Goff [4]	Keyes [8]	Ave.	Goff [4]	Keyes [8]
°C					
0	(1832)	1854	1843	(64.3)	93.8
10	1510	1520	1515	(34.7)	49.3
20	1260	1266	1263	(19.7)	27.6
30	1074	1070	1072	(11.7)	16.2
40	924	917	920	(7.18)	9.87
50	803	794	798	(4.51)	6.26
60	705	695	700	3.01	4.06
70	625	613	619	2.03	2.76
80	558	546	552	1.39	1.92
90	501	489	495	0.98	1.37
100	(453)	441	447	(.70)	0.99

Two sets of B_{ww_2} values are calculated from eq (14), one set from Goff's C_{www}, the other from Keyes' C_{www}. The results are given in table 2.

Other estimates may be obtained from assumptions about the intermolecular forces. We represent the interaction between two molecules as the sum of a spherically symmetric Lennard-Jones (12–6) interaction and the interaction between point dipoles embedded in the center of each molecule. The potential

energy $\varphi_{ij}(r)$ between molecules i and j a distance r apart is thus

$$\varphi_{ij}(r)=4\epsilon_{ij}\left[\left(\frac{\sigma_{ij}}{r}\right)^{12}-\left(\frac{\sigma_{ij}}{r}\right)^{6}\right]$$

$$-\frac{\mu_i\mu_j}{r^3}(2\cos\theta_i\cos\theta_j-\sin\theta_i\sin\theta_j\cos\phi) \qquad (15)$$

where μ_i and μ_j are the dipole moments, θ_i and θ_j are the angles between the dipole axes and the line of centers of the molecules, ϕ is the azimuth angle of the axes, and ϵ_{ij} and σ_{ij} are adjustable constants. If either dipole moment is zero, eq (15) reduces to the Lennard-Jones (12–6) potential, for which ϵ_{ij} is the depth of the potential well and $\varphi(\sigma_{ij})=0$. Equation (15) is usually called the Stockmayer potential [9].

TABLE 2. *Experimental and calculated values of the water monomer-dimer second virial coefficient*

Temp.	$-B_{ww_2}$, liter/mol					
	Exptl., eq (14) (Keyes' C_{www})	(Goff's C_{www})	Calc. eq (18)	Calc. eq (19)	Calc. eq (21a)	Calc. eq (21b)
°C						
0	25.4	17.4	21.53	11.91	3.39	5.08
10	16.3	11.5	17.52	9.84	2.66	3.99
20	11.0	7.80	12.96	8.20	2.25	3.15
30	7.56	5.46	10.44	6.72	1.89	2.56
40	5.36	3.90	8.21	6.13	1.62	2.20
50	3.92	2.8[illegible]	6.61	4.84	1.37	1.82
60	2.90	2.1[illegible]	5.58	4.22	1.21	1.55
70	2.23	1.64	4.27	3.67	1.09	1.36
80	1.74	1.26	3.65	3.16	0.96	1.18
90	1.38	0.99	3.10	2.73	.86	1.06
100	1.11	.79	2.63	2.46	.79	0.95

The values of ϵ_{ij} and σ_{ij} must be determined from some experimentally measured property. For pure air, which has no dipole moment, the values used by Mason and Monchick [5] and by Chaddock [10] are $\sigma_{aa}=3.522$ Å and $\epsilon_{aa}/k=99.2$ °K, where k is Boltzmann's constant. For pure water vapor, Rowlinson [11] gives $\sigma_{ww}=2.65$ Å and $\epsilon_{ww}/k=380$ °K from analysis of B_{ww}, and Monchick and Mason [12] give $\sigma_{ww}=2.71$ Å and $\epsilon_{ww}/k=506$ °K from analysis of viscosity data. Tabulations of virial coefficients for the Stockmayer potential are given in terms of a reduced dipole parameter, defined as

$$t^*_{ij}=\frac{\mu_i\mu_j}{\sqrt{8}\,\epsilon_{ij}\sigma^3_{ij}}. \qquad (16)$$

The value of t^*_{ww} is 1.2 according to Rowlinson and 0.85 according to Monchick and Mason, with the dipole moment of water taken as $\mu_w=1.83\times10^{-18}$ esu.

Stogryn and Hirschfelder [13] have shown how to estimate ϵ_{ij} and σ_{ij} for dimer-monomer interactions from those for monomer-monomer interactions, according to simple geometrical arguments. The results have been elaborated by Barua and Das Gupta [13] on the basis of the pressure dependence of the viscosity of superheated steam. They recommend the values

$$\epsilon_{ww_2}=1.32\epsilon_{ww},\ \sigma_{ww_2}=1.16\sigma_{ww}. \qquad (17)$$

Since we assume that the dimer consists of two monomers with their dipoles in a head-to-tail configuration, the dipole moment of the dimer is twice that of the monomer, $\mu_{w_2}=3.66\times10^{-18}$ esu.

Once ϵ, σ, and t^* are known, it is straightforward to calculate B_{ww_2} from published numerical tables [9, 11] for the Stockmayer potential.

The Rowlinson [11] parameters for water vapor, based on virial coefficient data, are considered first, since so far only virial coefficient data have been used in this presentation.

Equations (16) and (17) lead to

$$t^*_{ww_2}=1.2,\ \sigma_{ww_2}=3.07\text{ Å},\ \epsilon_{ww_2}/k=501\text{ °K}. \qquad (18)$$

The values of B_{ww_2} obtained from these parameters are found in table 2. The agreement between the values of $-B_{aw_2}$ calculated from eqs (14) and (18) is generally good, although the latter are somewhat higher except at 0 °C. The implication is that the assumptions made to derive our model are at least as reasonable an approximation of the true physical situation as those used in the derivation of the Stogryn and Hirschfelder [13] model.

If the viscosity-derived parameters of Mason and Monchick [5] for water vapor are used with eqs (16) and (17), we find

$$t^*_{ww_2}=0.83,\ \sigma_{ww_2}=3.14\text{ Å},\ \epsilon_{ww_2}/k=668\text{ °K}. \qquad (19)$$

The values of B_{ww_2} derived from these parameters are also given in table 2. The curve of this set of B_{ww_2} values versus T is flatter at the low temperature end than the three curves obtained above from virial coefficient data, but the agreement still is not unreasonable.

Since the values of B_{ww_2} derived from eq (14) do agree fairly well with those derived from other sources, we now seek, by curve fitting, improved Stockmayer potential parameters which will describe the values from eq (14). These will be needed in the calculation of C_{aww}.

The curve-fitting should be done so as to produce preferentially better agreement at high temperatures than at low temperatures for two reasons. First, the experimental values of C_{www} are less uncertain at high temperatures. Second, and more important, is the fact that the low-temperature values of B_{ww_2} are dominated more by $t^*_{ww_2}$ than are the high-temperature values, but the parameter $t^*_{ww_2}$ is of no interest for the present purposes, since it does not contribute at all to the determination of C_{aww}. In other words, we want the derived values of ϵ_{ww_2} and σ_{ww_2} to represent the spherical (12–6) part of the potential, not the dipole part, as there is no dipole contribution to B_{aw_2}.

Therefore, we require that the B_{ww_2} values obtained by fitting should lie between -0.79 liter/mol and -1.11 liter/mole at 100 °C, that is, between the values predicted respectively by using Goff's and Keyes' C_{www} in eq (14). At the same time the slopes of the curves in the 100 °C region must be almost the same to prevent any gross divergences at higher temperatures.

The limiting ranges of σ_{ww_2} and ϵ_{ww_2} are set arbitrarily, but not unreasonably, in the following manner. The lower limits are taken to be the corresponding values for pure water vapor given by Rowlinson [11]. This is equivalent to setting the coefficients of σ_{ww} and ϵ_{ww} in eq (17) equal to 1, a change of 13.8 percent in the former and 24.2 percent in the latter. The upper limits are set by raising the coefficients by the same percentages, and using the σ_{ww} and ϵ_{ww} parameters of Mason and Monchick [5] in eq (17). The limits on $t^*_{ww_2}$ are found by using the limiting values of ϵ_{ww_2} and σ_{ww_2} in eq (16).

This procedure leads to

$$\sigma_{ww_2} \geq (\sigma_{ww})_{\text{Rowlinson}} = 2.65 \text{ Å},$$

$$\epsilon_{ww_2}/k \geq (\epsilon_{ww}/k)_{\text{Rowlinson}} = 380 \text{ °K}, \qquad (20a)$$

$$t^*_{ww_2} \leq 2.4$$

$$\sigma_{ww_2} \leq 1.32(\sigma_{ww})_{\text{M. and M.}} = 3.58 \text{ Å},$$

$$\epsilon_{ww_2}/k \leq 1.64\,(\epsilon_{ww}/k)_{\text{M. and M.}} = 830 \text{ °K},$$

$$t^*_{ww_2} \geq 0.45. \qquad (20b)$$

Within these ranges, the predicted curves are slightly flatter in the 100 °C region than those predicted by eq (14). This means that a curve which predicts −1.11 liter/mole at 100 °C will diverge immediately from higher temperature B_{ww_2} values derived from Keyes' C_{www}. In order to prevent this immediate divergence, we changed the lower permissible B_{ww_2} limit at 100 °C from −1.11 liter/mol to −0.95 liter/mol, that is, midway between the limits set by eq (14).

Empirical curve fitting with B_{ww_2} matching at both −0.79 liter/mol and −0.95 liter/mol at 100 °C led respectively to these choices of parameters:

$$t^*_{ww_2} = 1.14,\ \sigma_{ww_2} = 3.41 \text{ Å},\ \epsilon_{ww_2}/k = 380 \text{ °K} \qquad (21a)$$

$$t^*_{ww_2} = 1.25,\ \sigma_{ww_2} = 3.30 \text{ Å},\ \epsilon_{ww_2}/k = 380 \text{ °K}. \qquad (21b)$$

The σ_{ww_2} values are not unreasonable. The fact that ϵ_{ww_2}/k is the same as the value for pure water vapor (lower limit) in both cases is perhaps annoying, but can be accepted in the present context without undue alarm.

The values of B^* versus T^* for the parameters were interpolated graphically between tabulated values of t^* [9], and these in turn were extrapolated graphically to the lowest temperatures. Therefore the derived parameters may not be the "best" ones in a least squares sense, but they are certainly close enough for our purposes.

The values of B_{ww_2} corresponding to eqs (21a) and (21b) are given in table 2, and clearly the agreement with the curves derived from eq (14) is poor except at the highest temperatures. The reason for the discrepancy is open to some speculation, but we remind the reader again that first, we demanded a fit at the high temperatures to have the σ and ϵ values be more representative of the spherical part of the potential, and second, we are seeking various estimates of σ_{ww_2} and ϵ_{ww_2} rather than attempting to derive B_{ww_2}.

Summarizing this section, we have obtained four sets of σ_{ww_2} and ϵ_{ww_2} parameters (t^* is of no further interest). Two were obtained through the method of Stogryn and Hirschfelder [13], using first experimental virial coefficient data and then experimental viscosity data, and two from curve-fitting, subject to several restraints, to the B_{ww_2} values derived with the methods of this paper. We also obtained what are thought to be reasonable outside limits on the values of σ_{ww_2} and ϵ_{ww_2}.

5. Calculation of C_{aww}

The various values of σ_{ww_2} and ϵ_{ww_2} derived in the previous section may now be used to obtain the parameters σ_{aw_2} and ϵ_{aw_2} for the air-dimer interaction, from which B_{aw_2} and finally C_{aww} may be obtained. The procedure is based on semi-empirical combining rules [9] for ϵ and σ,

$$\epsilon_{ij} = (\epsilon_{ii}\epsilon_{jj})^{1/2},\ \sigma_{ij} = (1/2)(\sigma_{ii} + \sigma_{jj}). \qquad (22)$$

These rules work fairly well for both polar and nonpolar molecules [15]. Applying these rules twice, we obtain expressions for the desired parameters ϵ_{aw_2} and σ_{aw_2},

$$\epsilon_{aw_2} = \epsilon_{ww_2}(\epsilon_{aa}/\epsilon_{ww})^{1/2},$$

$$\sigma_{aw_2} = \sigma_{ww_2} + (1/2)(\sigma_{aa} - \sigma_{ww}). \qquad (23)$$

The values of σ_{aw_2} and ϵ_{aw_2} are derived from the four sets of ww_2 parameters obtained in the previous section. For the three associated with virial coefficient data [eqs (18), (21a), (21b)] we use in eq (23) Rowlinson's [11] values for ϵ_{ww} and σ_{ww}, while for the set associated with viscosity data [eq (19)] we use in eq (23) the Mason and Monchick [5] values. We find

$$\epsilon_{aw_2}/k = 256 \text{ °K} \qquad \sigma_{aw_2} = 3.51 \text{ Å [from eq (18)]} \qquad (24a)$$

$$\epsilon_{aw_2}/k = 194 \text{ °K} \qquad \sigma_{aw_2} = 3.85 \text{ Å [from eq (21a)]} \qquad (24b)$$

$$\epsilon_{aw_2}/k = 194 \text{ °K} \qquad \sigma_{aw_2} = 3.74 \text{ Å [from eq (21b)]} \qquad (24c)$$

$$\epsilon_{aw_2}/k = 296 \text{ °K} \qquad \sigma_{aw_2} = 3.55 \text{ Å [from eq (19)]} \qquad (24d)$$

The last set is of particular interest, since it is derived entirely from viscosity data. The viscosity is relatively insensitive to the dipole interaction [12], so the values of ϵ_{ww_2} and σ_{ww_2} from which eq (24d) is derived should be good representations of the spherical part of the potential.

Two more sets of aw_2 parameters should be derived—namely, those associated with the limiting cases of the ww_2 parameters [eqs (20a) and (20b)]. From these we obtain respectively

$$\epsilon_{aw_2}/k = 194\ °\text{K} \qquad \sigma_{aw_2} = 3.09\ \text{Å} \tag{25a}$$

$$\epsilon_{aw_2}/k = 423\ °\text{K} \qquad \sigma_{aw_2} = 4.02\ \text{Å}. \tag{25b}$$

From each of these six sets of parameters, we calculate first B_{aw_2} and then, using eq (13), C_{aww}. The results of the latter are given in table 3.

TABLE 3.—*Calculated value of the third interaction virial coefficient* C_{aww} *based on the parameters of eqs (24) and (25)*

Temp	$-C_{aww}$, liter²/mol²					
	Virial			Viscosity*	Limits	
	Eq (24a)	Eq (24b)	Eq (24c)	Eq (24d)	Eq (25a)	Eq (25b)
°C						
0	0.152	0.121	0.111	0.203	0.062	0.549
10	.117	.090	.083	.156	.047	.424
20	.092	.072	.066	.123	.037	.332
30	.073	.057	.052	.098	.029	.266
40	.058	.046	.042	.080	.024	.216
50	.048	.037	.034	.065	.019	.178
60	.040	.030	.028	.054	.016	.148
70	.034	.025	.023	.046	.013	.123
80	.028	.021	.019	.039	.011	.105
90	.024	.018	.016	.033	.009	.090
100	.021	.015	.014	.028	.008	.077

*Best estimates.

Those derived from experimental viscosity values [i.e., from eq (24)] are felt to be the most reliable. This is based on the relative independence of viscosity on the dipole interaction, and on the success of the dimer-monomer model in predicting the pressure dependence of the viscosity of steam [13, 14].

The viscosity-based values differ from the limiting values derived for eq (25a, b) by at most a factor of three, and from all other values by no more than a factor of two.

We are confident that the values are accurate to within a factor of four, and probably to within a factor of two.

6. Discussion

We are now in a position to estimate the contributions of C_{aaw} and C_{aww} to the compressibility factor of moist air; that is, to estimate the magnitudes of the terms $(3x_a^2x_wC_{aaw}/V^2)$ and $(3x_ax_w^2C_{aww}/V^2)$, as compared to unity. Since the maximum water vapor content of air increases rapidly with increasing temperature, the largest contribution of these terms comes at high temperatures, even though C_{aaw} and C_{aww} decrease in magnitude with increasing temperature. At 100 °C the partial pressure of water vapor can be taken as 1 atm, and the mole fractions as

$$x_a = P_a/(P_a+1),\ x_w = 1/(P_a+1) \tag{26}$$

where P_a is the partial pressure of the air. These relations are only approximate for nonideal gases, but adequate here because in C_{mix} we are seeking only the highest-order deviation terms. Similarly, the molar volume of the mixture is

$$V = RT/(P_a+1). \tag{27}$$

Taking $C_{aaw} = +696$ (cm³/mol)² [5] and $C_{aww} = -2.8 \times 10^4$ (cm³/mol)² (table 3), we find from eqs (26) and (27) that

$$3x_a^2x_wC_{aaw}/V^2 = 2.23 \times 10^{-6}P_a^2/(P_a+1) \tag{28a}$$

$$3x_ax_w^2C_{aww}/V^2 = 0.90 \times 10^{-4}P_a/(P_a+1). \tag{28b}$$

Thus even for $P_a = 100$ atm the contribution of these two terms is only of the order of parts in 10^4.

The present results are readily extendable to higher or lower temperatures by means of the aw_2 parameters of eq (24d) in conjunction with tabulated virial coefficients for the (12–6) potential [9]. There is no loss in overall accuracy in PV/RT by extrapolation to low temperatures. For example, a calculation similar to that performed above, based on a temperature of −50 °C ($P_w = 3.9 \times 10^{-5}$ atm) with $P_a = 100$ atm and $C_{aww} = -1 \times 10^6$ (cm³/mol)², indicates that the contribution of the C_{aww} term to the compressibility factor is on the order of parts in 10^{11}. There is loss in accuracy by extrapolation to high temperatures because of the increasing water vapor content; how much extrapolation is permissible depends on how much uncertainty in PV/RT is acceptable. It must also be remembered that the physical model of dimer formation becomes less accurate as the temperature increases.

6. References

[1] J. A. Goff and A. C. Bates, Trans. ASHVE **47,** 373 (1941).
[2] J. A. Goff, J. R. Andersen, and S. Gratch, Trans. ASHVE **49,** 269 (1943).
[3] J. A. Goff and S. Gratch, Trans. ASHVE **51,** 125 (1945).
[4] J. A. Goff, Heating, Piping, and Air Conditioning (Journal Section) **21,** 118 (1949).
[5] E. A. Mason and L. Monchick, Humidity and Moisture, Vol. **III,** p. 257 (Rheinhold Publishing Corp., New York, 1965).
[6] H. W. Woolley, J. Chem. Phys. **21,** 236 (1953).
[7] A. K. Barua, P. K. Chakraborti, and A. Saran, Mol. Phys. **9,** 9 (1965).
[8] F. G. Keyes, J. Chem. Phys. **15,** 602 (1947).
[9] J. O. Hirschfelder, C. F. Curtiss, and R. B. Bird, Molecular Theory of Gases and Liquids (John Wiley & Sons, Inc., New York, N.Y., second printing, 1964).
[10] J. B. Chaddock, Humidity and Moisture, Vol. **III,** p. 273 (Reinhold Publishing Corp., New York, 1965).
[11] J. S. Rowlinson, Trans. Faraday Soc. **45,** 974 (1949).
[12] L. Monchick and E. A. Mason, J. Chem. Phys. **35,** 1676 (1961).
[13] D. E. Stogryn and J. O. Hirschfelder, J. Chem. Phys. **31,** 1531, 1545 (1959).
[14] A. K. Barua and A. Das Gupta, Trans. Faraday Soc. **59,** 2243 (1963).
[15] E. A. Mason and L. Monchick, J. Chem. Phys. **36,** 2746 (1962).

(Paper 71A3–454)

JOURNAL OF RESEARCH of the National Bureau of Standards—A. Physics and Chemistry
Vol. 71A, No. 3, May–June 1967

Recrystallization and Melting of Partially Melted Stark Rubber

Donald E. Roberts

Institute for Materials Research, National Bureau of Standards, Washington, D.C. 20234

(January 27, 1967)

Two specimens from a piece of stark rubber which had a melting temperature originally at 41 °C were partially melted at 38 °C and allowed to stand for 11 years, one at about 25 °C, the other at 38 °C. The first showed a continuous slow decrease in specific volume, while the second increased slowly in volume for 5 months and remained constant for about 5 months more before showing the continuous slow decrease. The melting temperature of the first increased to 45 °C and the melting range was broadened. The melting temperature of the second became 52 °C and the range was narrowed. Perfecting or enlarging of crystals and the effect of higher recrystallization temperatures have influenced the melting temperatures. The effect of heating rate is discussed in connection with slow increases in volume, attributed to relaxation of oriented regions, during melting.

Key Words: Crystal size, crystallized rubber, heating rate, melting range, melting temperature, oriented, partial melting, recrystallization, rubber, slow melting, stark rubber.

1. Introduction

The term "stark" was originally applied to hard crystalline regions which formed in bales of rubber during storage. The term can be used in referring to rubber which has been deformed in some way, then crystallized so that an oriented system of crystallites results which is stable above room temperature.[1] Its crystallization and melting are similar to those of undeformed rubber crystallized by cooling, except that the temperatures of these processes are shifted upward several degrees for stark rubber.

This paper presents the results of two experiments which are a continuation of work described in a previous paper on the nature of stark rubber [1].[2] The specimens used in the present work are from the same source as Sample II, illustrated in figure 1 of that paper, namely smoked sheet, highly milled, then kept in a basement for 15 years. After the sample was discovered to have become stark, it was returned to the laboratory and the several specimens were removed from it. The temperature during the storage period is not known, although it is unlikely that it differed appreciably from the range 15 to 25 °C. Orientation in stark rubber [2, 3] facilitates the crystallization near room temperature, where the rate of crystallization for undeformed rubber is negligible [4]. X-ray diffraction [1] indicated that the stark rubber crystallites were oriented as a result of the milling process. The *d*-spacings indicated that the crystalline form in stark rubber is the same as that in stretched or cooled rubber [1]. Molecular weights were not determined; a recent paper [5] discusses the effects of milling on the molecular weight of rubber. The observed melting temperature (T_m), without annealing, of Sample II in 1952 was 41 °C.

Stark rubber requires a very long time to approach phase equilibrium at any temperature below its T_m, therefore an experiment was started in which sufficient time could be allowed at a fixed temperature near T_m for the process to run through whatever changes might occur. At the same time another experiment was started to see if recrystallization of the partially melted stark rubber could be observed at room temperature. These experiments were begun in 1953 and finished in 1965.

2. Experimental Procedures

Two dilatometers were assembled, each containing about 2.7 g of the stark rubber. Their thermal histories are represented in figures 1 and 2. The dilatometers were heated from 30 to 38 °C in 7 days, remaining at 38 °C for one day, then one (Sample A) was returned to room temperature (avg 25 °C, limits 21.5 and 29.5 °C) and the other (Sample B) was kept at 38 °C (limits 37.7 and 38.3 °C). Sample B was unintentionally overheated for a period of a few hours during which the temperature briefly reached 39.8 °C. This occurred 2 weeks after the experiment began and resulted in a small irreversible increase in volume.

[1] Not to be confused with racked rubber, which has been severely and repeatedly stretched at elevated temperatures and cooled to yield a fiber.

[2] Figures in brackets indicate the literature references at the end of this paper.

In Sample A at room temperature an induction period of about 20 days was followed by a decrease in volume and the recrystallization[3] eventually progressed until a greater degree of crystallinity existed than that at room temperature before heating. In Sample B there was a continued increase in volume[4] until a maximum was reached after 5 months. This volume was constant for an additional 4 to 5 months, then a decrease began. Neither of these recrystallization rates had yet begun to diminish on a log time plot by the time the final heating was begun in 1964. Presumably the recrystallization might have gone on for many years longer. For the recrystallization, occurring in the presence of existing crystals, the Avrami exponent n is a little less than 1 for each of the two samples. Isotherms with n near 1 have been noted in seeded crystallization [6, 7, 8]. The crystallinities of the specimens, calculated from the specific volumes at 30 °C as shown in figures 1 and 2, were approximately as follows:

Amorphous rubber	1.1032 cm³/g	0%
Initial stark rubber	1.0807	23%
Recrystallized Sample A	1.0770	26.5%
Recrystallized Sample B	1.0875	16%
Ideal crystal calculated from unit cell	1.005	100%

After 11 years at the stated temperatures, Sample B was cooled to 30 °C, then the dilatometers were heated so as to reach 36 °C in 3 days and 38 °C in 7 days more. The subsequent heating rate was usually stepwise 1 deg C per week (6–8 days), which approximates the heating schedule used for Sample II in the previous work [1], and permits proper comparison of their melting temperatures. See figures 1 and 2.

[3] To simplify terminology the term "recrystallization" in this paper may be understood to include any of the processes which occur when a sample is stored or annealed: Crystallization, enlarging or thickening of crystals, and removal of voids and defects.

[4] Following the overheating, when the temperature had returned to 38 °C, the volume remained constant for 10 days then continued its upward crawl.

3. Results and Discussion

During the period each sample was held at 38 °C, some of the less stable crystals were melted, thus raising the average and narrowing the distribution of crystal sizes.

Upon first heating of the specimens, before the recrystallization, as well as in the melting of Sample II,

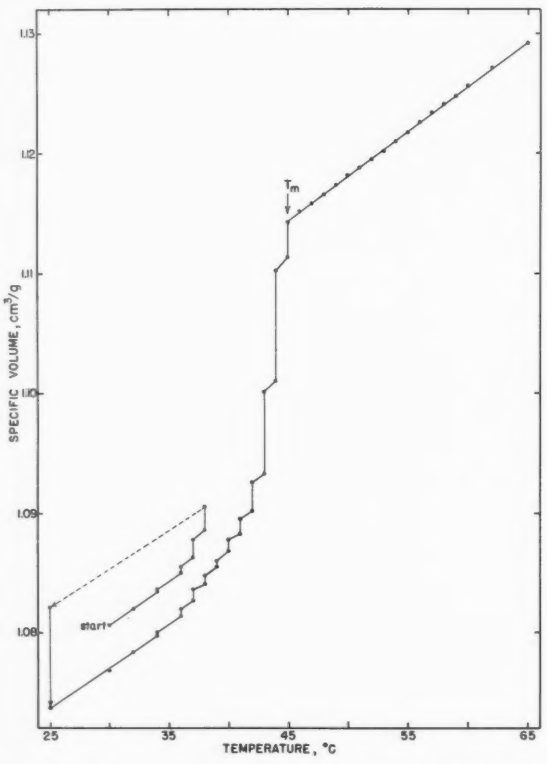

FIGURE 1. *Thermal history of stark rubber Sample A from 1953 to 1965.*

The vertical lines show the volume increases during the observation period at those temperatures. T_m is taken as that temperature at which volume increase with time ceases. Irregularities in the slopes of the "thermal expansion" lines result from differences in times of initial readings after heating.

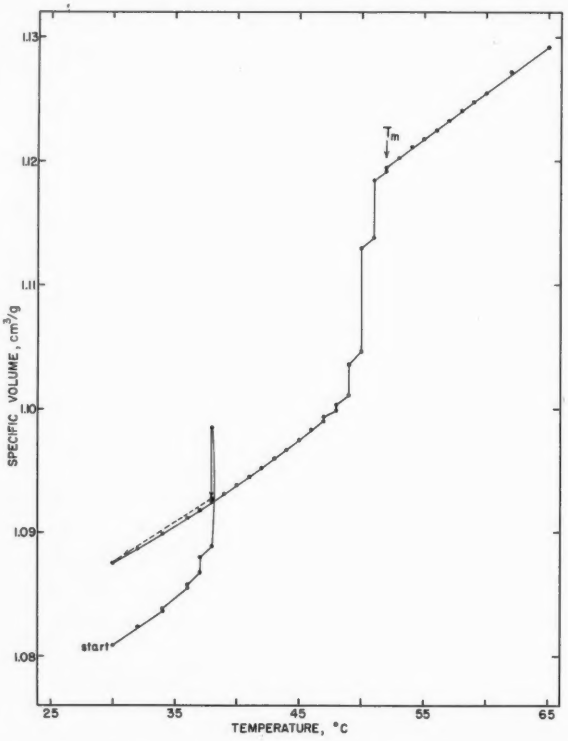

FIGURE 2. *Thermal history of Sample B.*

the melting process begins to produce an increase in volume (beyond normal thermal expansion) at about 34 °C. Also for Sample A, this is observed upon the final heating after recrystallization, and the melting range is broadened so that T_m is now 45 °C compared to 41 °C for the earlier specimen. Apparently a broader distribution (raising the upper limit) of crystallite size and perfection was developed by the long-time recrystallization at room temperature.

Upon final heating of Sample B, on the other hand, the additional increase of volume begins to appear at 47 °C, only 5 deg below T_m. In each case the increase of volume began at 9 deg above the recrystallization temperature. In previous work [4] at lower temperatures this difference ranged from 7 to a minimum of 4 deg, increasing to 9 deg as the crystallization temperature was raised to 15 °C. The annealing at 38 °C apparently tended to eliminate defects, raising the low end of the melting range by 13 deg. At the same time it produced larger crystallites at the expense of smaller ones, raising the T_m by 11 deg, to 52 °C.

Increases of melting temperatures of rubber and other polymers after prolonged storage have been reported, and these have been attributed to growth of crystals or thickening of lamellae [9, 10, 11, 12]. In the present work, perfecting or enlarging the crystals over a long time span and the effect of high temperatures of crystallization have operated similarly to raise the melting temperatures. At the same time the melting range for Sample B was narrowed from 7 deg to 5 deg, in accordance with previous observations [4, 13] of a narrowing of the melting range at higher crystallization temperatures. The slow melting of crystals while the temperature was held at 38 °C is in accordance with previous observations [1], where it was found to occur in stark rubber at temperatures above 35 °C. Figure 3 shows the volume-time relations observed for the final melting of Sample B, when it was held at each temperature for about a week.

The observed melting temperature in a sample of stark rubber having a given degree of orientation depends upon (1) the temperature of crystallization, (2) the age of the crystals, and (3) the heating rate. With regard to the heating rate, two influences are at work and the observed T_m will depend to some extent upon which of the two dominates. On one hand there is the effect of the slowness of melting, and on the other hand there is the effect of annealing during the heating schedule. The temperature range where slow volume increases are observed ("melting range") is the critical region where heating rate is concerned. Outside this range, volume equilibrium is attained at the same time as thermal equilibrium.

The heating rate of 1 deg/week used here does not allow time for the completion of phase changes below T_m. Consequently, the portions of the crystalline material that are unstable at a given temperature do not have time to melt completely, so that the volume increase at the next higher temperature is composed partly of the contribution from previously unstable crystals. This delay results in a higher observed T_m than would occur if slower heating were to be used, e.g., holding the temperature until maximum volume had been reached at each temperature in the melting range (see figs. 1 and 2). However, if sufficient time

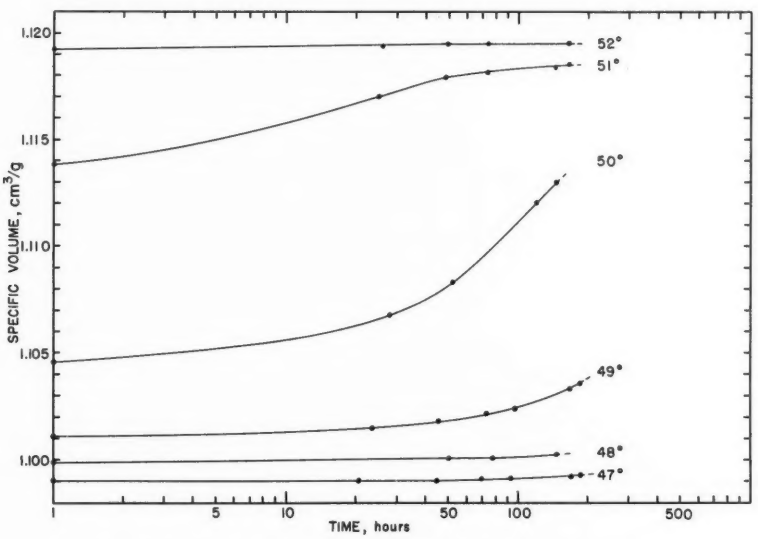

FIGURE 3. *Melting kinetics of Sample B in the range 47 to 52 °C* ($= T_m$).

A similar family of curves is obtained with Sample A between 34 and 45 °C. The average melting rates (cm³/g/hr) between the points shown on, for example, the 50 °C curve are 0.0000822, 0.0000634, 0.0000551, and 0.0000362.

(years) were to be allowed so that significant recrystallization could occur at each temperature, the crystallization temperature would be effectively raised and the T_m would be correspondingly higher. Table 1 gives estimates of the effect of heating rate on T_m in comparison with the present work. Another sample from the same source as Sample II melted 4 deg higher than that sample when heated at 1 deg/4 min.

It is not clear whether chain folded, extended chain or bundlelike crystals are present in stark rubber. Partially oriented systems might contain a mixture [14]. Considerable superheating in large, extended chain crystals has been reported [15].

TABLE 1

Heating rate one degree per	Influence of:		Effect on T_m compared with present work
	Delay	Annealing	
Hour	Strong	None	1–2 Deg higher.
Week	Some	None	Present work.
6 Months [a]	None	Slight	1–2 Deg lower.
10 Years [b]	None	Strong	10–15 Deg higher.

[a] Or until maximum volume is reached at each temperature. This heating rate avoids superheating and minimizes reorganization [15, 16], so that the observed melting temperature is that of the largest crystals formed at a given crystallization temperature.
[b] Or until appreciable recrystallization has occured at each temperature.

When Sample B was held at 38 °C, 3 deg below its initial T_m, this temperature was too low for complete melting to occur [1] (i.e., for the volume to reach the extrapolated liquidus) over a long time span. As judged by the volume change, the melting was about 45 percent [5] complete before recrystallization began to predominate. Partial melting and recrystallization are common to semicrystalline polymers below their melting temperatures, but they require a very long time for this rubber. Presumably, if the same specimen had been held at 39 or 40 °C, it would have completely melted,[6] since upon heating to that temperature only a small amount of crystallinity would have remained (see fig. 1 of ref. [1]), and the orientation between crystalline regions would have been partially disrupted. Somewhere between $T_m - 3$ deg and T_m lies a point of no return, probably corresponding to the temperature where maximum volume increase occurs during the observation period (50 °C in figs. 2 and 3). Another specimen of stark rubber, from a different source (the "Cramer" sample of refs. [4 and 17]), whose melting point was found in a separate experiment (heating at 1 deg/6 weeks) to be 36.5 °C, reached the liquidus in 23 days at 35 °C, after being heated to 35 °C at 1 deg/5 min. There is some evidence [18] that a polymer which was quickly heated into the melting range and held there would go on and completely melt, but if slowly heated, it would not.

After Sample B had been kept at 38 °C for about 10 days, the rate of increase in volume was slow enough so that more than 24 hr was required to be sure that the volume was indeed increasing. After 2 months, the volume *appeared* to remain constant for 2 to 4 weeks at a time, but a slight increase was actually occurring, as became evident over a longer time. Slow increases in volume near the melting temperature have been observed elsewhere [11, 18, 19, 20, 21], although in unoriented systems this does not result in complete melting.

It seems reasonable to interpret the broad melting behavior of Sample A as consisting of two melting ranges overlapped. At the lower temperatures (34 to 41 °C) there is a long succession of small volume increases, representing the melting of the less stable room temperature crystals of more recent vintage, whereas the steep rise and upper shoulder result from the melting of the larger, older crystals. In figure 1 it can be seen that the heights of the increases in volume with time become larger at each temperature from 34 to 37 °C, diminish from 37 to 39 °C, then increase again toward T_m. (This remains true after allowing for differences in time intervals.) In the work described in ref. [4] two distinct melting ranges were observed for a specimen of stark rubber which had undergone additional crystallization. In Sample B, the 38 °C crystals and the older ones all melt within a narrow (5 deg) range.

The slow rate of recrystallization of stark rubber might be expected at these temperatures, but the apparently slow rate of melting above 34 °C requires some explanation. Analysis of unpublished data in this laboratory shows stark rubber to have melting rates (equal to $\Delta\overline{V}/\Delta$ time at a given temperature) similar to those of rubber crystallized by cooling alone in corresponding parts of the melting curves, but the process of melting takes longer to reach static volume in stark rubber. At 38 °C this process was observed for a long time, resulting in a relatively large increase in volume. It would seem that this is connected with a slow (because of high viscosity) cooperative relaxation of residual stress in the oriented rubber. The mechanism for this is not clear.

Heating stark rubber several degrees above its T_m destroys the orientation so that crystallization by cooling and subsequent melting are the same as in ordinary rubber [1]. Consequently it may be asked whether or not the new crystals formed on storage after the partial melting at 38 °C are still oriented. Unoriented rubber crystallized by cooling has a negligible rate of recrystallization above 20 °C and melts near 30 °C or below. In view of the finite rates of recrystallization at 25 and 38 °C as well as the high melting temperatures found in the present work, it seems very likely that the new crystals formed on storage of stark rubber are oriented. Direct evidence for this orientation was not obtained. Such orientation would arise from

[5] The 60 percent melting referred to in ref. [1] is a numerical error.
[6] This would eliminate the upper "tail" [13] usually observed in the melting curve. See figures 1 and 2.

a "memory" of previous sites (oriented liquid) or surface nucleation on oriented crystals.

Recrystallization and melting of stark rubber should be possible at still higher temperatures than those observed in this work.

This research was initiated in collaboration with Leo Mandelkern. The author acknowledges many helpful conversations with J. J. Weeks, and appreciates comments and suggestions by P. K. Sullivan, A. J. Bur, and L. A. Wood.

4. References

[1] D. E. Roberts and L. Mandelkern, J. Res. NBS **54,** 167 (1955) RP2578.
[2] C. J. Newton, L. Mandelkern and D. E. Roberts, J. Res. NBS **55,** 143 (1955) RP2613.
[3] C. J. Newton, L. Mandelkern and D. E. Roberts, J. Appl. Phys. **26,** 1521 (1955).
[4] L. A. Wood and N. Bekkedahl, J. Appl. Phys. **17,** 362 (1946); J. Res. NBS **36,** 489 (1946) RP1718; or Rubber Chem. and Technol. **19,** 1145 (1946).
[5] D. J. Harmon and H. L. Jacobs, J. Appl. Polymer Sci. **10,** 253 (1966).
[6] J. D. Hoffman, J. J. Weeks and W. M. Murphey, J. Res. NBS **63A,** 67 (1959).
[7] P. H. Geil, "Polymer Single Crystals," Interscience, New York, p. 361–366, 1963. Some of the curves in figs. V–48 and V–52 yield calculated values of n near 1 (Data of Gubler, Rabesiaka and Kovacs).
[8] R.-J. Roe and W. R. Krigbaum, Polymer **6,** 231 (1965).
[9] A. van Rossem and J. Lotichius, Kautschuk **5,** 2 (1929); or Rubber Chem. and Technol. **2,** 378 (1929).
[10] J. D. Hoffman, SPE Transactions **4,** 315 (1964).
[11] J. J. Weeks, J. Res. NBS **67A** (Phys. and Chem.) No. 5, 441 (1963).
[12] J. D. Hoffman and J. J. Weeks, J. Chem. Phys. **42,** 4301 (1965).
[13] J. D. Hoffman and J. J. Weeks, J. Res. NBS **66A** (Phys. and Chem.) No. 1, 13 (1962).
[14] J. D. Hoffman and J. I. Lauritzen, Jr., J. Res. NBS **65A** (Phys. and Chem.) No. 4, 297 (1961).
[15] E. Hellmuth and B. Wunderlich, J. Appl. Phys. **36,** 3039 (1965); also Tamio Arakawa and B. Wunderlich, J. Polymer Sci. A2, **4,** 53 (1966).
[16] B. Wunderlich, Polymer **5,** 611 (1964); also D. Bodily and B. Wunderlich, J. Polymer Sci. A2, **4,** 25 (1966).
[17] L. A. Wood, N. Bekkedahl and C. G. Peters, J. Res. NBS **23,** 571 (1939) RP1253; or Rubber Chem. and Technol. **13,** 290 (1940); also L. A. Wood, N. Bekkedahl and R. E. Gibson, J. Res. NBS **35,** 375 (1945) RP1677; or J. Chem. Phys. **13,** 475 (1945).
[18] P. J. Flory, L. Mandelkern and H. K. Hall, J. Am. Chem. Soc. **73,** 2532 (1951).
[19] R. Chiang and P. J. Flory, J. Am. Chem. Soc. **83,** 2857 (1960).
[20] D. E. Roberts and L. Mandelkern, J. Am. Chem. Soc. **77,** 781 (1955).
[21] R. D. Evans, H. R. Mighton and P. J. Flory, J. Am. Chem. Soc. **72,** 2018 (1950).

(Paper 71A3–455)

JOURNAL OF RESEARCH of the National Bureau of Standards—A. Physics and Chemistry
Vol. 71A, No. 3, May–June 1967

Effects of a Distribution of Volume Relaxation Times in the Annealing of BSC Glass

P. B. Macedo and A. Napolitano

Institute for Materials Research, National Bureau of Standards, Washington, D.C. 20234

(February 20, 1967)

The influence of a distribution of relaxation times is studied in annealing experiments. A two-relaxation time model is proposed, which permits the calculation of the distribution of relaxation times from the crossover data of Spinner and Napolitano as well as that of Ritland. This model also characterizes the structure of any glass in terms of two parameters. Thus, quenched equilibrium as well as nonequilibrium glass were compared with rate cooled glasses with respect to their behavior upon further annealing as well as their conductivity at low temperatures with excellent agreement.

Borosilicate crown glass was found to have a narrow distribution of relaxation times which is particular to associated liquid monomers rather than polymers. The results can be explained in terms of a topological model for the distribution of relaxation times. The temperature dependence of the viscosity is due to a true activation energy rather than a free volume effect.

Key Words: Annealing, borosilicate crown glass, glass, index of refraction, relaxation times, two relaxation time model, volume relaxation.

1. Introduction

This study deals with the analysis of some annealing experiments performed on a borosilicate glass by Spinner and Napolitano [1].[1] They established time-index of refraction isotherms for their glass in the transformation region. It is well known that the index of refraction of glass at room temperature is dependent on its thermal history, i.e., the type of heat treatment that the parent liquid received as it was cooled through the transformation region. The index of refraction (N) has been used throughout this study because, of the various physical properties which reflect this change in structure, the refractive index of glass can be most accurately measured. It is assumed throughout that the mechanical deformations associated with change of temperature are purely dilatations.

The thermal history of the glass in the transformation region is shown graphically in figure 1 where the indices of refraction (N) have been plotted versus time and temperature. The equilibrium indices (line AC) for corresponding temperatures are shown on the left in figure 1. The glass at temperature T_1, in equilibrium, will have a constant index of refraction A versus time. If the temperature is changed instantaneously to some lower value T_2, the index of refraction gradually increases to a new equilibrium value C corresponding to the new temperature T_2. The time dependence B–C of this property can be represented as either

(a) a linear (i.e., nonamplitude dependent) distribution of relaxation times or as
(b) a nonlinear single relaxation (i.e., at any instant there is only one relaxation time, but at subsequent intervals the relaxation time changes with the distance from equilibrium) [2].

Even though any curve can be represented by (a) or (b), a systematic series of such curves cannot be

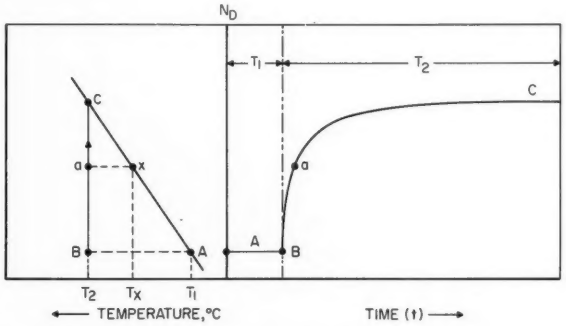

FIGURE 1. *Plot of index of refraction versus temperature and time.*

[1] Figures in brackets indicate the literature references at the end of this paper.

represented by either (a) or (b) [3] only. Unfortunately none of the previous investigators has been able to extract either the distribution of relaxation times or the nonlinear effects [3].

The purpose of this paper is to show how one can find a distribution of relaxation times from such annealing experiments.

The time dependence of the physical properties of liquids has also been investigated by measuring the frequency dependence of these same properties. The time and frequency experiments are equivalent and a mathematical procedure will be considered which can interrelate both types of measurements.

2. Pertinent Viscoelastic Theory

When a distribution of relaxation times is present in a fluid, the complex modulus of compression, K^*, is frequency dependent and can be written [4]

$$K^* = K' + iK'' = K_0 + (K_\infty - K_0)\left[\int_0^\infty \frac{g(\tau)(\omega\tau)^2 d\tau}{1+(\omega\tau)^2} + i\int_0^\infty \frac{g(\tau)\omega\tau d\tau}{1+(\omega\tau)^2}\right] \quad (1)$$

where $K_0 = \lim_{\omega \to 0} K^*$,

$K_\infty = \lim_{\omega \to \infty} K^*$,

ω = the angular frequency,

τ = the relaxation times,

$g(\tau)$ = the relaxation spectrum.

Although this is in many ways a convenient form in which to represent material properties, it is seldom possible to find a unique spectrum to represent a measured response function (either a steady-state function of frequency like the above or a transient function of time like the annealing measurements). This results both from the experimental uncertainty of the measured function and the fact that a complete response function is seldom measured. As an example of the difficulty of finding a unique spectrum, figure 2 due to Macedo and Litovitz [5] shows a plot of reduced modulus versus $\omega\bar{\tau}$, as well as two different $g(\tau)$. First, $g(\tau)$ was assumed to be of the form

$$g(\tau) = (b/(\tau\sqrt{\pi}))\ \exp\left[-b^2(\ln(\tau/\tau'))^2\right] \quad (2)$$

which is a symmetric spectrum in the logarithm of τ centered at τ' whose width is determined by the value of b.

The second fit was obtained by using two delta functions for $g(\tau)$ such that

$$K' = K_0 + \left(\frac{K_\infty - K_0}{2}\right)\left[\frac{(\omega\tau_1)^2}{1+(\omega\tau_1)^2} + \frac{(\omega\tau_2)^2}{1+(\omega\tau_2)^2}\right]. \quad (3)$$

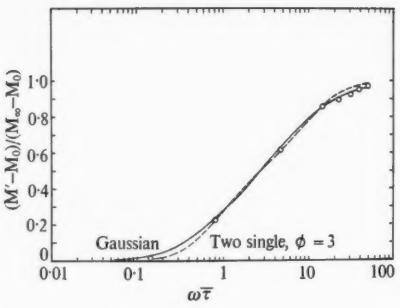

FIGURE 2. *Normalized real part of the modulus versus normalized frequency for B_2O_3 at 550 °C from reference 5.*
$\varphi = (\tau_2/\tau_1)^{1/2}$

Depending on the experiment and subsequent data reduction, one can obtain the relaxation time spectrum at different thermal conditions. In the above example where the modulus was calculated from ultrasonic velocity measurements, one has a spectrum corresponding to a stress relaxation modulus at constant entropy and strain. In the annealing experiment one is measuring the relaxation of a thermally induced strain at constant temperature and stress. Even though there is a rigorous mathematical connection between the constant stress spectrum (retardation) and the constant strain spectrum (relaxation) at either constant temperature or constant entropy, no simple relation between the spectra for the two limiting thermal conditions is available.

3. Analysis of Annealing Experiments

3.1. Thermal History of Crossover

Spinner and Napolitano [1], following some work of Ritland [6] and Kovacs [7], transferred a sample from the middle of an approach curve having an index (a), see figure 1, to a furnace whose temperature (T_x) was so adjusted that the equilibrium value of the index (x) was equal to the approach index (a). This change in temperature was designated as a crossover. The changes in index with time at two of these crossovers are shown in figure 3. The thermal history of these specimens follows:

(a) All specimens were held at 585 °C until the structure was at equilibrium. (Index of refraction was constant with time.)

(b) The specimens were reintroduced into the furnace set at 470 °C for Crossover A and at 500 °C for Crossover B. The curves through the open circles represent the values of index of the specimens for the respective approach curves.

(c) The change in index with time was followed by frequent measurements. When the index had reached a value close to the equilibrium value for a temperature of 544 °C, the sample was transferred to the furnace set at 544 °C and the subsequent change in index followed until it had reached its final equilibrium.

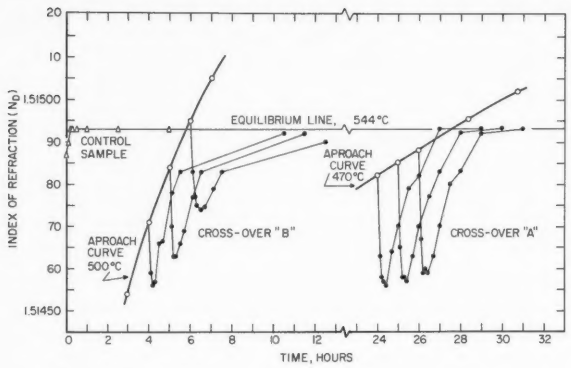

FIGURE 3. *Index versus time at two selected crossovers.*
Equilibrium temperature for both crossovers is 544 °C. Approach temperature for crossover A is 470 °C, and for crossover B, is 500 °C. Data from reference 1.

Several different starting points for this final crossover curve (solid circles) were selected on each of the two approach curves, as shown in figure 3.

3.2. Effect of Distribution of τ on Annealing

Reexamining figure 1, one observes that upon an instantaneous change in temperature from T_1 to T_2, a thermal strain of $N_\infty(T_1)$-$N_\infty(T_2)$, $(B-C)$, is applied to the sample. We will proceed to study the decay or relaxation of this strain.

As noted in the introduction, one cannot represent a series of volume-time curves in terms of any given sum of exponentials with given relaxation times and weighting factors if the total volume change is very large. However, we might well expect, if the total range of volume covered by the final (crossover) curves is small, that a series of such curves could be represented by a sum of exponentials without changing the constants. We shall find that the curves analyzed here can be so represented for any given final equilibrium temperature, even though the various crossover curves are started from different points on the same approach curve or from points on two different approach curves. We will term such behavior "linear."

The simplest such representation which could describe the type of behavior shown in figure 3 is two exponential terms with equal weighting factors, which may be set equal to 1/2. If we were describing the index-time relation between two equilibrium conditions (starting with the glass in equilibrium at one temperature and following the index as a function of time after suddenly changing the temperature to a second value which is then held constant), we would write:

$$N(t)=N_\infty+N(1/2\ e^{-t/\tau_1}+1/2\ e^{-t/\tau_2})$$
$$=1/2\ (M_1(t)+M_2(t)) \qquad (4)$$

where $M_i(t)=N_\infty+N_i e^{-t/\tau_i}$

where $N_1=N_2=N$.

This formulation can be thought of as describing the relaxation (change of volume) to a final equilibrium value following a change in temperature (analogous to an isothermal recovery function) in terms of two separate mechanisms, the first of which relaxes appreciably faster than the second. N_1 and N_2 are measures of the total relaxation undergone by the two separate mechanisms in reaching equilibrium. If the starting point is one of equilibrium ($M_1(0)=M_2(0)$) the two mechanisms will have to relax the same total amount, $N_\infty(T_1)-N_\infty(T_2)$, and N_1 will equal N_2. However, when starting from a nonequilibrium approach curve, N_1 and N_2 will depend on the particular approach curve being followed, as well as on the actual measured index at the crossover point, and in general, will not be equal. To represent this situation eq (4) can be generalized to:

$$N(t)=1/2\ (M_1(t)+M_2(t))=N_\infty$$
$$+1/2\ (N_1e^{-t/\tau_1}+N_2e^{-t/\tau_2}). \qquad (5)$$

Figure 4 shows schematically the time dependence of N, M_1, and M_2 for a glass initially at equilibrium. As the structure rearranges itself to the new equilibrium, M_1 will rise faster since it is associated with the shorter relaxation time τ_1, while M_2 will change more slowly. Thus, around the bend of the approach curve, there will be the largest difference between M_1 and M_2 in the glass. As time progresses, M_1 will reach its equilibrium value for T_2 first and stay there. From then on the spread between M_1 and M_2 narrows because the slow relaxation process continuously approaches the same equilibrium value at a slower rate. Finally, when the structure is completely at the new equilibrium the spread becomes zero, and one has again an equilibrium glass ($M_1=M_2$). At a crossover (a) the fast relaxation time (τ) corresponds to an index M_1 higher than the (average) measured value, N, and the slow relaxation time (τ_2) corresponds to an index M_2 lower than N.

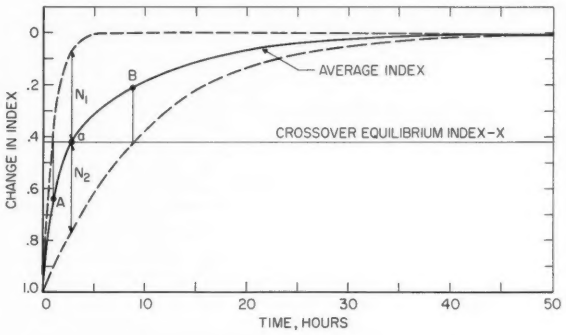

FIGURE 4. *Illustration of two relaxation times represented by upper and lower dashed curves.*
The average or measured index is given by the solid line. The crossover equilibrium index x and the transfer point are also shown.

248-733 O-67—4

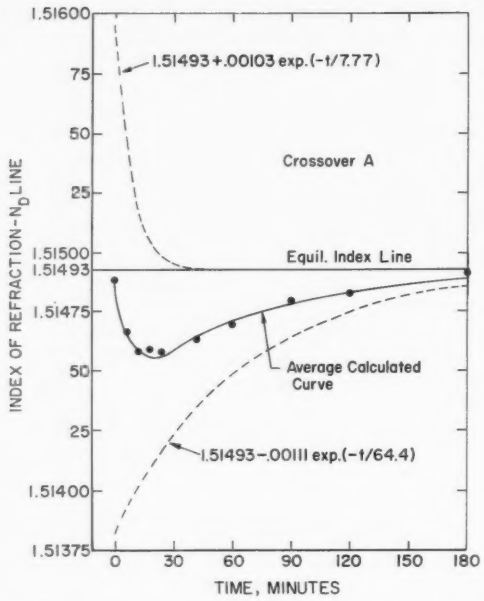

FIGURE 5. *Crossover A—Solid curve is the average of the two dashed curves, each having a single relaxation time; the fast relaxation time ($\tau_1 = 7.77$ min), above; and the slow relaxation time ($\tau_2 = 64.4$ min) below the equilibrium line $N_\infty = 1.51493$.*

Here $N_1 = 0.00103$ and $N_2 = -0.00111$. Points are third experimental set from crossover A, in figure 4. Data from reference 1.

If the index at the point of crossover, $N(0)$, is equal to the equilibrium index, $N(\infty)$ at the crossover temperature T_x, then $N_2 = -N_1$. A prerequisite for a minimum in the crossover is that N_1 and N_2 have opposite signs. This is fulfilled when N has a value between A and B in figure 4.

The crossover curves were analyzed as follows:

(a) The logarithm of the difference between the equilibrium index and actual index was plotted as a function of time. From the best straight line through the final points, both τ_2 and N_2 were calculated, assuming $t \gg \tau_1$ so $M_1(t)$ in eq (5) can be set equal to N_∞.

(b) From the initial value of the index at crossover, N_0 and the equilibrium value, N_∞, N_1 was calculated from

$$\Delta = N_0 - N_\infty = \frac{N_1 + N_2}{2}. \tag{6}$$

(c) From the time, t_m, at which the index reached its minimum value, τ_1 was calculated from the equation

$$\frac{\partial N}{\partial t} = -[N_1 \exp(-t_m/\tau_1)]/\tau_1 - [N_2 \exp(-t_m/\tau_2)]/\tau_2 = 0. \tag{7}$$

The results of this computation for the crossover A curve with N_0 closest to N_∞ is shown in figure 5. The solid line is the average of the upper curve, M_1, and the lower curve, M_2. The agreement of the solid calculated curve with the actual experimental points is seen to be good.

3.3. Nonlinearity in Crossover Region

The definition of linearity adopted requires that the relaxation times at a crossover are independent of amplitude (i.e., N_1 and N_2). Since in the linear case the relaxation times are characteristic of the equilibrium temperature rather than the approach curve, two crossovers having the same equilibrium temperature will have the same τ_1 and τ_2 and the same weighting factors (½), regardless of approach temperature.

The two crossovers in figure 3 present themselves as a natural check for linearity. This is done by applying τ_1 and τ_2, already computed for crossover A, to crossover B. Equations (5) and (6) were combined to give:

$$N - N_\infty = \frac{N_1}{2}[\exp(-t/\tau_1) - \exp(-t/\tau_2)] + \Delta \exp(-t/\tau_2). \tag{8}$$

Solving for N_1 gives:

$$N_1 = 2\,\frac{(N - N_\infty) - \Delta \exp(-t/\tau_2)}{\exp(-t/\tau_1) - \exp(-t/\tau_2)}. \tag{9}$$

From this equation the average value of N_1 for crossover B was obtained using τ_1 and τ_2 from crossover A and Δ from eq 6. Figure 6 compares the calculated curve (solid line) with the corresponding experimental points (the middle set from crossover B in fig. 3). This fit is seen to be comparable with that observed for crossover A (fig. 5). Linearity of the relaxation process in the crossover region with respect to a given equilibrium temperature is thus demonstrated to within the experimental uncertainty.

3.4. Further Experiments

Spinner and Napolitano (1) also reported data for a third crossover (C) which corresponds to an initial equilibrium temperature of 585 °C, approach temperature 477 °C, and equilibrium 527 °C. The results of a calculation performed as above are shown in figure 7. Inasmuch as this crossover contains the largest number of experimental points, the agreement of the computed curve with these experimental points is even more impressive than that for the other two crossovers shown. For this crossover, τ_1 was computed to be 75 min and τ_2, 540 min.

An encouraging result is that $(\tau_2/\tau_1)_{527\,°C} = 7.2$ is within the experimental uncertainty of the value of 8.3 found at 544 °C. Since the distribution of relaxation times is temperature independent in most liquids, one can assume that this is the case here, even though the temperature range is not large enough to justify a conclusive statement.

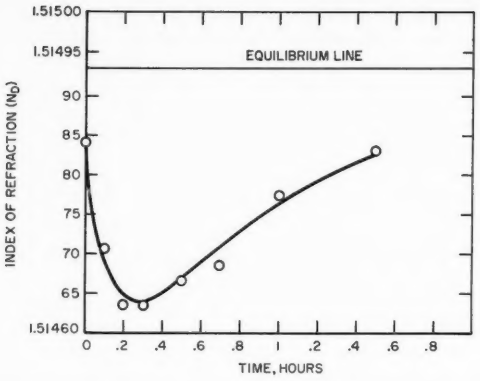

FIGURE 6. *Crossover B—Solid curve is computed result using fast and slow relaxation times found for crossover A.*

In this case $N_1 = +0.00069$ and $N_2 = -0.00088$. Points are middle experimental set (ref. [1]) from crossover B, in figure 4.

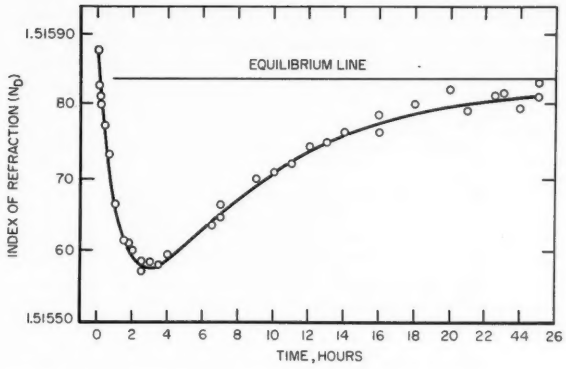

FIGURE 7. *Crossover C—Equilibrium temperature 527 °C and $N_\infty = 1.51584$, approach temperature 477 °C.*

Solid line is computed curve based on two single relaxation decay curves (not shown), and shows fit to experimental points (ref. [1]). Here $\tau_1 = 75$ min; $N_1 = 0.00094$; and $\tau_2 = 540$ min, $N_2 = -0.00086$.

The annealing experiments of Spinner and Napolitano are based on the following experiment of Ritland [6]. A sample of BSC glass was cooled through the glass transformation range at a constant rate. Later it was reintroduced in a furnace whose temperature matched the sample's fictive temperature. Figure 8 shows the time dependence of the specimen after reinsertion. Even though the dip is slightly shallower the curve is similar. Unfortunately, Ritland did not take enough data at "long" times for accurate description of τ_2. Since the composition of Ritland's glass is very close to that of Spinner and Napolitano, it was decided to use the same ratio of $\tau_2/\tau_1 = 8$ and fit the dip by adjusting the average τ and the initial spread in index. Again, a good fit was obtained, indicating once more, that the distribution of relaxation times is a property of BSC glass and not of the thermal history.

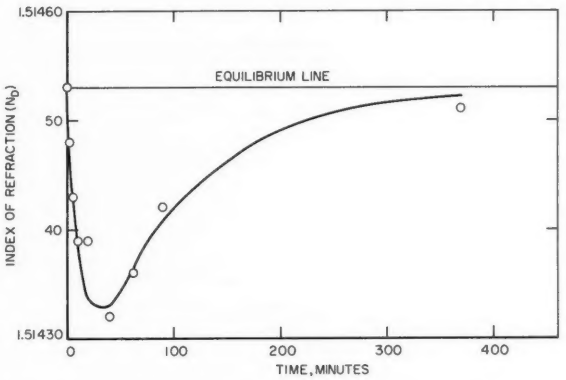

FIGURE 8. *Solid line is computed curve based on two single relaxation decay curves.*

Here $\tau_1 = 12$ min, $N_1 = 0.00064$ and $\tau_2 = 96$ min, $N_2 = -0.00064$, $N_\infty = 1.51453$, and shows fit to experimental points [6]. Initial distribution of index was obtained by rate cooling samples.

3.5. Comparison of $\bar{\tau}_{vs}$ and $\bar{\tau}_s$

The distribution of volume relaxation times has been calculated at two temperatures (544 and 527 °C) for BSC glass. From these a weighted average relaxation time at constant pressure and temperature can be defined by:

$$\bar{\tau}_{pT} = \Sigma g_i \tau_i = 1/2\tau_1 + 1/2\tau_2 . \tag{10}$$

On the basis of the values of $\bar{\tau}_{pT}$ for each of these temperatures the apparent activation energy for volume relaxation, H_b, was computed from the well-known relation

$$\bar{\tau}_{pT} = Ae^{H_b/RT} \tag{11}$$

where A is an arbitrary constant. H_b was found to be 155 kcal/mole (6.49×10^5 J/mole). This value is comparable with the activation energy for shear viscosity, $H_s = 140$ kcal/mole (5.86×10^5 J/mole), over about the same temperature range, based on direct measurement of the shear viscosity by the fiber elongation method [8].

According to a tabulation by Litovitz and Davis [9] the ratio of the average adiabatic isochoric relaxation time for dilatation, $\bar{\tau}_{vs}$, to Maxwell's average shear relaxation time, $\bar{\tau}_s$, turns out to be between about 0.79 and 4.60 for a number of associated liquids. Hence a calculation of this ratio should give us a check on whether the relaxation times as calculated here to represent thermally induced volume changes can reasonably be equated to relaxation times associated with purely mechanical deformations.

The isothermal isobaric average relaxation (retardation) time, $\bar{\tau}_{PT}$, at 544 °C was calculated from eq (10) to be 2.17×10^3 sec. It is assumed that the relationship

$$\bar{\tau}_{PT}/\bar{\tau}_{vs} = (\kappa_{T_0}/\kappa_{T_\infty})(C_{v_0}/C_{v_\infty}) \tag{12}$$

derived for a single relaxation mechanism will be adequate for the comparison desired here. This gives, using isothermal compressibilities, κ_T, and isochoric specific heat, C_v, from references [11, 12, and 13] $\bar{\tau}_{vs}=653$ sec.

The average shear relaxation time $\bar{\tau}_s$, was computed [4] from

$$\bar{\tau}_s=\eta_s/G_\infty \tag{13}$$

where G_∞ is the glass modulus of rigidity [14] and at 544 °C, was found to be 303 sec. Thus, the ratio $\bar{\tau}_{vs}/\bar{\tau}_s$, was 2.2, a value in good agreement with the above mentioned Litovitz and Davis compilation for associated liquids. Therefore, the relaxation times calculated here can reasonably be equated with the relaxation process associated with purely mechanical deformations.

The width of the distribution found in BSC glass, as given by $\tau_2/\tau_1=8$ is comparable with that found in most liquids. For example, B_2O_3 at 550 °C (fig. 2) is a little wider, $\tau_2/\tau_1=9$, but at higher temperatures it is narrower [5]. The associated organic liquids, whose distributions are the best known, have about the same width provided they are monomeric [9]. For polymeric liquids this ratio is meaningless but would be from 10^3 to 10^6. Thus one can conclude that BSC is not polymeric.

4. Discussion

The only physical model that would readily predict two relaxation times would be two immiscible phases. Even though there is a possibility that these relaxation times be single they should be separated by many orders of magnitude, since one of the immiscible phases in the silicate system is usually almost pure SiO_2 with its associated high viscosity (very long relaxation time). Also, had there been such an immiscibility then the temperature cycling of Spinner and Napolitano would not have been reproducible.

We will now present a microscopic model to explain the distribution of relaxation times. The topological model will consist of a distribution of micro regions in space, each with a different relaxation time. Such regions have been postulated by various authors. For example, Bockris et al. [15], pictured an "iceberg structure" for silicate glasses. Litovitz and McDuffie [16] and Macedo and Litovitz [5] have proposed that the distribution of relaxation times as well as the non-Arrhenius temperature dependence of the structural relaxation time in associated liquids is due to the cooperative behavior of molecules and the possible existence of clusters.

In order to explain the conductivity experiments, which will be described below, the glass is assumed to have two microdisperse regions which are interconnected. This should be expected from both the immiscibility work of Haller [17] and the immiscibility precursor stage investigated by Ohlberg and Parsons [18]. The dimension of these micro regions must be smaller than 150 Å in order not to be detected by light scattering or (ordinarily) by the electron microscope. (Zarzycki and Mezard [19] claim to have seen such regions even in single component glasses by an elaborate process using transmission in an electron microscope.) It is assumed that the relaxation time of each region is a function only of its own structure, i.e.,

$$\tau_i=f(M_i, T)\neq f'(M_{j\neq i}). \tag{14}$$

This equation is equivalent to assuming that the hybrid equation of Macedo and Litovitz [20] is good for each separate region, rather than for the average values.

Evidence for the topological model can be obtained from the conductivity experiments of Ritland [6]. These conductivity measurements were made well below the glass transition and there were no structural rearrangements taking place during the measurements. The conductivity of a glass below T_g is known to be due to alkali diffusion through the immobile lattice. This ionic diffusion has been shown to have a distribution of relaxation times. From rate theory one can calculate the conductivity due to ionic jumps for a single relaxational process to be

$$\sigma=\frac{a^2n}{ckT\tau_l} \tag{15}$$

where a is the "jump distance"; n, the number density of ions; τ_l, the ionic relaxation time; and c, a geometrical constant. Let us consider the effect of these two microdispersed regions on the conductivity. First, whatever caused region one to have a shorter volume relaxation time, such as higher disorder, less intramolecular bonding, etc., may reasonably be assumed to cause the ionic relaxation time in region one to be shorter. Thus, one can write for the conductivity of each region:

$$\sigma_i=\frac{a^2n}{ckT\tau_{li}}, \tag{16}$$

where the nonindex quantities are the same for both regions. Since each region is interconnected, the measured conductivity can be approximated by

$$\sigma=\sigma_1+\sigma_2=\frac{a^2n}{ckT}\qquad\left(\frac{1}{\tau_{l_1}}+\frac{1}{\tau_{l_2}}\right). \tag{17}$$

In fact, if $\tau_{l_1}\cong(1/8)\tau_{l_2}$, then the conductivity is controlled primarily by τ_{l_1}. Note that here is where the topological model differs from the phenomenological approach. Had one assumed a distribution of relaxation times in a homogeneous material then

$$\sigma=\frac{a^2n}{ckT(\tau_{l_1}+\tau_{l_2})}, \tag{18}$$

and, provided $8\tau_{l_1}\cong\tau_{l_2}$, the conductivity would have been controlled by τ_{l_2}.

Figure 9 due to Ritland shows resistivity versus index for glasses that were either cooled at constant rate through the glass transformation region (rate cooled) or quenched from an equilibrium configuration (soaked). It can be seen from this figure that the variation of resistivity with thermal history for a given index is of the same order of magnitude as the variation with index for a given type of annealing experiment. The resistivity is not a single valued function of the average structure as represented by the index. Thus, any model in which the relaxation is a function of the average structure, such as Tool's fictive temperature [21], must be ruled out. In the topological model the conductivity is only a function of τ_1, which in turn is a function of M_1 and not M_2.

In a previous section, it was found that the rate cooled glass with an index of 1.51453 had $M_1 = 1.51517$ associated with τ_1 and $M_2 = 1.51389$ associated with τ_2. Since as a first approximation resistivity is only controlled by structure 1, the resistivity of the rate cooled sample having an index 1.51453 should be the same as that of the soaked sample having an index 1.51517 because both have the same values of M_1. This point is shown plotted in figure 9. If a line is drawn through the Ritland's soak specimen data points it will intercept his rate cooled curve. This intersection should only occur when the rate sample's cooling rate approaches the cooling rate of the chilled specimen. Therefore, these lines through the rate cooled and chilled specimen data points should be almost parallel. Thus for comparison a line is drawn parallel to the rate cooled specimen and through the "theoretical" point. Since this line is above one experimental point and below the other, it is considered within the experimental accuracy of the soaked data. Note, that eq (18) due to the phenomenological approach would predict that σ is a function of either M_2 or $M_1 + M_2$ depending on the assumed functional dependence of τ_2, neither of which will fit the data. Even though the data are sparse in this experiment it has been shown that the two-parameter topological model represents the state of the glass regardless of the heat treatment.

Rate Cooling. The best experiment to show whether the apparent temperature dependence of the viscosity is directly due to temperature or indirectly due to structure is the rate cooling process.

When a glass sample is cooled through the glass transition region at a constant rate, initially the sample will follow the equilibrium index curve (see fig. 10). When the long volume relaxation time, τ_2, becomes comparable with the cooling rate, M_2 will lag behind the equilibrium value N_∞. As the temperature continues to lower τ_2 becomes longer and longer compared with the cooling rate, and eventually the structure is thermally arrested at a value of the relaxation time, τ_R, which is governed by the cooling rate. Upon further cooling M_2 remains constant. M_1 will follow a similar history and τ_1 will also be finally arrested at the same value, τ_R.

Thus as a sample is cooled through the glass transition at a constant rate each relaxing process will be thermally arrested at the same value of relaxation time, τ_R, which is a function of the cooling rate. If the values of the relaxation times are only a function of structure, then, at any temperature, all the relaxation times in a rate cooled glass cooled at the same rate should be equal. The crossover data of Ritland, figure 8, clearly demonstrates that this is not the case.

If we assume that the hybrid equation is completely controlled by the activation energy (i.e., $f(T)$ is given by eq (11)), the difference in index $M_1 - M_2$ in the rate cooled glass represents the difference in temperatures required for τ_1 to equal τ_2. One, then, can write for the activation energy

$$H_b = R \ln (\tau_2/\tau_1)\{1/T_1 - 1/T_2\}^{-1} \qquad (19)$$

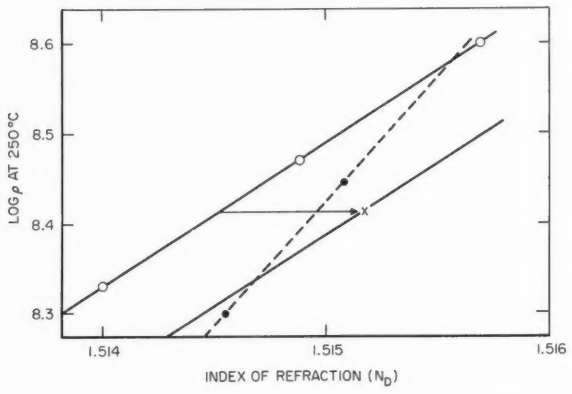

FIGURE 9. *Resistivity versus refractive index for rate cooled,* O, *and soak,* ●, *samples;* X *predicted value. Data from reference* [6].

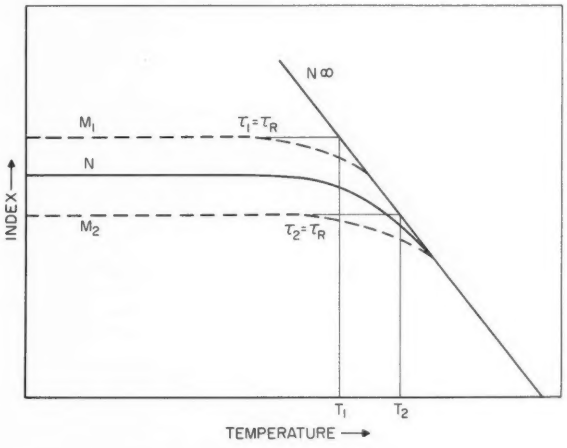

FIGURE 10. *Plot of index versus temperature for a rate cooled sample.*
Equilibrium index (N_∞) curve is also shown plotted.

in which $T_1 = T_R - N_1 \Big/ \frac{\partial N}{\partial T}$ and similarly for T_2; T_R is the crossover temperature of Ritland; and $\partial N/\partial T$ was taken from Spinner and Napolitano. The activation energy calculated from eq (19) is 122 kcal/mol (5.12×10^5 J/mol) which corresponds favorably with the 140 kcal/mol (5.86×10^5 J/mol) obtained from the viscosity data.

One must conclude that most of the apparent activation energy of viscous flow is due to a true activation energy effect. This is in direct contradiction with recent papers on the interpretation of the Fulcher equation by W.L.F. [22], Cohen and Turnbull [23], but agrees with the work of Maurer [24], who annealed glass under pressure.

5. Conclusion

It has been shown how one can obtain the distribution of relaxation times by proper analysis of annealing experiments. A physical model for the distribution was proposed, and it, the topological model, was found to explain not only the temperature dependence of viscosity, but also the resistivity experiments of Ritland. In doing so, Tool's fictive temperature was extended to two parameters, which can explain both equilibrium and nonequilibrium behavior of glasses. The temperature dependence of the viscosity was found to be due to a true activation energy rather than a free volume effect. The stress (thermal) strain experiment gives a distribution many decades narrower than the stress (pressure) strain work previously done [25, 26] in the relaxation region. Since no pressure was applied, no "delayed elastic relaxation" takes place in the thermal experiment. Thus, there is the added advantage of only measuring the structural distribution of relaxation times.

This analysis was applied to a borosilicate crown glass, and it was found that $\tau_2/\tau_1 \approx 8$ (Gaussian $b=0.6$). This narrow distribution indicates that the flow in this material is monomeric rather than polymeric ($10^3 < \tau_2/\tau_1 \leqq 10^6$). The monomeric nature of silicate glasses has been postulated by Bockris et al. [15], from zero frequency compressibility measurements at high temperatures, but was questioned when Westman [27] proved that phosphate glasses are polymeric. The present work together with Macedo and Litovitz [5] distribution of relaxation times in B_2O_3 indicates that the iceberg picture of Bockris is correct for the borates and silicates. The ratio of the average volume to average shear relaxation time was found to be ≈ 2, in good agreement with other associated liquids [9].

6. References

[1] S. Spinner and A. Napolitano, J. Res. NBS **70A** (Phys. and Chem.), No. 2, 147–152 (1966).
[2] E. U. Condon, The Glass Industry **33**, 307, 322–3 (1952).
[3] M. Goldstein, Modern Aspects of the Vitreous State, Vol. **3**, pp. 90–125 (Butterworths, Washington, D.C., 1964).
[4] K. F. Herzfeld and T. A. Litovitz, Absorption and Dispersion of Ultrasonic Waves (Academic Press, New York and London, 1959).
[5] P. B. Macedo and T. A. Litovitz, Phys. and Chem. of Glasses **6**, 69 (1965).
[6] H. N. Ritland, J. Am. Ceram. Soc. **39**, 403 (1956).
[7] A. J. Kovacs, Fortschr. Hockpolym-Forsch. **3**, 394 (1963).
[8] A. Napolitano and E. G. Hawkins, J. Res. NBS **68A** (Phys. and Chem.), No. 5, 439–448 (1964).
[9] T. A. Litovitz and C. M. Davis, Physical Acoustics, Vol. **II**, ch. 5 (Academic Press, New York and London, 1965).
[10] H. J. Bauer, Physical Acoustics, Vol. **II**, ch. 2 (Academic Press, New York and London, 1965).
[11] Handbook of Glass Manufacture, F. V. Tooley, editor (Ogden Publishing Co., New York, N.Y., 1953).
[12] A. Cooper, private communication.
[13] H. N. Ritland, J. Am. Ceram. Soc. **37**, 370 (1954).
[14] S. Spinner, J. Am. Ceram. Soc. **39**, 113 (1956).
[15] J. O'M Bockris and Kojoneu, J. Phys. Chem. **82**, 4493 (1960).
[16] T. A. Litovitz and G. McDuffie, J. Chem. Phys. **39**, 729 (1963).
[17] W. Haller, J. Chem. Phys. **42**, 686 (1965).
[18] S. M. Ohlberg and J. M. Parsons, Physics of Non-Crystalline Solids, Delf Conference (North Holland Publishing Co., Amsterdam, 1964).
[19] J. Zarzycki and R. Mezard, J. Phys. and Chem. of Glasses **3**, 163 (1962).
[20] P. B. Macedo and T. A. Litovitz, J. Chem. Phys. **42**, 245 (1965).
[21] (a) A. Q. Tool, J. Am. Ceram. Soc. **29**, 240 (1948). (b) A. Q. Tool, L. W. Tilton and J. B. Saunders, J. Res. NBS **38**, 519 (1947) RP1793.
[22] M. L. Williams, R. F. Landel, and J. D. Ferry, J. Am. Chem. Soc. **77**, 3701 (1955).
[23] M. H. Cohen and D. Turnbull, J. Chem. Phys. **31**, 1164 (1959).
[24] R. D. Maurer, J. Am. Ceram. Soc. **40**, 211 (1957).
[25] C. R. Kurkjian, Phys. and Chem. of Glasses **4**, 128 (1963).
[26] J. DeBast and P. Gilard, Phys. and Chem. of Glasses **4**, 117 (1963).
[27] A. E. R. Westman, Modern Aspects of the Vitreous State, Vol. **I**, pp 63–91 (Butterworths, Washington, D.C. 1960).

(Paper 71A3–456)

JOURNAL OF RESEARCH of the National Bureau of Standards—A. Physics and Chemistry
Vol. 71A, No. 3, May–June 1967

Publications of the National Bureau of Standards*

Selected Abstracts

Infrared reflectances of metals at cryogenic temperatures—a compilation from the literature, P. F. Dickson and M. C. Jones, *Tech. Note 348 (Oct. 14, 1966), 40 cents.*
Spectral and total reflectances for metals at cryogenic temperatures in the infrared wavelength region are compiled from the literature. Information concerning sample preparation and purity, radiation source, and methods of reflectance measurement are also presented. Observations regarding the effects on reflectance of temperature, oxide layer, wavelength, and sample preparation are given.

Key Words: Compilation, cryogenic, infrared, metals, reflectance.

The design and operation of a high voltage calibration facility, W. W. Scott, Jr., *Tech. Note 349 (Nov. 10, 1966), 25 cents.*
The high-voltage calibration facility, in operation for seven years at the National Bureau of Standards Radio Standards Laboratory (RSL) but now at NBS Washington, is described with emphasis on several novel construction features and calibration techniques. The more usual calibration techniques are also outlined for the assistance of those personnel in standards laboratories assigned the task of calibrating with high accuracy, electrostatic voltmeters, resistive dividers, and potential transformers at high voltage. Precautions, based on experience in the calibration and use of high voltage standards, are given so that certain errors may be avoided by the users.

Key Words: Alternating-current, calibration, direct-current, high-voltage, ratio, safety, standards enclosure, transformer, voltage-divider, voltmeter.

Fortran programs for the calculation of Wigner 3*j*, 6*j*, and 9*j* coefficients for angular momenta 80, R. S. Caswell and L. C. Maximon, *Tech. Note 409 (Nov. 15, 1966), 40 cents.*
Fortran II and Fortran IV programs are given for the calculation of Wigner 3*j*, 6*j*, and 9*j* coefficients containing individual angular momenta less than or equal to 80. The large numbers, resulting from the factorials which appear in the expressions for these coefficients, are handled by taking logarithms and performing most of the pertinent arithmetic with the logarithms. The alternating series involved in the expressions for the 3*j* and 6*j* coefficients are summed arithmetically in double precision. We present two versions of the basic program for the calculation of these coefficients (each version being given both in Fortran II and in Fortran IV). All programs are called as single-precision Fortran functions. The difference between Versions I and II is in the internal structure of these programs. In Version I, only the series summation is in double precision, resulting in a faster program which occupies less memory in the computer, the computation time being of the order of 0.001 to 0.01 sec per 6*j* and 0.1 to 1 sec per 9*j*. Version II, being entirely in double precision internally, is much more accurate (the errors being of the order of one percent of the errors in Version I), but the computation time for a given coefficient is approximately 50 percent greater than in Version I. Information relative to the accuracy and memory requirements of the two versions of the program is provided, and Fortran II and IV lists of the programs and calling instructions are given.

Key Words: Fortran program, Wigner coefficients, quantum theory of angular momentum, 3*j* coefficient, 6*j* coefficient, 9*j* coefficient, Clebsch-Gordan coefficients.

Abstraction of hydrogen atoms from isobutane-d_9 by methylene, M. L. Halberstadt and J. R. McNesby, *J. Chem. Phys.* **45,** *No. 5, 1666–1669 (Sept. 1, 1966).*
The photolysis of ketene at 3130 Å in the presence of isobutane-d_9 was carried out at 320 °C in order to determine the mechanism of methyl radical formation. The two possibilities considered are:
Mechanism I—insertion followed by internal relaxation and finally expulsion of a methyl radical.
Mechanism II—direct abstraction.
Mechanism II was found to be the only detectable mode of methyl radical formation. The effect of pressure on the isotopic methane distribution was studied and an attempt is made to explain the effect in terms of a DeMore-Benson process.

Key Words: Abstraction, isobutane-d_9, ketene, methylene, photolysis.

Chemisorption of nitric oxide on tungsten, J. T. Yates, Jr., and T. E. Madey, *J. Chem. Phys.* **43,** *No. 5, 1623–1634 (Sept. 1, 1966).*
The chemisorption of NO on polycrystalline W has been investigated using a combination of ultrahigh vacuum techniques: flash desorption mass spectroscopy and field emission microscopy. It has been found that NO chemisorbs non-dissociatively on W at room temperature. Dissociation occurs at elevated temperature with an activation energy of about 47 kcal/mol (197 kJ/mol). Kinetic evidence indicates that dissociation involves the interaction of an adsorbed NO molecule with a neighbor empty site. At high NO coverage, dissociation is rate controlling for the liberation of ω-mode nitrogen near 1000 °K. Heating of an NO-shadowed W field emission tip above ~ 700 °K results in the formation of a *receding* boundary which remains sharp during the entire course of its backward motion over the initially covered region. This behavior is consistent with a model involving dissociation of NO at the boundary where empty sites are available. For monolayer NO (1.4×10^{15} molecules cm^{-2}) on polycrystalline W, $\Delta\phi=+1.85\pm0.10$ eV; this corresponds to an average surface dipole moment of 0.35 debye per chemisorbed NO molecule at full coverage.

Key Words: Chemisorption, nitric oxide, dissociation, tungsten, field emission microscopy, kinetic, adsorption, desorption, surface diffusion, surface, work function.

Electron affinity of tungsten determined by its positive and negative self-surface ionization, M. D. Scheer and J. Fine, *Phys. Rev. Letters* **17,** *No. 6, 283–284 (Aug. 8, 1966).*
It has been shown that negative as well as positive ions are evaporated from an incandescent tungsten surface thereby establishing that the tungsten atom has a positive electron affinity. When equilibrium is assumed between the metal surface and the evaporating ions, a quantitative estimate of the electron affinity can be obtained from a measurement of the positive to negative ion emission ratio at some known surface temperature. Measurements in the 2260 to 2350 °K temperature range yield a value of 0.5 eV for the electron affinity of tungsten.

Key Words: Electron affinity, tungsten, positive and negative self-surface ionization.

Mass-spectrometric investigation of the nickel-fluorine surface reaction, J. D. McKinley, *J. Chem. Phys.* **45,** *No. 5, 1690–1693 (Oct. 1, 1966).*
Mass spectrometic measurements have been made of the reaction of polycrystalline nickel at temperatures between 900 and 1600 °K

with fluorine at pressures between 10^{-7} and 10^{-4} torr. Gaseous NiF, NiF_2 and F are the major products, and are formed rapidly on the surface at rates linear with fluorine pressure. NiF is present on the surface over the entire temperature range and desorbs above 1100 °C; the desorption step involves rupture of a Ni(substrate)–NiF bond and has an activation energy of 28 kcal mol^{-1}. NiF_2 formation and desorption are important between 900 and 1600 °K with a maximum rate at 1250–1300 °K. The rate limiting step in the formation of NiF_2 has an activation energy of 39 kcal mol^{-1} and is probably dissociation of fluorine on the surface.

Key Words: Nickel, fluorine, surface reaction, kinetics, high temperature, mass spectrometry.

Mass-spectrometric study of the rate of the reaction CO + OH, J. T. Herron, *J. Chem. Phys.* **45,** *No. 5, 1854–1855 (Sept. 1, 1966).*
The rate constant of the reaction $CO + OH \rightarrow CO_2 + H$ has been directly measured at 300 °K to be $5.4 \pm 2.0 \times 10^{10}$ cm^3 $mol^{-1}sec^{-1}$. This value combined with published high temperature rate data leads to $k = 9.2 \times 10^{11} \exp(-1000/RT)$.

Key Words: Hydroxyl-radical, carbon-monoxide, rate-constant, activation-energy, reaction, carbon dioxide, hydrogen atom, gas phase, atom-transfer.

Matrix-isolation study of the photolysis of cyanogen azide. II. The symmetric stretching fundamental of the free radical NCN, D. E. Milligan and M. E. Jacox, *J. Chem. Phys.* **45,** *No. 5, 1387–1391 (Sept. 1, 1966).*
The photolysis of $Ar:N_3CN$ samples at 14 °K with the full light of a cadmium arc has been found to permit complete conversion of the cyanogen azide to the free radical NCN, plus molecular nitrogen. At the high concentration of NCN thus achieved a weak absorption appears at 2672 cm^{-1}. The photolytic behavior of this feature and its shifts upon isotopic substitution support its assignment as the combination band ($\nu_1 + \nu_3$) of NCN, permitting deduction of a value of 1197 cm^{-1} for ν_1 of this species. The thermodynamic properties of NCN have been revised in accord with this assignment. The carbon-nitrogen stretching force constant approaches a value characteristic of a doubly bonded species, and the stretching interaction constant is relatively large and positive. Cyanogen azide photolyzes in both its 2750 and its 2200 A absorption regions to produce $NCN + N_2$. However, NCN itself photolyzes when subjected to radiation near 2500 A, producing carbon atoms in the ^3P state, which, in turn, may react with N_2 to form the free radical NCN.

Key Words: Carbon atom production, carbon atom reactions, cyanogen azide, force constants, infrared spectrum, NCN free radical, thermodynamic properties, ultraviolet photolysis.

Pseudonatural orbitals as a basis for the superposition of configurations. I. He_2^+, C. Edmiston and M. Krauss, *J. Chem. Phys.* **45,** *No. 5, 1833–1839 (Sept. 1, 1966).*
The use of pseudonatural orbitals (PNO) is proposed to improve the rate of convergence in the superposition of configurations (SOC). Natural orbitals are determined for selected electron pairs in the Hartree-Fock field of the *n*-2 electron core and are then used as the basis for the total SOC calculation. Since these natural orbitals are not natural for the *n*-electron system they are considered false or pseudonatural orbitals when used in the *n*-electron problem.
The PNO basis has been applied to He_2^+ and H_3 to test the convergence. Complete results are reported here only for He_2^+. The PNOs are quite successful in speeding up the convergence of the SOC and rendering the calculation of correlation energy quite practical in general. Gaussian type orbitals (GTO) are used throughout and were not a serious impediment to obtaining quantitative accuracy. In fact the large number of unoccupied Hartree-Fock orbitals consequent upon the use of a GTO basis permit a straightforward determination of the PNO orbitals.

Key Words: Molecular quantum mechanics, electronic energy, pseudonatural orbitals, He_2^+.

A zero-range treatment of the three-body photodisintegration cross section of ^3H and ^3He, J. M. Knight, J. S. O'Connell, and F. Prats, *Phys. Letters* **22,** *No. 3, 322–325 (Aug. 15, 1966).*
Zero-range theory is used to construct bound and continuum state wave functions. The total and differential electric dipole photodisintegration cross sections for three-body breakup of ^3He and ^3H are calculated using these wave functions.

Key Words: Zero-range, ^3H, ^3He, photodisintegration, cross section, differential cross section.

Bandlike structure from continuum-continuum emission: the He_2 600-Å bands, F. H. Mies and A. L. Smith, *J. Chem. Phys.* **45,** *No. 3, 994–1000 (Aug. 1, 1966).*
The continuous spectrum produced by the radiative deexcitation of metastable atoms by atom impact is an example of molecular continuum-continuum transitions. It is shown that if the upper molecular state has a deep attractive well and the lower state is repulsive, the continuous spectrum will show banded structure similar to that obtained in bound-continuum transitions from high vibrational states. The analysis is applied to the radiative deexcitation of $He(2^1S)$ by He, which gives rise to the "600 Å bands." The structure and temperature dependence of these bands are well explained as banded continuum-continuum emission. Structured continua observed in other rare gases are discussed in terms of the molecular states involved.

Key Words: Theory, continuous, spectra, He_2, vacuum-ultraviolet, atomic, collisions, He, metastable, radiative, deexcitation.

Determination of the effective force constants between a substitutional impurity and its nearest neighbors in an alkali halide crystal, R. A. MacDonald, *Phys. Rev.* **150,** *No. 2, 597–602 (Oct. 14, 1966).*
The forces between a substitutional impurity and its nearest neighbors in an alkali halide crystal with rocksalt structure are determined in the harmonic approximation. The deformation dipole model is used for the lattice dynamics of the perfect crystal. Two independent force constants are involved in the problem which is treated in two ways. First, the two force constants are obtained from the equation of motion for the local mode of vibration using experimental values of the local mode frequencies due to H^- and D^- impurities in NaCl and KCl, and assuming that the force constants are the same for different isotopes of the impurity. This method yields no real solutions for the force constants for *U*-centers in KCl. The second method assumes that the force constants for the impurity (say H^-) are the same as those in an alkali hydride crystal having the same lattice spacing as the alkali halide crystal. A Born-Mayer interatomic potential is used for this calculation. The first method gives 45 percent softening of the force constants for *U*-centers in NaCl, the second method gives 70 percent softening. The results are compared with those of previous theories and with experimental results on the $KBr:Li^+$ system.

Key Words: Alkali halide crystal, Born-Mayer potential, deformation dipole model, effective force constants, isotopic impurities, local mode frequencies, nearest-neighbor interaction, substitutional impurity, *U*-centers.

Motions of water molecules in potassium ferrocyanide trihydrate, water, and ice: a neutron scattering study, J. J. Rush, P. S. Leung, and T. I. Taylor, *J. Chem. Phys.* **45,** *No. 4, 1312–1317 (Aug. 15, 1966).*
The motions of H_2O molecules in ferroelectric $(K_4Fe(CN)_6 \cdot 3H_2O$ (KFCT), water and ice have been investigated by total cross-section and differential inelastic scattering measurements with cold neutrons. The results show no significant change in the average rotational or translational freedom of the water molecules in KFCT at or near its ferroelectric transition. The inelastic neutron spectra for KFCT exhibit peaks at about 425 and 160 cm^{-1}, both above and below the transition, which are assigned to the librational and optic translational modes of the H_2O molecules, respectively. Moreover, both the total cross-section and inelastic scattering results indicate a greater freedom of motion of the H_2O molecules in the KFCT lattice than in either water or ice. In addition a decrease in the total cross-section of H_2O, and in its variation with neutron wavelength, is observed at the water-ice transition, indicating a significant

change in the frequency distribution. The neutron results are compared with the results of n.m.r. and infrared measurements.

Key Words: $K_4Fe(CN)_6 \cdot 3H_2O$; H_2O; ice; neutron scattering; neutron spectra; neutron cross-sections; inelastic scattering; ferroelectrics; libration; low-frequency modes; phase transition.

Photodetachment cross section, electron affinity, and structure of the negative hydroxyl ion, L. M. Branscomb, *Phys. Rev.* **148,** *No. 1, 11–18 (Aug. 5, 1966).*
Experimental data on the cross section for photodetachment of OH^- and OD^- ions are given and used to argue that $r_e(OH^-) = r_e(OH) \pm 0.0002$ Å, that $\omega_e(OH^-) = 3700 \pm 560$ cm^{-1} and that the OH electron affinity E.A. (OH) $= 1.83 \pm 0.04$ eV. Thus, the structure of OH^- and OH are remarkably similar, which is consistent with the theoretical predictions of Cade.

Key Words: Photodetachment, OH^- ions, OD^- ions, cross section, electron affinity, negative hydroxyl ion, molecular structure.

Acidity functions for amphiprotic media, R. G. Bates, *Book, Chemistry of Nonaqueous Solvents, I, Sect. III, 97–128 (Academic Press Inc., New York, N. Y., 1966).*
The several acidity functions of possible use in amphiprotic solvents are reviewed critically and intercompared. Some of these functions represent an attempt, thus far not completely successful, to express the acidity of all amphiprotic media with reference to a common standard state for the Gibbs energy of the proton, usually that conventionally adopted for aqueous solutions. The most promising approaches are based on a single scale for electrode potentials in different solvents and on the investigation of ionic solvation energies. Acidity functions based on indicators are also discussed. The practical barriers to an ideal acidity scale are examined in the light of the behavior of acids and bases in amphiprotic solvents, and it is shown that the selection of the most suitable acidity function often depends on the nature of the problem at hand.

Collagen aggregation phenomena, J. M. Cassel, *Biopolymers* **4,** *989–997 (1966).*
Three processes by which tropocollagen units associate to yield highly specific aggregates have been examined. From the temperature coefficients of the amounts aggregated it is concluded that the complex "native" aggregation is endothermic whereas both end-to-end and lateral aggregation are exothermic. These results combined with additional information lead to the conclusion that "native" aggregation is an entropy driven process in which hydrophobic bonding plays the dominant role. In contrast the reactions producing the lateral aggregate and the aggregate in which end-to-end bonding is dominant are electrostatically governed.

Studies of molten alumina in the arc-image furnace, J. J. Diamond and A. L. Dragoo, *Rev. Hautes Temper. et Refract.* **3,** *272–279 (1966).*
Aluminum oxide was melted in vacuum and in atmospheres of H_2, He, O_2, N_2, Ar, air, and water vapor with an arc-image furnace. Water vapor was found to dissolve rapidly in molten alumina and to boil out vigorously when it was made supersaturated in a water vapor atmosphere. In spite of this solubility water vapor does not appreciably enhance the vaporization of molten alumina. The rate of vaporization of molten alumina in vacuum was determined in the temperature range 2493 to 2606 °K and the mean third law heat of vaporization found to be 729.0 kcal mol^{-1}, with a standard error in the mean of 0.9 kcal mol^{-1}. Some problems associated with the measurement of the temperature of molten alumina were studied and are discussed.

Key Words: Alumina, arc-image furnace, heat of vaporization, molten alumina, temperature measurement, vapor pressure, vaporization, water in alumina, water vapor.

Effect of certain crystalline substances on physical properties of elastomers. I. Stress-strain behavior, F. J. Linnig, E. J. Parks, and R. D. Stiehler, *Rubber Chem. Technol.* **39,** *No. 4, Pt. 1, 1041–1052 (Sept. 1966).*
Some crystalline organic compounds containing a β-naphthyl group have been found under certain conditions to produce a pronounced stiffening of rubber vulcanizates. When these materials are removed by extraction, the reinforcing effect vanishes. Reinforcement by the most effective of the materials examined, phenyl β-naphthylamine is obtained with vulcanizates made from various elastomers and vulcanizing agents, and is essentially independent of the state of cure. In some instances about 5 percent PBNA produces the same stiffness on first extension as 30 to 40 percent carbon black but the stiffness is markedly reduced by flexing. Less than 3 percent crystalline PBNA may produce an isotropic Young's modulus of about 20 kg/cm² at room temperature. At higher concentrations of PBNA, "anisotropic" effects are observed. The temperature coefficient of Young's modulus is negative analogous to that for vulcanizates containing carbon black. The addition of PBNA to a rubber vulcanizate does not affect significantly the glass-transition temperature.
The loss of reinforcement on removal of the PBNA indicates that primary valence bonds are not involved. However, the effect is not in accord with existing physical theories of reinforcement. This work strongly suggests that profound reinforcement can result from other than primary valence bonds.

The adsorption kinetics of nitrogen on rhenium, M. D. Scheer and J. D. McKinley, *Surface Sci.* **5,** *No. 3, 332–344 (Nov. 1966).*
The adsorption of room temperature nitrogen on atomically clean polycrystalline rhenium has been studied. The sticking coefficients at zero coverage were found to be 0.060, 0.009, and 0.007 at rhenium surface temperatures of 205, 300, and 373 °K, respectively. These values are between one and two orders of magnitude smaller than those in the nitrogen-tungsten system. The dependence of the sticking coefficient upon surface coverage and temperature could be accounted for by assuming an intermediate state weakly bound to an adsorption site. These sites were assumed to be uniformly distributed over the surface. Their concentration was found to be less than 1/10 of the number of substrate rhenium atoms/cm². The binding energies of the intermediate state and the permanently adsorbed state were in the ratio of about 1/20 for both the nitrogen-rhenium and nitrogen-tungsten systems. In view of this similarity, it is difficult to account for the large difference in sticking probabilities unless one assumes that tungsten absorbs energy from the intermediate binding state much more efficiently than does the rhenium.

Key Words: Adsorption kinetics, sticking coefficient, surface coverage, rhenium, nitrogen.

An ultrasonic pressure gage, P. L. M. Heydemann, *Am. Soc. Mech. Eng. Publ. No. 66–WA/PT–5 (1966).*
The transit time of short ultrasonic pulses in solid rods is used to measure pressures throughout the fluid range. Self-excited regenerating circuits are used. Measurements to 3500 bar with an uncertainty of .3 bar and to 20 kb with an uncertainty of 2 bar are reported. Further improvements, temperature compensation and stability are discussed.

Key Words: Gage, high pressure, ultrasonics, velocity of sound, delay line, temperature compensation, self-excited pulse repetition, frequency stability.

The melting point of Al_2O_3 in vacuum, S. J. Schneider and C. L. McDaniel, *Rev. Hautes Temper. et Refract.* **3,** *351–361 (1966).*
The National Bureau of Standards has initiated a program to determine, under a variety of environmental conditions, the melting points of a number of the more refractory metal oxides. The present paper, the first in a series, reports results obtained in an investigation of the melting point of Al_2O_3 (corundum) in vacuum. Equipment has been constructed which will permit the heating of small samples under blackbody conditions to 3000 °C in vacuum or inert atmosphere. The furnace essentially consisted of two concentric covered tungsten crucibles supported by three tungsten rods in the center of a water-cooled, copper, load concentrator. The outer crucible served as the susceptor for induction heating. The inner crucible acted as both the specimen container and the blackbody enclosure for temperature measurements. Theoretical calculations as well as experimental testing indicated that the blackbody-container had an effective emittance of 0.999 at 2000 °C. Temperatures were continuously monitored with a recording photoelectric

spectral pyrometer which has a sensitivity of ±0.2° at 1063 °C and ±1° at 2000 °C. Experiments were conducted on specimens obtained from three different sources of Al_2O_3, each having a purity in excess of 99.9 percent. The data indicated that the melting point of Al_2O_3 in vacuum ($\sim 6.5 \times 10^{-5}$ torr) is 2051 °C (IPTS). The overall maximum uncertainty of the melting point was estimated to be no greater than ±4 °C. Precision of the measurements was within ±1.5 °C.

Temperature measurement in high temperature chemistry: 1000–3000 °C, R. F. Walker, *Rev. Hautes Temper, et Refract.* **3,** *301–308 (1966).*
The uncertainty of temperature measurements is one of the principal causes of error in the measurement of the thermodynamic and kinetic properties of substances above the gold point. In terms of international standards, the ultimate accuracy of temperature measurements depends on the consistency of the International Practical Temperature Scale (IPTS) with the thermodynamic temperature scale. The accuracy achieved in measuring other properties depends on the accuracy of calibration of the temperature measuring instruments in accordance with the IPTS, and on the ability to use the instruments under prescribed physical and chemical conditions. The higher the temperatures, the more difficult it becomes to meet these prescribed conditions.
The present status of the IPTS is reviewed briefly. A summary is given of the precision and accuracy achievable with common temperature measuring instruments. The potential advantages and limitations of newer instruments, such as photoelectric pyrometers, are also indicated. It is concluded that in the field of high temperature chemistry the principal limitation is the inability to use the instruments under ideal conditions. Higher precision and accuracy would be achievable if additional internal checks, such as internationally recognized secondary reference points, were available to the experimentalist. Severe problems of both a chemical and physical nature are, however, attendant on the provision of such reference points, and these are briefly discussed.

Key Words: High temperature chemistry, international temperature scale, melting points, pyrometry, secondary reference points, temperature measurement.

Accurate microscopical determination of optical properties on one small crystal, C. P. Saylor, *Book, Advances in Optical and Electron Microscopy, ed. R. Barer and V. E. Cosslett, 1, 41–76 (Academic Press Inc., New York, N.Y., 1966).*
By rotating a crystal about one axis and using phase, double diaphragm, or interference contrast, refractive indices of a typical crystal can be microscopically determined for any wavelength with an error that is not greater than 0.00002. For such accuracy, the diameter of the crystal must be about 20 μ or larger. Precautions involve careful orientation, precise matching of index with that of immersion, fluid, and correct determination of the refractive index of the fluid.

Effect of nuclear alinement on the 14-MeV total neutron cross section of ^{165}Ho, H. Marshak, A. C. B. Richardson, and T. Tamura, *Phys. Rev.* **150,** *No. 3, 996–1010 (Oct. 21, 1966).*
The effect of nuclear alinement on the total cross section of the highly deformed ^{165}Ho nucleus has been measured using 14 MeV neutrons. The alined ^{165}Ho target was obtained by cooling a metal single crystal to 0.33 °K. A finely collimated beam of 14 MeV neutrons was produced by careful collimation of the alpha particle produced in the ^{3}H(d,n)^{4}He reaction and by detecting it in fast coincidence with its associated neutron. The measured total cross section is (5.29 ± 0.10) b. The fractional change in the total cross section, for our value of nuclear alinement ($f_2 = 0.31$), is + (3.52 ± 0.75) percent, where the positive sign indicates a larger cross section for nuclei alined perpendicular to the incident beam than for randomly oriented nuclei. These results are in excellent agreement with the predictions of the optical model using an adiabatic coupled-channel calculation. The optical-model parameters used are in good agreement with those obtained from other measurements, and in particular the value of the deformation parameter $\beta = +0.30$ is the same as that used in our earlier work. It was also found that 14 MeV is not yet a sufficiently high energy to use the black nucleus model to interpret our results.

Key Words: Black nucleus model, cryogenic target, coupled-channel calculation, nuclear alinement, nuclear deformation, 14 MeV neutrons, ^{165}Ho, Van de Graaff, optical model.

Electron microscopy and diffraction of synthetic corundum crystals. II. Dislocations and grain boundaries in impurity-doped aluminum oxide, D. J. Barber, and N. J. Tighe, *Phil. Mag.* **14,** *No. 129, 531–544 (Sept. 1966).*
Boules of aluminum oxide containing various impurities, grown by the Verneuil technique, have been examined by transmission electron microscopy. Most of the samples have dislocation densities $\sim 6 \times 10^5$ cm^{-2}, excluding grain boundaries. This is two orders of magnitude higher than that for comparable undoped crystals. There is a higher incidence of low angle boundaries and the characteristics of these are described. The samples rarely contain internal precipitates; furthermore, precipitates in sapphire do not normally create significant numbers of dislocations.
The interactions of a singularity with a basal network of dislocations with $\frac{1}{3}\langle 1120\rangle$ Burgers vectors are analyzed. The configuration is not consistent with the singularity being a $\langle 10\bar{1}0\rangle$ dislocation, but it can be explained by assigning the singularity a $\frac{1}{3}\langle 10\bar{1}1\rangle$ vector.

Key Words: Aluminum oxide, dislocations, electron microscopy, grain boundaries, impurities, sapphire.

Exact vibrational matrix elements for molecular hydrogen and the intensity of the qudarupole rotation-vibration spectrum, T. C. James, *Astrophys. J.* **146,** *No. 2, 572–580 (Nov. 1966).*
Accurate vibrational overlap integrals and matrix elements of $\xi = (r-re)/re$, ξ^2, and ξ^3 have been calculated for lines in the 1–0, 2–0, 3–0, and 4–0 rotation-vibration bands of molecular hydrogen. The affect of rotation-vibration interaction has been considered and values are given for Q, S, and some O branch lines. The calculations were carried out using a computer program written by R. N. Zare. These results are used to analyze the intensity measurements in the quadrupole rotation-vibration spectrum which have been made by Rank and his associates. The possibility of predicting the intensity of the 4–0 band, and of using the 2–0, and 3–0 bands for rotational temperature measurements is discussed.

Key Words: Hydrogen, intensity, quadrupole spectrum, rotation-vibration interaction, vibrational matrix elements.

Interference in the photo-ionization of molecules, H. D. Cohen and U. Fano, *Phys. Rev.* **150,** *No. 30–33 (Oct. 7, 1966).*
Atoms of a molecule exposed to Far-UV light may be treated approximately as separate sources of photoelectrons. Interference from these sources modulates the spectrum of photoabsorption in accordance with Samson's observations on N_2 and O_2. A Born approximation calculation for H_2^+ displays details of this effect.

Key Words: Photoionization, ultraviolet, diatomic molecule, interference.

The absorption spectrum of cesium deuteride. The $A^1\Sigma$ state of CsH, I. R. Bartky, *J. Mol. Spectry.* **21,** *No. 1, 25–28 (1966).*
An analysis of the visible absorption spectrum of CsD has shown that the vibrational numbering of the $A^1\Sigma$ state of CsH must be increased by 3. From this and previous reassignments of the $A^1\Sigma$ states of KH and RbH, it is now possible to exhibit the trends of the vibrational and rotational constants for the alkali metal hydrides.

Key Words: Absorption spectroscopy, alkali metal hydrides, hydrides, isotope relations, molecular constants.

The absorption spectrum of RbD. Vibrational numbering of the A^1 state of RbH, I. R. Bartky, *J. Mol. Spectry.* **21,** *No. 1, 1–3 (1966).*
RbD has been observed in absorption from 5200–5400 Å. Of the several bands observed in this region, two have been analyzed in detail. The RbD spectrum correlates with the RbH spectrum only if the vibrational numbering of the $A^1\Sigma$ state of RbH is increased by 3. Revised molecular consants for RbH are given.

Key Words: Absorption spectroscopy, alkali metal hydrides, hydrides, isotope relations, molecular constants.

The momentum autocorrelation function in a Bernoulli chain, R. J. Rubin and P. Ullersma, *J. Math. Phys.* **7,** *No. 10, 1877–1885 (Oct. 1966).*

This paper is devoted to the study of the statistical dynamics of the small amplitude coplanar vibrations of a compound pendulum consisting of $N+1$ particles suspended in series by weightless strings in a gravitational field. All particles have the same mass m except for the top particle whose mass is $m(1+2)$; and all strings are of equal length. The behavior of this system in the limit in which $N \to \infty$ is of particular interest because the maximum normal mode frequency is proportional to $N^{1/2}$. In the limit $N \to \infty$ asymptotic formulas with error estimates are obtained for the time-dependence of the momentum autocorrelation function of: (1) the top particle when $2=0$; (2) the bottom particle when $2=0$; and (3) the top particle when $N \gg 2 \gg 1$.

Key Words: Statistical dynamics, coupled harmonic oscillators, momentum autocorrelation function, statistical mechanics.

Other NBS Publications

J. Res. NBS 71B (Math. and Math. Phys.), No. 1 (Jan.–Mar. 1967), 75 cents.

Algorithms for frames and lineality spaces of cones. R. J. B. Wets and C. Witzgall.

The coefficients of the powers of a polynomial. M. Newman.

Stable evaluation of polynomials. C. Mesztenyi and C. Witzgall.

On involutions. O. Shisha and C. B. Mehr.

Minimum number of subsets to distinguish individual elements. P. R. Meyers.

E-transforms. F. M. Ragab.

Three observations on nonnegative matrices. A. J. Hoffman.

Additional remarks on a theorem of M. Riesz. J. M. Smith.

Heat treatment and properties of iron and steel, T. G. Digges, S. J. Rosenberg, and G. W. Geil, Mono. 88 (Nov. 1, 1966), 35 cents. (Supersedes Circular 495 and Monograph 18.)

Standard Reference Materials: Viscosity of a standard lead-silica glass, A. Napolitano and E. G. Hawkins, Misc. Publ. 260–11 (Nov. 7, 1966), 25 cents.

Critical Phenomena. Proceedings of a Conference held in Washington, D.C., April 1965, ed. M. S. Green and J. V. Sengers, Misc. Publ. 273 (Dec. 1, 1966), $2.50.

The National Bureau of Standards 1966, Misc. Publ. 282 (Nov. 1966), 35 cents.

Thermal conductivity of selected materials, R. W. Powell, C. Y. Ho, and P. E. Liley, NSRDS–NBS 8 (Nov. 25, 1966), $1.00.

Notes on the state-of-the-art of benefit-cost analysis as related to transportation systems, J. D. Crumlish, Tech. Note 294 (Nov. 1, 1966), 30 cents.

A grammar for component combination in Chinese characters, B. K. Rankin, III, S. Siegel, A. McClelland, and J. L. Tan, Tech. Note 296 (Dec. 1966), 60 cents.

Calculation of the heating value of a sample of high purity methane for use as a reference material, G. T. Armstrong, Tech. Note 299 (Dec. 15, 1966), 25 cents.

A new near-zone electric field-strength meter, F. M. Greene, Tech. Note 345 (Nov. 15, 1966), 35 cents.

A standard for accurate phase-angle measurements at audio frequencies, W. W. Scott, Jr., Tech. Note 347 (Oct. 14, 1966), 25 cents.

Radiochemical analysis: activation analysis, instrumentation, radiation techniques, and radioisotope techniques July 1965 through June 1966, ed. J. R. DeVoe, Tech. Note 404 (Sept. 30, 1966), $1.25.

Dissociation constant of morpholinum ion and related thermodynamic quantities from 0 to 50°, H. B. Hetzer, R. G. Bates, and R. A. Robinson, J. Phys. Chem. **70,** No. 9, 2869–2872 (Sept. 1966).

Dissociation of 4-aminopyridinium ion in 50 percent methanol-water and related acidity functions from 10 to 40 °C, M. Paabo, R. A. Robinson, and R. G. Bates, Anal. Chem. **38,** No. 11, 1573–1575 (Oct. 1966).

Kinetics and statistics of structural changes in polyacrylonitrile, K. Noh and H. Yu, J. Polymer Sci. Letters **4B,** No. 10, 721–726 (Oct. 1966).

Momentum autocorrelation function for systems with finite spatial boundaries, R. Nossal, J. Chem. Phys. **45,** No. 4, 1097–1100 (Aug. 15, 1966).

Translational diffusion in polymer solutions, R. Zwanzig, J. Chem. Phys. **45,** No. 5, 1858–1859 (Sept. 1, 1966).

A device for use in applying strain gages to cylindrical specimens, T. W. Butler and R. L. Bloss, Experimental Mechanics **6,** No. 10, 528 (Oct. 1966).

A simplified method for the prediction of multi-component adsorption equilibria from single gas isotherms, A. J. Kidnay and A. L. Myers, AIChE J. **12,** No. 5, 981–986 (Sept. 1966).

Calibration and use of laminar flowmeters, H. H. Allion, (Proc. 25th Annual Gas Measurement Short Course, Aug. 25, 1965), West Virginia Univ. Tech. Bull. **77,** pp. 34–43 (1965).

Coincident summer weather characteristics of six selected cities in the United States, T. Kusuda and P. R. Achenbach, ASHRAE **J. 8,** No. 11, 34–42 (Nov. 1966).

Embrittlement of high strength AISI 4340 steel in boiling NaCl solution, H. L. Logan and J. M. Wehrung, Corrosion **22,** No. 9, 265–269 (Sept. 1966).

Some effects of notch geometry on the tensile behavior of annealed type 310 stainless steel, G. W. Geil, J. Materials **1,** No. 3, 583–608 (Sept. 1966).

Monte Carlo studies of lattice-model polymer chains. I. Correlation functions in the statistical-bead model, P. H. Verdier, J. Chem. Phys. **45,** No. 6, 2118–2121 (Sept. 15, 1966).

Monte Carlo studies of lattice-model polymer chains. II. End-to-end length, P. H. Verdier, J. Chem. Phys. **45,** No. 6, 2122–2128 (Sept. 15, 1966).

A nonmagnetic laboratory for the National Bureau of Standards, F. K. Harris, IEEE Spectrum **3,** No. 11, 85–87 (Nov. 1966).

A scattering chamber for use with cooled large area lithium-compensated silicon radiation detectors, W. R. Dodge, J. A. Coleman, and S. R. Domen, Nucl. Instr. Methods **42,** 181–187 (July 1966).

Anomalous energy spreads in electron beams, J. A. Simpson and C. E. Kuyatt, J. Appl. Phys. **37,** No. 10, 3805–3809 (Sept. 1966).

Classification of the $Y_1(1765)$ and $Y_0(1520)$ resonances in the 1134 representation of SU(6), J. J. Coyne, S. Meshkov, and G. B. Yodh, Phys. Rev. Letters **17,** No. 12, 666–668 (Sept. 19, 1966).

Dielectric constants of $PbMoO_4$ and $CaMoO_4$, W. S. Brower and P. H. Fang, Phys. Rev. **149,** No. 2, 646 (Sept. 16, 1966).

Effect of surface patch fields on field-emission work-function determinations, R. D. Young and H. E. Clark, Phys. Rev. Letters **17,** No. 7, 351–353 (Aug. 15, 1966).

EPR in single crystals of $NiBr_2$, J. S. Wells and D. R. Winder, J. Chem. Phys. **45,** No. 1, 410–411 (July 1, 1966).

Erratum: Statistical model for the beta zirconium hydrides, T. B. Douglas, J. Chem. Phys. **45,** No. 3, 1080 (Aug. 1, 1966).

Lithium compensated silicon focal plane detectors for electron scattering spectrometers, W. R. Dodge, J. A. Coleman, S. R. Domen, and J. K. Whittaker, Rev. Sci. Instr. **37,** No. 9, 1151–1159 (Sept. 1966).

Measurement of the mean energy required to create an electron-hole pair in silicon between 6 and 77 °K, W. R. Dodge, S. R. Domen, T. F. Leedy, and D. M. Skopik, Phys. Rev. Letters **17,** No. 12, 653–655 (Sept. 19, 1966).

Microwave spectrum of CF_2, F. X. Powell and D. R. Lide, Jr., J. Chem. Phys. **45,** No. 3, 1067–1068 (Aug. 1, 1966).

Multiple diffraction in the Weissenberg methods, A. Santoro and M. Zocchi, Acta Cryst. **21,** Pt. 3, 293–297 (Sept. 1966).

The structure of field-evaporated hexagonal close-packed surfaces: rhenium and ruthenium A. J. Melmed, Surface Science **5,** No. 3, 359–379 (Nov. 1966).

Zeeman effect and magnetic hyperfine structure in the low frequency transitions of H_2CO, H. Takuma, K. M. Evenson, and T. Shigenari, J. Phys. Soc. **21,** 1622–1623 (1966).

Government, industry and engineering. NBS in a new setting, S. Lichtenstein, Automotive Ind. **135,** No. 10, 119–124 (Nov. 15, 1966).

Progress in nuclear electronics, L. Costrell, Bock, Radioisotopes for Aerospace, Part 1. Advances and Techniques, p. 1–13 (Plenum Press Inc., New York, N.Y., 1966).

Hadamard matrices of order cube plus one, K. Goldberg, Proc. Am. Math. Soc. **17,** No. 3, 744–746 (June 1966).

State standards and laboratories, T. M. Stabler, Scale J. **53,** No. 1, 3–14 (Oct. 1966).

The measurement of solar radiation, with principal emphasis on the ultraviolet component, R. Stair, Air Water Pollut, Int. J. **10,** 665–688 (1966).

Angle and channel dependence of resonance in e-He scattering near 60 eV, J. A. Simpson, J. G. Menendez, and S. R. Mielczarek, Phys. Rev. **150,** No. 1, 76–78 (Oct. 7, 1966).

Anomalous work function of the tungsten (110) plane, R. D. Young and H. E. Clark, Appl. Phys. Letters **9,** No. 7, 265–268 (Oct. 1, 1966).

Oxidation products in an oxygen-blown Kuwait asphalt, P. G. Campbell and J. R. Wright, I&EC Product Res. Devel. **5,** No. 4, 319–323 (Dec. 1966).

Proton broad-line N.m.r. study of ($^2H_6$) dimethoxy (^{11}B) borane, T. C. Farrar, J. Cooper, and T. D. Coyle, Chem. Commun. **17,** 610–611 (1966).

Compressibility, gas, J. M. H. L. Sengers, Encyclopedia of Physics, p. 118–120 (Reinhold Publ. Corp., New York, N.Y., 1966).

Pyrometry, optical, H. J. Kostkowski, Encyclopedia of Physics, p. 563–564 (Reinhold Publ. Corp., New York, N.Y., 1966).

Resonances in inelastic electron scattering from H_2, M. G. Menendez and H. K. Holt, J. Chem. Phys. **45,** No. 8, 2743–2744 (Oct. 15, 1966).

The $A^1\Sigma$ transition of ^{39}KH and ^{39}KD. Vibrational numbering and molecular constants, I. R. Bartky, J. Mol. Spectry. **20,** No. 4, 299–311 (1966).

What environment—for whom? B. E. Auman, Civil Service J. **7,** No. 1, 6–11 (July–Sept. 1966).

X-ray fiber optics, L. Marton, Appl. Phys. Letters **9,** No. 5, 194–195 (Sept. 1, 1966).

**Publications for which a price is indicated are available by purchase from the Superintendent of Documents, U.S. Government Printing Office, Washington, D.C. 20402 (foreign postage, one-fourth additional). The NBS nonperiodical series are also available from the Clearinghouse for Federal Scientific and Technical Information, Springfield, Va. 22151. Reprints from outside journals and the NBS Journal of Research may often be obtained directly from the authors.*

U.S. GOVERNMENT PRINTING OFFICE : 1967 OL—248-733

SJR-A OCT 46129
UNIVERSITY MICROFILMS INC
ATTN SERIALS SECTION
300 NORTH ZEEB RD
ANN ARBOR MICH 48106

UNITED STATES
GOVERNMENT PRINTING OFFICE
DIVISION OF PUBLIC DOCUMENTS
WASHINGTON, D.C. 20402

OFFICIAL BUSINESS

POSTAGE AND FEES PAID
U.S. GOVERNMENT PRINTING OFFICE

JOURNAL OF RESEARCH of the National Bureau of Standards
A. Physics and Chemistry

Vol. 71A, No. 3 May–June 1967

Contents

Page

Measured relative enthalpy of anhydrous crystalline aluminum trifluoride, AlF_3, from 273 to 1173 °K and derived thermodynamic properties from 273 to 1600 °K. Thomas B. Douglas and David A. Ditmars. 185

The heat of formation of boron trifluoride by direct combination of the elements. Eugene S. Domalski and George T. Armstrong. 195

An equation of state for fluid parahydrogen from the triple-point to 100 °K at pressures to 350 atmospheres. Robert D. Goodwin. 203

The dissociation constants of some disubstituted anilines and phenols in aqueous solution at 25 °C. R. A. Robinson. 213

Third virial coefficient for air-water vapor mixtures. R. W. Hyland and E. A. Mason. 219

Recrystallization and melting of partially melted stark rubber. Donald E. Roberts. 225

Effects of a distribution of volume relaxation times in the annealing of BSC glass. P. B. Macedo and A. Napolitano. 231

Publications of the National Bureau of Standards. 239

Library of Congress Catalog Card Number: 62–37059

For sale by the Superintendent of Documents, U.S. Government Printing Office, Washington, D.C. 20402. Price $1.00 (single copy).
Subscription price: $5 a year; $1.00 additional for foreign mailing.
UNITED STATES GOVERNMENT PRINTING OFFICE, WASHINGTON : 1967